# Functional analysis of the insulin receptor substrate protein of 53 kDa (IRSp53) in the brain of *Mus musculus* *(Linnaeus 1758)*

**Dissertation**

for achieving the degree

Doctor rerum naturalium (Dr. rer. nat.)

at the Faculty of Mathematics, Informatics and Natural Sciences
Department of Biology
of the University of Hamburg

submitted by
Kristin Bobsin
from Bautzen

Hamburg 2013

Genehmigt vom Fachbereich Biologie
der Fakultät für Mathematik, Informatik und Naturwissenschaften
an der Universität Hamburg
auf Antrag von Priv. Doz. Dr. H.-J. KREIENKAMP
Weitere Gutachterin der Dissertation:
Frau Professor Dr. S. DOBLER
Tag der Disputation: 20. Dezember 2013

Hamburg, den 05. Dezember 2013

Professor Dr. C. Lohr
Vorsitzender des
Fach-Promotionsausschusses Biologie

Katrin Lehmann
Schlegelstraße 5
07747 Jena

Universität Hamburg
Fachbereich Biologie
Fachbereichsleitung
Prof. Dr. Axel Temming
Ohnhorststraße 18
22609 Hamburg

14.11.2013

**Bestätigung der Korrektheit der englischen Sprache**

Sehr geehrte Damen und Herren,

hiermit bestätige ich, dass die Dissertation „Functional analysis of the insulin receptor substrate protein of 53 kDa (IRSp53) in the brain of *Mus musculus (Linnaeus 1758)*“, eingereicht von Kristin Bobsin, in korrekter englischer Sprache abgefasst ist.

Mit freundlichen Grüßen

Katrin Lehmann
Staatl. Geprüfte Fremdsprachenkorrespondentin
Level 2 Certificate in English (ESOL) der University of Cambridge
Mit fünfjähriger Berufserfahrung im Kundendienst und Marketing des UK NARIC,
Cheltenham, UK

I hereby declare that I wrote this dissertation independently and used no other sources and tools than indicated and that the textual and cited quotations of the references were marked. Furthermore, I declare that this manuscript was not submitted to another Faculty either in this or another written form.

Hamburg, 22/10/2013

Kristin Bobsin

*For Markus and my family.*

# Abstract

The postsynaptic density (PSD) of excitatory synapses in the central nervous system (CNS) is a tightly packed compartment that integrates, processes and transmits input signals. A reorganisation of the postsynapse enables the modulation of synaptic efficacy; this phenomenon is known as synaptic plasticity and underlies learning and memory formation. One abundant postsynaptic protein is the insulin receptor substrate protein of 53 kDa (IRSp53). IRSp53 is a powerful regulator of the actin cytoskeleton and therefore a suitable candidate to promote postsynaptic reorganisation. However, *in vivo* analysis of IRSp53 knock out (ko) mice unveiled no morphological alterations in the CNS. Instead, IRSp53 null-mice displayed severe cognitive impairments in simple learning tasks. A cellular model for synaptic improvement implicated in memory formation is the long-term potentiation (LTP), which is significantly enhanced in the hippocampus of IRSp53 ko mice. How does IRSp53 contribute to synaptic plasticity?

One hypothesis is that a critical amount of IRSp53 is required for the protein to fulfil its function. A suitable approach to test a reduction of IRSp53 in a physiological context was to analyse IRSp53 heterozygous (+/d) mice. Indeed, these mice show a severe cognitive deficit in the contextual fear-conditioning assay, similar to that observed for IRSp53 ko mice. Quantification of the IRSp53 amounts reveal different IRSp53 accumulation levels in the PSD of different forebrain regions of IRSp53 haploinsufficient mice; as a significantly larger proportion of the protein is located in the hippocampal PSD. Expression studies in primary neurons indicate that the IM- and CRIB domains of IRSp53, as well as the PDZ ligand are important for the synaptic localisation. Live imaging indicates that IRSp53 reaches the postsynapse by diffusion where it is tethered by its postsynaptic interaction partners.

As known from prior experiments the amount of NMDA receptors is increased in the PSD of IRSp53 ko mice; this could be responsible for the enhanced LTP. Analysis of the compositions of PSD with respect to proteins involved in cognition shows a changed distribution of ionotropic glutamate receptors in the cortex, hippocampus and striatum. During the development the NMDA receptor subunit GluN2B is exchanged by the GluN2A subunit. This developmental switch seems to be retarded in the cortex and hippocampus due to the reduction or loss of IRSp53. Although the total number of NMDA receptors remains constant, the number increases in the PSD of the hippocampus. However, no change in the NMDA receptor surface expression was detectable. Therefore, a shift of the extrasynaptic GluN2B containing NMDA receptors towards the synapse can be assumed.

Biochemical analysis of the NMDA receptor dependent LTP via chemical stimulation of acute hippocampal slices shows an altered phosphorylation pattern of different signalling molecules. Both the loss and the reduction of IRSp53 results in an increased phosphorylation of the transcription initiation factor CREB. Otherwise, the activation of the kinases ERK1/2 and Akt1 decreases. Both kinases are responsible for boosting the translational capacity of the cell required to stabilise and maintain LTP as well as for memory formation. Thus, IRSp53 seems to affect not only the quantity and composition of postsynaptic NMDA receptors but also the NMDA receptor-mediated signal transduction and gene expression that are essential for memory formation.

# Zusammenfassung

Die postsynaptische Dichte (PSD) exzitatorischer Synapsen ist ein dicht gepacktes Netzwerk von Proteinen, welches verantwortlich ist für die Integration, Verarbeitung und Weiterleitung eingehender Signale. Eine Umstrukturierung der Postsynapse ermöglicht eine Anpassung ihrer Effizienz; dies ist bekannt als synaptische Plastizität, welche der Gedächtnisbildung zugrunde liegt. Ein in der PSD angereichertes Protein ist das Insulin Rezeptor Substrat Protein von 53 kDa (IRSp53). Funktionelle Analysen in auf Zellkulturen basierenden Systemen weisen IRSp53 als einen einflussreichen Regulator des Aktinzytoskeletts aus, der essentiell für die Umstrukturierung der PSD sein könnte. Analysen IRSp53-defizienter Mäuse zeigten jedoch keine morphologischen Veränderungen des neuronalen Netzwerkes. Stattdessen zeigten IRSp53 knock out (ko) Mäuse massive kognitive Beeinträchtigungen in einfachen Verhaltenstests. Ein zelluläres Modell für die Steigerung der synaptischen Effizienz ist die Langzeitpotenzierung (LTP), welches signifikant im Hippocampus von IRSp53-defizienten Tieren erhöht ist.

Ziel dieser Arbeit ist die Erforschung des Proteins IRSp53 im zentralen Nervensystem in Bezug auf dessen Rolle in der synaptischen Plastizität. Für die Analyse eines möglichen Gendosiseffektes wurden IRSp53 heterozygote (+/d) Mäuse mittels Angstkonditionierung untersucht. Die Tiere zeigen, wie ihre IRSp53 ko Geschwister, deutliche kognitive Beeinträchtigungen. Die biochemische Quantifizierung der IRSp53 Proteinmenge offenbarte eine unterschiedlich starke Anreicherung von IRSp53 in der PSD verschiedener Gehirnregionen bei IRSp53-haploinsuffizieten Tieren; so ist im Hippocampus der IRSp53 +/d Tiere ein deutlich größerer Anteil des Proteins in der PSD angereichert. Expressionsstudien in kultivierten Primärneuronen zeigen eine Beteiligung der IRSp53 IM- und CRIB Domäne sowie des PDZ Liganden an dessen postsynaptischer Akkumulation. Mittels Diffusion scheint IRSp53 an die Postsynapse zu gelangen, wo es durch seine Interaktionspartner verankert wird.

Bereits publizierte Daten demonstrieren eine Erhöhung der NMDA-Rezeptormenge in der PSD, die vermutlich verantwortlich für die Erhöhung der LTP ist. Untersuchungen abundanter Proteine der PSD ergaben eine veränderte Verteilung der ionotropen Glutamatrezeptoren im Cortex, Hippocampus und Striatum IRSp53-haploinsuffizienter und -defizienter Mäuse. Während der Entwicklung des ZNS erfolgt ein Austausch von NMDA-Rezeptoren, welche anstelle von GluN2B GluN2A Untereinheiten beinhalten. Im Cortex und Hippocampus von IRSp53 +/d und d/d Tieren scheint dieser Entwicklungsschritt verzögert zu sein. Während die Gesamtmenge konstant bleibt, ist die Anzahl der NMDA Rezeptoren in der PSD des Hippocampus signifikant erhöht. Es konnte keine veränderte Oberflächenexpression der NMDA Rezeptoren im Hippocampus nachgewiesen werden. Dies lässt eine Verschiebung der extrasynaptischen NMDA Rezeptoren hin zur Synapse vermuten.

Untersuchungen des NMDA-Rezeptor-abhängigen LTPs mittels chemischer Stimulation akuter hippocampaler Schnitte zeigten ein verändertes Phosphorylierungsmuster verschiedener Signalmoleküle. Sowohl der Verlust als auch die Reduktion von IRSp53 verursacht eine erhöhte Aktivierung des Transkriptionsinitiationsfaktors CREB. Andererseits sinkt die Aktivierung der Kinasen ERK1/2 und Akt1. Diese steigern die Kapazität der Zelle zur Proteinsynthese, welche benötigt wird für die Stabilisierung und Konsolidierung des LTPs so-

wie für die Gedächtnisbildung. Demzufolge scheint IRSp53 nicht nur die Menge und Zusammensetzung der postsynaptischen NMDA-Rezeptoren zu beeinflussen, sondern auch die NMDA-Rezeptor vermittelte Signaltransduktion und Genexpression, die für die Gedächtnisbildung essentiell sind.

# I Content

# II Register of Tables

# III Register of Illustrations

# IV Abbreviations

| | |
|---|---|
| 4-AP | 4-aminopyridine |
| A | Ampere |
| A (amino acid) | alanin |
| A (nucleotide) | adenosin |
| AC | adenylate cyclase |
| ACSF | artificial cerebrospinal fluid |
| Ad | adenovirus |
| AD | alzheimer diseases |
| ADHS | attention deficit hyperactivity disorder |
| AKAP | adenylate-kinase anchoring protein |
| AMPA | α-Amino-3-Hydroxy-5-Methyl-4-Isoxazolepropionic acid |
| ANOVA | analyis of variance |
| AP | action potential |
| APS | ammonium persulfate |
| as | anti-sense |
| ASD | autism spectrum disorder |
| AStr | amygdalstriatal transmission area |
| ATP | adenosin-triphosphate |
| BAI-1 | brain-specific angiogenesis inhibitor 1 |
| BAIAP2 | BAI-associated protein 2 |
| BBS | N,N-Bis(2-hydroxyethyl)-2-aminoethanesulfonic acid |
| BIC | bicuculline |
| bp | base pair |
| BSA | bovine serum albumine |
| C (nucleotide) | cytosine |
| C-terminal | carboxy-terminal |
| CA | closed arm |
| Ca | calcium |
| CA1/2/3 | field CA1/2/3 of the hippocampus |
| CamKII | calcium/calmodulin-dependent kinase II |

| | |
|---|---|
| Cdc42 | cell devision control protein 42 |
| cDNA | complementary DNA |
| CeMAD | central amygdaloid nucleus |
| CGH | comparative genomic hybridization |
| CHO | chinease hamser ovary |
| CIPP | channel-interacting PDZ domain protein |
| CMV | cytomegalovirus (promotor) |
| CNS | central nervous system |
| CNV | copy number variations |
| $CO_2$ | carbone dioxide |
| CoIP | coimmun precipitation |
| Cp | basal cerebral peduncle |
| CPu | caudate putamen |
| CRIB | Cdc42 and Rac interacting binding |
| CS | cover slip |
| Cu | cupper |
| Cx | cerebral cortex |
| Cypin | cytosolic PSD95 interactor |
| Da | Dalton |
| DAPI | 4',6-diamidino-2-phenylindole |
| DEn | dorsal endopiriform nucleus |
| DG | dentate gyrus |
| DHPG | dihydroxyphenylglycine |
| DIV | days in vitro |
| DMEM | dulbeco's modified eagle's medium |
| DMSO | dimethyl sulfoxide |
| DNA | desoxyribonucleic acid |
| dNTP | desoxy-nucleosid triphosphate |
| ds | double strand |
| E (amino acid) | glutamic acid |
| E. coli | Escherichia coli |
| e. g. | exempli gratia |
| EDTA | ethylenediaminetetraacetic acid |
| eEPSC | evoked excitatory postsynaptic current |
| EGFP | enhanced green fluorescent protein |
| EGTA | ethylene glycol tetraacetic acid |

| | |
|---|---|
| EPM | Elevated-plus maze |
| ER | endoplasmatic reticulum |
| ERK1/2 | p42/44 MAP kinase |
| EtBr | ethidium bromide |
| EtOH | ethanol |
| FACS | Fluorescence-activated cell sorting |
| FBS | fetal calve serum |
| g | graphity of Earth |
| G (amino acid) | glycine |
| G (nucleotide) | guanine |
| $GABA_A$ receptor | γ-aminobutyric acid receptor type A |
| GAPDH | glyceraldehyde 3-phosphate dehydrogenase |
| GFP | green fluorescent protein |
| GKAP | guanylate kinase-associated protein |
| GluA1 | AMPA receptor subunit 1 |
| GluN1/2/3 | NMDA receptor subunit 1/2/3 |
| GRIP | glutamate receptor interacting protein |
| GST | gluthation-S-transferase |
| GTP | guanosine triphosphate |
| GTPγS | guanosine 5'-O-[gamma-thio]triphosphate |
| h | hour |
| HBSS | Hanks balanced salt solution |
| HCl | hydrochloride acid |
| HEK293 | human embryonic kidney cell line 293 |
| HEPES | 4-(2-hydroxyethyl)-1-piperazineethanesulfonic acid |
| HRP | horseradish peroxidase |
| I (amino acid) | isoleucin |
| ICC | Immunocytochemistry |
| i. e. | id est |
| ICH | immunhistochemistry |
| IGF-I | insulin-like growth factor 1 |
| IMD | IRSp53 missing-in-metastasis domain |
| IP3 | inositide-triphosphate |
| IRSp53 | insulin receptor substrate protein of 53 kDa |
| K (amino acid) | lysine |
| kb | kilo base |

| | |
|---|---|
| KCl | potassium chloride |
| kg | kilo gramm |
| $KH_2PO_4$ | potassium phosphate monobasic |
| ko | knock out |
| l | litre |
| LB | Lysogeny broth |
| LTD | long-term depression |
| LTP | long-term potentiation |
| M | Molar |
| MAGUK | membrane associated guanylate kinase |
| mg | milligramm |
| $MgCl_2$ | magnesium chloride |
| mGluR | metabotropic glutamate receptor |
| $MgSO_4$ | magnesium sulfate heptahydrate |
| mHB | medial habenular nucleus |
| min | minute |
| MR | mental retardation |
| mRNA | messenger RNA |
| N (amino acid) | asparagine |
| N-terminal | amino-terminal |
| N-WASH | Wiskott-Alddrich syndrom protein homolog N |
| N-WASP | Wiskott-Alddrich syndrom protein N |
| N2 | nitrogen |
| $Na_2HPO_4$ | sodium tetraborate hydrate |
| NaAc | sodium acetide |
| NaCl | sodium chloride |
| NaDOC | sodium deoxycholate |
| NaOH | sodium hydroxide |
| NB | Neurobasal |
| Neo | neomycin |
| NETBAG | network-based analysis of genetic associations |
| NGS | normal goat serum |
| nm | nano meter |
| NMDA | N-Methyl-D-aspartic acid |
| NP-40 | nonindet P40 |
| nt | nucleotide |

| | |
|---|---|
| OA | open arm |
| OD | optical density |
| ORF | open reading frame |
| p | plasmid |
| P | postnatal |
| P (amino acid) | proline |
| p-value | probability value |
| PaLM | lateral paraventricular hypothalamic nucleus |
| PaMM | medial paraventricular hypothalamic nucleus |
| PBS | phosphate buffered saline |
| PBS-T | PBS-Tween 20 |
| PCR | polymerase chain reaction |
| PDZ | PSD95 - large disc - Zona occludens 1 |
| PFA | paraformaldehyde |
| PI(4,5)P2 | phosphatidylinositol (4,5) bispohsphate |
| Pir | pirifom cortex |
| PKA/C | protein kinase A/C |
| PLC | phospholipase C |
| PLL | Poly-L-Lysin |
| PM | plasma-membrane |
| pmol | pico mol |
| pnl | postnuclear lysate |
| PPF | paired-puls fascilitation |
| PSD | postsynaptic density |
| PSD95 | synaptic density protein 95 |
| PSD93 | postsynaptic protein 93 |
| R&F | rolipram and forskolin |
| rAAV | recombinant adeno-associated virus |
| RFP | red fluorescent protein |
| RIPA | radioimmunoprecipitation assay buffer |
| RNA | ribonuceic-acid |
| rpm | revolutions per minute |
| RT | room temperature |
| s | sense |
| SAM | sterile alpha motif |
| SAP102 | synapse-associated protein 102 |

| | |
|---|---|
| SAP97 | synapse-associated protein 97 |
| SAPAP | SAP90/PSD-95-associated protein |
| SC | Schaffer colateral |
| SCZ | schizophrenia |
| SD | standard deviation |
| SDS | sodium dodecyl sulfate |
| SE | standard error |
| sec | second |
| SH3 | Src homology 3 |
| Shank protein | SH3 and multiple ankyrin repeat domains protein |
| siRNA | small interfering RNA |
| ss | single strand |
| SSTR5 | somatostatin receptor subtype 5 |
| SynGAP | synaptic Ras-GTPase activating protein |
| T (amino acid) | threonin |
| T (nucleotide) | thymine |
| TAE | Tris-acetate-EDTA |
| TARP | transmembrane AMPA receptor regulating protein |
| TBS | Tris buffered saline |
| TBS-T | TBS-Tween 20 |
| TEMED | tetramethylethylenediamine |
| Th | thalamus |
| tr. IMD | truncated IMD |
| TU | transduction unit |
| U | Unit |
| UV | Ultra-violett |
| V | Volt |
| V (amino acid) | valine |
| VP | viral partical |
| WAVE2 | WASP-family verprolin-homologous protein 2 |
| wt | wild type |
| X-Gal | 5-brom-4-chlor-3-indoxyl-β-D-galactopyranosid |
| Y2H | yeast two-hybrid |
| β-Gal | β-galactosidase |
| µm | micro meter |

# 1 Introduction

## 1.1 The postsynaptic density – The interface of information transmission in the central nervous system

Neurons are the core component of the central nervous system (CNS); they form a complex network by connecting to each other and transmitting information via electrical or chemical signals. A neuron comprises of a soma, an axon and highly branched dendrites containing hundreds to thousands of spines. An electrical signal is induced at the axon hillock and propagates to the axon terminal where the signal is then conveyed to the next neuron by the release of neurotransmitters at so called chemical synapses (Kandel *et al.*, 2000). Excitatory synapses in the CNS are glutamatergic containing ionotropic glutamate receptors such as N-methyl-D-aspartate (NMDA) and α-amino-3-hydroxy-5-methyl-4-isoxazole proprionate (AMPA) receptors as well as metabotropic glutamate receptors (mGluR). At the tip of a dendritic spine these synapses have a characteristic postsynaptic electron-dense membrane thickening, the postsynaptic density (PSD) (Kennedy, 2000; Feng & Zhang, 2009).

The PSD includes up to a thousand different proteins with wide-ranging functions such as membrane receptors, ion channels, adhesion molecules, scaffolding proteins, various signalling molecules, membrane-trafficking proteins, cytoskeleton proteins and proteins involved in protein synthesis (Scannevin & Huganir, 2000; Laumonnier *et al.*, 2007). These diverse proteins enable the PSD to combine and coordinate many processes in space and time that underlie synaptic plasticity and memory formation (Kennedy, 2000; Murakoshi & Yasuda; 2012). A simplified schematic illustration of the PSD is shown in Figure 1 and the main features of the architectural build-up will be described in the following text.

Roughly, the PSD can be divided into three different levels of organisation. The first level contains transmembrane proteins such as glutamate receptors and adhesion molecules. The next layer comprises different scaffold proteins, which on the one side stabilise the glutamate receptors at the PSD and on the other side couple the receptors to the third level. Here, further scaffolding and adaptor proteins build a bridge to the cytoskeleton as well as to various effector

proteins including signalling proteins and cytoskeletal regulators (Kim & Sheng, 2004; Laumonnier et al., 2007; Feng & Zhang, 2009).

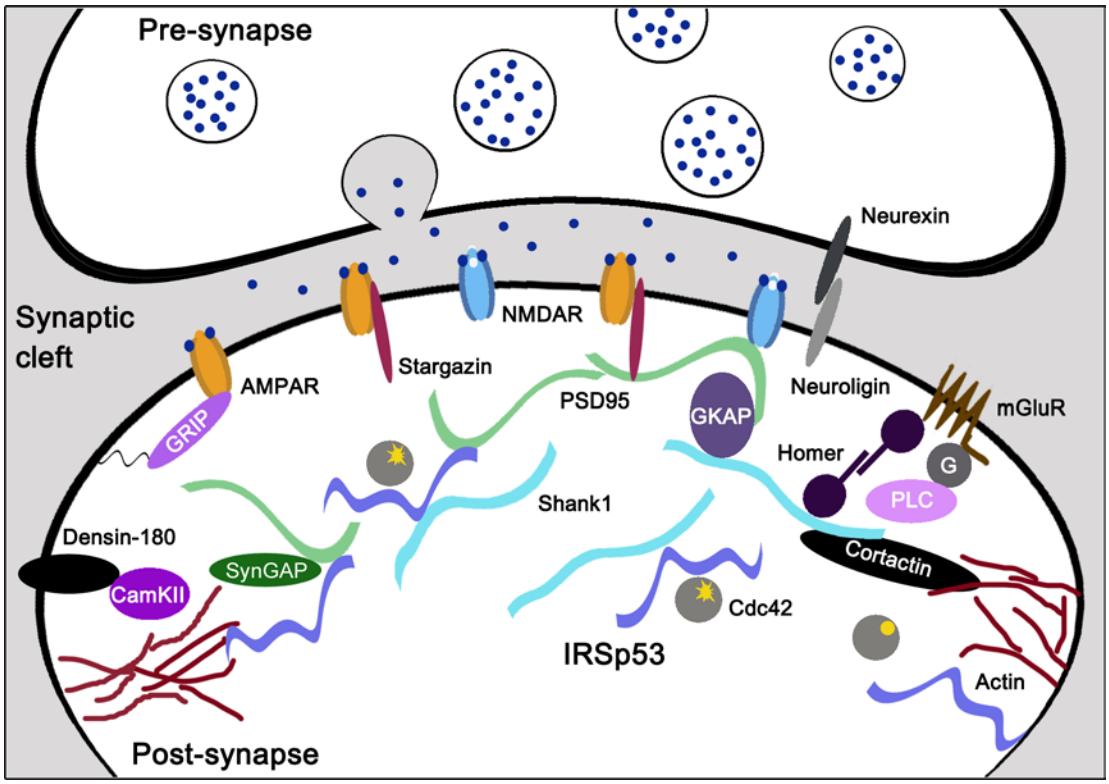


**Figure 1 Illustration of a glutamatergic synapse focusing on the PSD.** The PSD is composed of thousands of proteins that are organised in distinct structural and functional complexes including membrane receptors, ion channels, adhesion molecules, scaffolding proteins, various signalling molecules and cytoskeleton proteins. Membrane bound glutamate receptors (AMPA and NMDA receptors, mGluR) are connected through the scaffold proteins Shank and PSD95 to effector molecules such as IRSp53 and SynGAP which are components of downstream signalling pathways. The axon terminal with its presynapse is fixed to the postsynapse via the cell-adhesion molecules neurexin and neuroligin. AMPAR = α-amino-3-hydroxy-5-methyl-4-isoxazole proprionate receptor, CamKII = calcium/calmodulin-dependent kinase II, Cdc42 = cell devision control protein 42, G = G-protein, GKAP = guanylate kinase-associated protein, GRIP = glutamate receptor interacting protein, IRSp53 = insulin receptor substrate protein of 53 kDa, mGluR = metabotropic glutamate receptors, NMDAR = N-methyl-D-aspartate receptor, PSD95 = postsynaptic density 95, PLC = phosphoinositid-phospholipase C; SynGAP = synaptic Ras-GTPase activating protein.

Considering the huge amount of different proteins and their organisation specific molecular tools are needed to keep this complex together. One “master” module is the PSD95 - Discs-large - Zona occludens 1 (PDZ) domain that enables the formation of macro-molecular complexes by protein-protein interactions (Ranganathan & Ross, 1997; Scannevin & Huganir, 2000; Feng & Zhang, 2009; Kim & Sheng, 2004; Lee & Zheng, 2010). PDZ domains typically interact with the C-termini of target proteins and rarely recognise internal sequences of interaction partners (Lee & Zheng, 2010). A second standard interaction motif is the Src homology 3 (SH3) domain binding preferentially to prolin-rich sequences. With a low affinity and modest specificity to their targets (Mayer, 2001), SH3 domain-containing proteins may promote synaptic plasticity through rapid assembly/disassembly of different interaction partners. Several scaffolding proteins of the

PSD contain multiple PDZ domains and often SH3 domains allowing manifold interactions with various protein classes such as membrane-receptors and signalling proteins, thus connecting receptor activation to effector-pathways (Kennedy, 2000; Scannevin & Huganir, 2000; Laumonnier *et al.*, 2007; Gardoni, 2008; Kreienkamp, 2008). Two abundant scaffolding protein families in the PSD are the membrane associated guanylate kinase (MAGUK) protein family and the SH3 and ankyrin repeat domains (Shank) protein family (Gardoni, 2008; Kreienkamp, 2008; Feng & Zhang, 2009; Zheng *et al.*, 2011).

The MAGUK protein family consists of the post-synaptic density 95 (PSD95), synapse associated protein 97 (SAP97), chapsyn-110/PSD93 and SAP102, which are differentially expressed and distributed throughout the brain (Scannevin & Huganir, 2000; Kim & Sheng, 2004; Gardoni, 2008; Zheng *et al.*, 2011). All MAGUK proteins consist of 3 PDZ domains followed by a SH3 and a guanylate kinase (GK) domain (Kim & Sheng, 2004; Feng & Zhang, 2009). PSD95 is the most frequent scaffolding protein found in the PSD (Cheng *et al.*, 2006) located in the second organisation level. By interacting with the NMDA receptor subunit 2 (GluN2) PSD95 anchors NMDA receptors at the PSD and furthermore links the receptor directly to effectors and the cytoskeleton. A further PSD95 interaction partner is stargazin which binds to AMPA receptors (Lee & Zheng, 2010; Zheng *et al.*, 2011). Moreover, PSD95 provides a stage for the synaptic Ras-GTPase activating protein (SynGAP), another abundant protein of the PSD. Following NMDA receptor opening and calcium/calmodulin-dependent kinase II (CamKII) activation through $Ca^{2+}$ entry, SynGAP gets phosphorylated. This leads to the inhibition of Ras and results in the suppression of the Ras-dependent activation of the p42/44 MAP kinase (ERK1/2) cascade (Kennedy, 2000; Scannevin & Huganir, 2000; Kim & Sheng, 2004; Zheng *et al.*, 2011). PSD95 also interacts with the adenylate-kinase anchoring protein (AKAP), a platform for protein kinase A (PKA) signalling (Scannevin & Huganir, 2000; Kim & Sheng, 2004; Zheng *et al.*, 2011). Via the adaptor protein guanylate kinase-associated protein (GKAP/SAPAP) PSD95 is connected to the members of the Shank protein family, which belongs to the third organisation level. A further protein interacting with PSD95 and Shank proteins is the insulin receptor substrate protein of 53 kDa (IRSp53) (Bockmann *et al.*, 2001; Soltau *et al.*, 2002; Soltau *et al.*, 2004; Choi *et al.*, 2005; Kreienkamp, 2008; Zheng *et al.*, 2011).

The Shank protein family consists of three members, named Shank1 – 3, that are strongly expressed in the central nervous system (CNS) and almost entirely accumulated at the PSD. These multidomain scaffold proteins contain besides a PDZ and an SH3 domain, a Shank/ProSAP N-terminus (SPN) region, an ankyrin repeat region (ARR) and a C-terminal sterile alpha motif (SAM) (Mameza *et al.*, 2013). The SAM domain preferably interacts with other SAM domains and therefore Shank proteins have a strong ability to self-associate to form large multimeric platforms. Shank proteins further bind to the scaffold protein Homer, which interacts

with the G-protein coupled mGluR1/5. Consequently, Homer represents a bridge to link mGluRs and NMDA receptors via the Shank-GKAP-PSD95 network. In addition, Homer binds to the inositol triphosphate (IP3) receptors, which are located at the smooth entoplasmatic reticulum (ER) allowing the influx of $Ca^{2+}$ from internal stores (Kennedy, 2000; Kreienkamp, 2008). Further binding partners are the actin-binding protein cortactin and α-fodrin (Du *et al.*, 1998; Boeckers *et al.*, 2001; Kreienkamp, 2008).

In the last decades several postsynaptic proteins were functionally analysed by gene targeting in mice, allowing the investigation of functional and behavioural consequences in a physiological context. The genetic deletion of PSD95, Shank2 and Shank3 in mice depicts diverse phenotypic manifestations. PSD95 null-mice demonstrate an impaired spatial learning in the hidden-platform Morris water maze (Migaud *et al.*, 1998). A Shank2 mutant mouse strain generated by a deletion of exon 6 and 7 displays impaired spatial learning in the Morris water maze, too (Won *et al.*, 2012). In contrast, deletion of exon 7 of Shank2 in mice demonstrates no learning impairment. Otherwise, these mice demonstrate hyperactivity and impaired social communication (Schmeisser *et al.*, 2012). Deletion of the major Shank 3 isoform termed $Shank3^{e4-9}$ leads to impaired cognition in the Morris water maze and novel object recognition, which is accompanied by an alteration in the PSD composition. As already observed for Shank2 deletions, $Shank3^{e4-9}$ deficient mice display impaired social communication and repetitive behaviour, which are major symptoms of autism spectrum disorders (ASD) (Wang *et al.*, 2011). Thus, the deletion of single postsynaptic protein in mice results in behavioural abnormalities and learning deficits comparable to symptoms of distinct neurological diseases.

## 1.2 Long-term potentiation – A cellular model to improve synapses

In 1953 a surgical destruction of the hippocampus of the patient H.M. resulted in a dramatic impairment in the formation of new memories (Squire, 2009). About 10 years later, Tere Lømo described for the first time a persistent synaptic enhancement in the rabbit hippocampus, which was later termed LTP (Lømo, 2003). These exceptional discoveries placed the hippocampus in the focus of attention in the formation of memory and marked LTP as a possible cellular mechanism underlying information storage in the human/mammalian brain.

LTP is characterised by a persistent change of synaptic efficacy, which is stable from hours to months (Abraham & Williams, 2003; Andersen, 2003). In recent decades, the knowledge of the molecular and cellular basis of LTP has considerably increased. An intricate network of concurrent processes depending on a large number of proteins with wide-ranging functions has been

disclosed. Three phases of LTP can be distinguished considering duration and accompanying molecular and cellular changes. An increase in the synaptic efficacy for a few hours is called early LTP and depends on post-translational modifications of pre-existing postsynaptic proteins. The late LTP is the longest form of synaptic enhancement lasting for weeks and months. This form requires *de novo* protein synthesis and the transport of the newly synthesised proteins to recently activated synapses (Sweatt, 1999; Abraham & Williams, 2003; Kelleher *et al.*, 2004; Raymond, 2007). Some researchers also describe an intermediate phase of LTP that requires the translation of mRNAs but not nuclear gene transcription (Kelleher *et al.*, 2004; Raymond, 2007).

To induce long-lasting synaptic changes, the simultaneous repetitive activation of several synapses is crucial (Sweatt, 1999; Abraham & Williams, 2003; Kelleher *et al.*, 2004; Raymond 2007). The molecular sensor capable of translating this input signal into the induction and maintenance of LTP is the NMDA receptor. This particular ion channel is a coincidence detector that needs the binding of the neurotransmitter glutamate and an initial depolarisation of the membrane to remove the $Mg^{2+}$ block, which seals the NMDA receptor ion pore. The initial membrane depolarisation is induced by an ion flow through AMPA receptors impermeable for $Ca^{2+}$ (Dingledine *et al.*, 1999; Lisman *et al*., 2002; Lynch, 2004). Following repeated stimulation, the NMDA receptor opens and allows the influx of $Ca^{2+}$. This is detected by diverse calcium sensors, which trigger post-translational modifications and the activation of multiple signalling pathways (Bliss & Collingridge, 1993; Raymond, 2003).

One important kinase activated after $Ca^{2+}$-influx is CamKII, which is the most abundant kinase accumulated at synapses (Lisman *et al.*, 2002; Cheng *et al.*, 2006; Murakoshi & Yasuda, 2012; Lynch, 2004). CamKII is directly anchored to NMDA receptors (Lisman *et al*. 2002), PSD95 or densin-180 (Lynch, 2004). Further signalling molecules that are activated after $Ca^{2+}$ elevation are CamKIV and the adenylate cyclase (AC) responsible for the activation of PKA via an increase in cyclic adenosine monophosphate (cAMP) (Lynch, 2004). In the early phase of LTP AMPA receptors are post-translationally modified by phosphorylation through CamKII and PKA, leading to an increase in their conductance (Bliss & Collingridge, 1993; Lisman *et al.*, 2002; Lynch, 2004; Murakoshi & Yasuda, 2012). Moreover, within the first minutes following high frequency stimulation GluA1-containing AMPA receptors are inserted into the PSD in a CamKII and PKA dependent manner (Abraham & Williams, 2003; Lisman *et al.*, 2002; Lynch, 2004; Murakoshi & Yasuda, 2012). Besides the opening of ionotropic glutamate receptors after presynaptic glutamate release, mGluRs are activated leading to the induction of the small GTPase Ras, the protein kinase C (PKC) and the phosphoinositide 3-kinase (PI3K) (Bliss & Collingridge, 1993; Murakoshi & Yasuda, 2012). Activation of the mGluR-signalling pathway results the production of inositide-triphosphate ($IP_3$), which binds to $IP_3$ receptors to initiate the opening of intracellular $Ca^{2+}$ stores.

Thus, a further increase of the postsynaptic $Ca^{2+}$ concentration is achieved (Bliss & Collingridge, 1993; Raymond, 2007), which is assumed to propagate to the nucleus and/or initiate the activation of further signalling molecules outside the postsynaptic compartment (Bading, 2000).

Downstream targets of CamKII, PKA, PKC and Ras are the MAP kinases ERK1/2 (Ahn *et al.*, 2000; Abraham & Williams, 2003; Lynch, 2004). On the one hand phosphorylated ERK1/2 regulates transcription-dependent protein synthesis. On the other hand it increases the translational capacity of the cell via signalling to the S6 kinase and phosphorylation of translation initiation factors (Lynch, 2004). The facilitation of translation allows the fast delivery of proteins to recently activated synapses in the intermediate phase of LTP independent on nuclear transcription (Kelleher *et al.*, 2004). Nevertheless, activation of the ERK1/2 pathway is not sufficient to trigger the initiation of protein translation and needs to be accompanied by activation of the mammalian target of Rapamycin (mTOR) pathway triggered via PI3K and proteinkinase B (Akt) signalling (Lynch, 2004; Kelleher *et al.*, 2004; Raymond, 2007). Synergic activation of both pathways allows efficient dendritic translation (Kelleher *et al.*, 2004) e.g. of the activity-regulated cytoskeleton-associated protein (Arc), CamKII and Shank proteins (Steward & Worley, 2001; Lynch, 2004).

To stabilise and maintain LTP *de novo* gene transcription is obligatory. The ERK1/2 pathway is involved in the initiation of the serum response element (SRE)-dependent transcription (Raymond, 2007) and induces the cAMP response element (CRE) dependent transcription via activation of the cAMP response element-binding protein (CREB). Interestingly, the ERK1/2 pathway influences the histone modification of chromatin and thereby facilitates *de novo* gene transcription (Ahn *et al.*, 2000; Levenson *et al.*, 2004; Chwang *et al.*, 2006). The key initiation factor for activity-dependent gene transcription is CREB, which may be directly activated by PKA, CamKII and CamKIV (Ahn *et al.*, 2000; Abraham & Williams, 2003; Johannessen *et al.*, 2004). CREB is activated by phosphorylation which seems to occur in a biphasic manner meaning a primary fast initiation e.g. by CamKIV and a later induction by the ERK1/2 pathway (Ahn *et al.*, 2000; Johannessen *et al.*, 2004; Lynch, 2004). Proteins that are newly synthesised following LTP induction are for example GluA1, GluN2A/B, mGluR1/5 and the brain-derived neutrophic factor (BDNF) as well as its tyrosin-kinase receptor TrkB (Abraham & Williams, 2003; Kelleher *et al.*, 2004). Astonishingly, BDNF itself induces synaptic potentiation, which is dependent on translation (Lynch, 2004). A simplified model of kinase-dependent signalling cascades activated following LTP is illustrated in Figure 2.

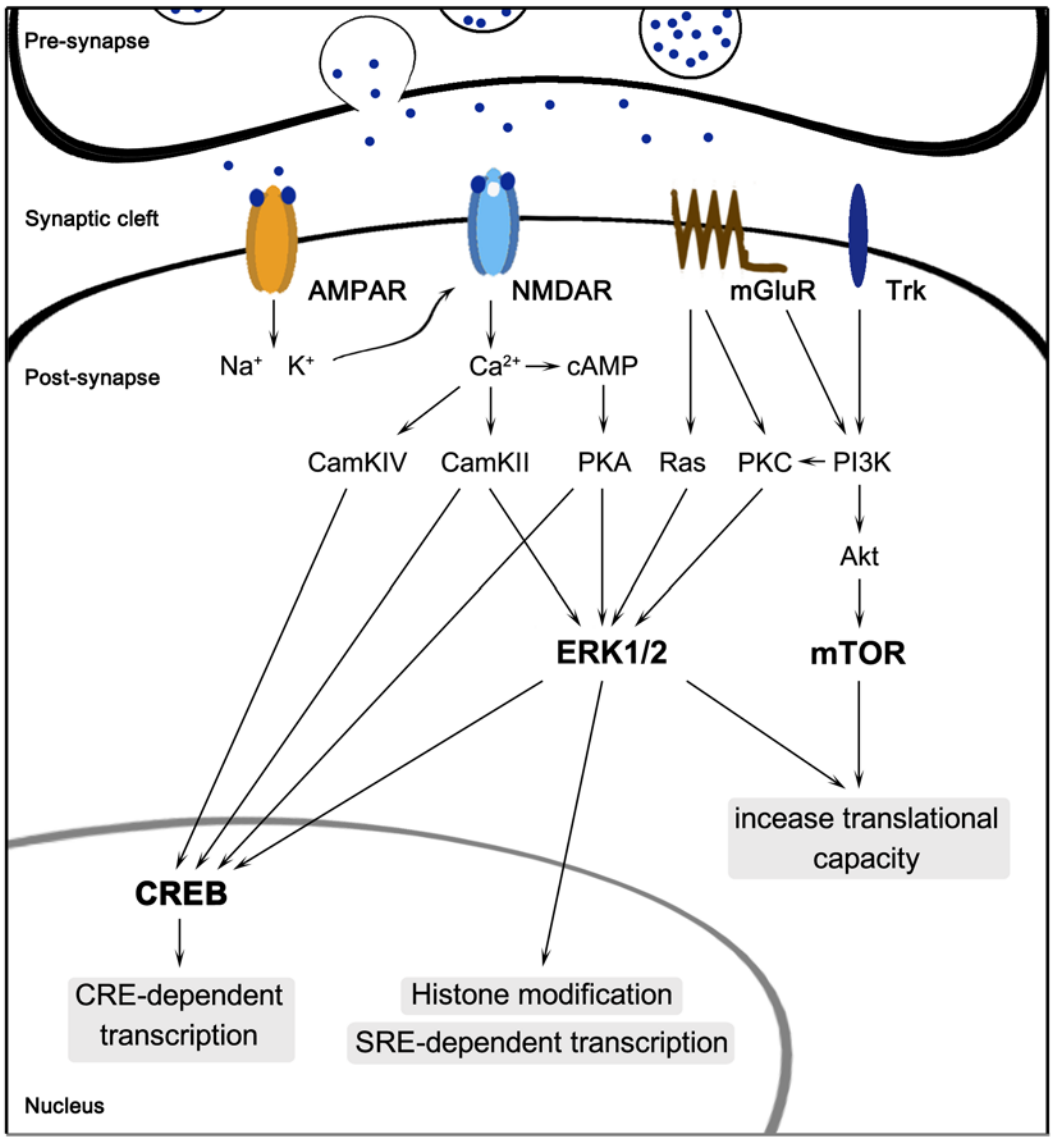


**Figure 2 NMDA receptor dependent signalling following LTP induction.** Following presynaptic glutamate release the AMPA receptors are activated and depolarise the postsynaptic membrane. This results in the opening of NMDA receptors allowing the influx of $Ca^{2+}$. The postsynaptic increase in $Ca^{2+}$ triggers the activation of several kinases like CamKII, CamKIV and PKA leading either to the activation of the ERK1/2/MAP kinase pathway or directly to the phosphorylation of CREB. Besides the opening of ionotropic glutamate receptors the G-protein coupled mGluRs are activated, which further trigger signal transmission via the small GTPase Ras as well as the kinases PKC and PI3K to ERK1/2 and mTOR signalling cascades. Additionally, Trk receptor induction also initiates the ERK1/2 and mTOR signalling pathways both required for boosting the translational capacity of the cell. LTP-dependent transcription is primarily initiated by CREB and is supported by ERK1/2 dependent remodelling of the chromatin structure by histone modification. This cooperative signal integration allows the induction and maintenance of long-lasting synaptic changes underlying learning and memory. Akt = protein kinase B; cAMP = cyclic adenosine monophosphate; CRE = cAMP response element; CREB = cAMP response element-binding protein; ERK1/2 = p42/44 MAP kinase; PI3K = phosphoinositide 3 kinase; PKA/C = protein kinase A/C; mTOR = mammalian target of Rapamycin; SRE = serum-response element; Trk = tyrosine-kinase receptor.

## 1.3 Proteins of the PSD are often affected in neurological diseases

Mutations in genes coding for postsynaptic proteins are often observed in mental/psychiatric diseases. Mental disorders based on synaptic dysfunction are called synaptopathies and include ASD, mental retardation (MR), schizophrenia (SCZ), Alzheimer diseases (AD) and epilepsy/seizures (Garber, 2007; Gardoni, 2008; Grabrucker *et al.*, 2011).

The Shank ko mouse lines introduced above demonstrate behavioural patterns consistent with symptoms observed in patients suffering from ASD. ASD is a complex genetic disorder featuring impaired social interaction, delayed speech development, a limited assortment of interests and repetitive behaviours with a varying degree of severity (Garber 2007; Geschwind, 2008; Kelleher III & Bear, 2008; Marshall *et al.*, 2008; Walsh *et al.*, 2008; Gilman *et al.*, 2011). *De novo* structural variations of chromosomes and rare sequence mutations seem to be common risk factors in the manifestation of ASD (Marshall *et al.*, 2008; Levy *et al.*, 2011; Schaaf & Zoghbi, 2011). In 5 to 7% of autism cases mutations in single genes can be identified. These genes are often coding for proteins which play a determining part in synapse formation and function such as neuroligin3 and 4, neurexin1 and Shank3 (Garber 2007; Geschwind, 2008; Kelleher III & Bear, 2008; Marshall *et al.*, 2008; Walsh *et al.*, 2008; Gilman *et al.*, 2011; Schaaf & Zoghbi, 2011). Interestingly, many of these proteins are connected in a trans-synaptic network. MR, epilepsy or hyperactivity can accompany autistic behaviour. For example, patients affected by *Shank3* deletions, translocation or missense mutations suffer from MR, ASD as well as epilepsy (Grabrucker *et al.*, 2011). Concerning the low number of cases caused by single genes the appearance of multiple mutations is likely. Gilman *et al.* (2011) used a network-based analysis of genetic associations (NETBAG) to identify molecular networks affected in ASD by using rare *de novo* CNV data from Levy *et al.* (2011). This analysis identified processes ranging from synapse formation and maturation over maintenance of synaptic function to downstream signalling pathways controlling protein biosynthesis, cytoskeleton rearrangements and neuronal survival.

One of the proteins found in this NETBAG analysis is the BAI-associated protein 2 (BAIAP2), the human homolog of the protein IRSp53. This protein was also suggested as susceptibility factor for autism in two other studies. Celestino-Soper *et al.* (2011) used an array comparative genomic hybridisation (CGH) screen to ascertain exonic CNVs in autism families and detected besides common known genetic factors causing ASD, also a rare *de novo* deletion of the *BAIAP2* gene in a male patient. A study by Toma *et al.* (2011) gives further evidence for the participation of *BAIAP2* in the manifestation of autism. Interestingly, another study analysing a German cohort implicates a contribution of *BAIAP2* in adulthood attention deficit hyperactivity disorder (ADHS) (Ribases *et al.*, 2009). Recently, post mortem analysis of the PSD composition

of AD patients unveiled a reduced expression of IRSp53 (Zhou *et al.*, 2013). The evidence from these studies suggests that IRSp53 plays an important role for proper synaptic function.

## 1.4 IRSp53 - A powerful regulator of the actin cytoskeleton

In 1996, Yeh and co-workers identified IRSp53 as a tyrosine receptor kinase substrate in Chinese hamster ovary (CHO) cells following insulin and insulin-like growth factor 1 (IGF-I) stimulation. A few years later the human homolog was termed BAIAP2 as it was identified in a yeast two-hybrid (Y2H) screen using brain-specific angiogenesis inhibitor 1 (BAI1) as 'bait' (Oda *et al.*, 1999). In humans four IRSp53 isoforms (L, M, S and T form) were found due to alternative splicing (Miyahara *et al.*, 2003). Interestingly, comparisons of the human and mouse complementary desoxyribonucleic acid (cDNA) sequence of the full-length IRSp53 demonstrates a 87% match and a 97% identical amino acid (aa) sequence pointing to a high conservation among mammals (Alvarez *et al.*, 2002).

Northern blot analysis and *in situ* hybridisations demonstrate IRSp53 messenger ribonucleic acid (mRNA) expression predominantly in the brain (Abbott *et al.*, 1999; Oda *et al.*, 1999; Thomas *et al.*, 2001). Highest mRNA levels were detected in the forebrain structures cerebral cortex (layer II/III, V and VI), striatum, hippocampus and olfactory bulb as well as in the cerebellum (Bockmann *et al.*, 2001; Thomas *et al.*, 2001), later verified by Kim *et al.* (2009) and Sawallisch *et al.* (2009).

IRSp53 is a multidomain protein consisting of four functional motifs: the IRSp53/missing-in-metastasis domain (IMD), a partial Cdc42 and Rac interacting binding (CRIB) domain, a SH3 domain and a PDZ ligand (PDZL). Through its multiple domains IRSp53 is able to interact with a variety of proteins (Figure 3) (Scita *et al.*, 2007). The IRSp53 IM domain preferentially binds phosphatidylinositol (4,5) bisphosphate ($PI(4,5)P_2$) rich membranes (Mattila *et al.*, 2007; Futo *et al.*, 2013) but is thought to interact also with filamentous actin (F-actin) (Millard *et al.*, 2005; Mattila *et al.*, 2007; Vaggi *et al.*, 2011) and GTP bound Rac (Miki & Takenawa, 2000). The CRIB domain of IRSp53 is shorter than the known CRIB domains and only interacts with GTP bound Cdc42 but not with Rac (Govind *et al.*, 2001; Soltau *et al.*, 2002). Interaction with actin regulatory proteins like Eps8 (Disanza *et al.*, 2006), WAVE2 (Miki & Takenawa, 2002), N-WASP (Lim *et al.*, 2008), mDia (Fujiwara *et al.*, 2000), Mena (Krugmann *et al.*, 2001), synaptopodin (Yanagida-Asanuma *et al.*, 2007), SPIN90 (Teodorof *et al.*, 2009), espin (Sekerkova *et al.*, 2003) and Cypin (Barilari & Dente, 2010) takes place at the SH3 domain of IRSp53. Beside actin regulators the IRSp53 SH3 domain associates with the PSD key scaffold proteins Shank1 (Soltau *et al.*, 2002)

and Shank3 (Bockmann *et al.*, 2001). Interaction partners of the IRSp53 PDZL are PSD95 (Choi *et al.*, 2005; Kreienkamp, 2008; Zheng *et al.*, 2011), MALS/Lin-7 (Hori *et al.*, 2003) and CIPP (Barilari & Dente, 2010). Thus, IRSp53 function as a platform connecting the small GTPases Rac and Cdc42 to various actin regulators and/or other scaffolding proteins. In addition, the N-terminal IRSp53 IM domain belongs to the inverse Bin-amphiphysin-Rvs (I-BAR) domains contributing to the deformation of membranes. Therefore, IRSp53 also links the plasma-membrane (PM) to actin dynamics (Millard *et al.*, 2005; Cory & Cullen, 2007; Mattila *et al.*, 2007; Scita *et al.*, 2007; Saarikangas *et al.*, 2009; Zhao *et al.*, 2011).

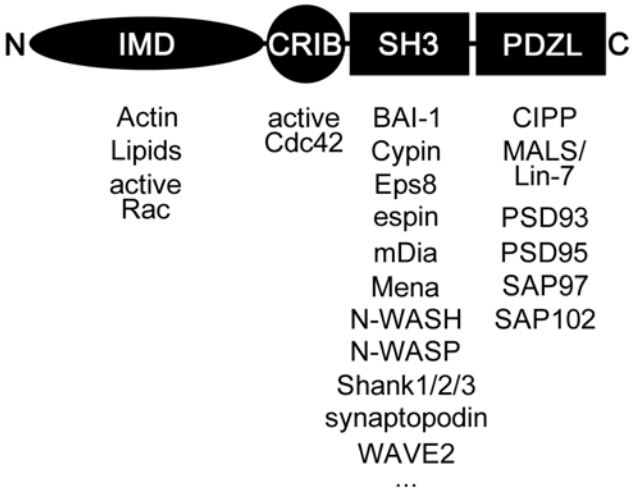


**Figure 3 Domain structure and known interaction partners of IRSp53.** IRSp53 consists of four functional motifs: the IM domain, CRIB domain, SH3 domain and a PDZ ligand. Through these multiple domains IRSp53 constitutes a scaffold for the interaction with various proteins like PSD scaffolding proteins and actin-regulatory proteins. BAI-1 = brain-specific angiogenesis inhibitor 1, Cdc42 = cell division cycle 42, CIPP = channel-interacting PDZ domain protein, Cypin = cytosolic PSD95 interactor, N-WASH = Wiskott-Alddrich syndrom protein homolog N, N-WASP = Wiskott-Alddrich syndrom protein N, WAVE2 = WASP-family verprolin-homologous protein 2.

The interplay of actin polymerisation, depolymerisation and retrograde flow ("actin treadmilling") is important to establish membrane protrusions such as lamellipodia and filopodia, known to be regulated by the small GTPases Rac and Cdc42 (Luo, 2002). IRSp53 is able to bind both GTPases and couples them to effector proteins. Taken together with its membrane-deformation activity this makes IRSp53 a suitable candidate to promote cell motility and morphogenesis.

An immense number of studies in non-neuronal culture systems support the role of IRSp53 in the regulation of cellular morphology. In summary, IRSp53 seems to function as an effector protein promoting the remodelling of the actin cytoskeleton. (1) Through the IM domain IRSp53 is able to deform membranes by itself (Suetsugu *et al.*, 2006; Mattila *et al.*, 2007, Saarikangas *et al.*, 2009). (2) It links the small GTPases Rac and Cdc42 to various actin-regulators, which enables the formation of membrane protrusion (Miki *et al.*, 2000; Govind *et al.*, 2001; Miki & Takenawa, 2002; Disanza *et al.*, 2006; Lim *et al.*, 2008; Misra *et al.*, 2010; Rajagopal *et al.*, 2010; Morimura *et al.*, 2011; Vaggi *et al.*, 2011). (3) The function of IRSp53 can be regulated through the interaction partner 14-3-3 (Robens *et al.*, 2010; Cohen *et al.*, 2011) and/or the activation of several growth factor receptors (Morimura *et al.*, 2011; Lewis-Saravalli *et al.*, 2013; Oh *et al.*, 2013).

What is the cellular function of IRSp53 in neuronal cells? Only a few studies elucidate this question. Immunofluorescence staining depicts the majority of IRSp53 at synapses. Analysis of the IRSp53 accumulation in the PSD outlines similar enrichment levels as observed for the NMDA receptor subunit GluN1 and the signalling molecule CamKII (Abbott *et al.*, 1999). The deletion of the PDZ ligand as well as the mutation of the SH3 domain of IRSp53 disrupts its PSD localisation in primary neuronal culture (Choi *et al.*, 2005). Recently, Ferrari *et al.* (2012) found that the silencing of Lin-7 obstructed the recruitment of IRSp53 into Triton-X-100 insoluble complexes. An overexpression of IRSp53 markedly increases the spine density, whereas small interfering RNA (siRNA) based knock down leads to shrinkage. Interestingly, Hori et al. (2009) demonstrates that stimulation of primary cultured neurons through glutamate or NMDA induces an IRSp53 translocation to synapses dependent on NMDA receptor activation.

## 1.5 The loss of IRSp53 leads to severe cognitive deficits and altered LTP

In 2009 IRSp53 knock out (ko) lines were generated and characterised by Kim *et al.* (2009) as well as Sawallisch *et al.* (2009). Considering that IRSp53 is a powerful regulator of the actin-cytoskeleton shown in *in vitro* experiments in non-neuronal cells and primary neuronal cultures, an altered neuronal morphology was predicted upon loss of IRSp53. However, in *in vivo* experiments no morphological changes in hippocampal neurons were detected in ko animals compared to wt ones. Furthermore, no obvious differences were found in spine density (Kim *et al.*, 2009; Sawallisch *et al.*, 2009) but analysis of the PSD ultrastructure demonstrated a slight decrease in the size of the PSD (Sawallisch *et al.*, 2009). Interestingly, during embryonic development IRSp53 is expressed only in peripheral tissues, whereas expression in the CNS is switched on postnatally. Expression analysis demonstrates a weak expression in postnatal day (P) 1 hippocampal brain tissue, which increases gradually until P21. The Shank expression profile in juvenile neurons seems to partially correlate with the IRSp53 expression (Sawallisch *et al.*, 2009). Thus, the SH3 domain of IRSp53 is probably covered by Shank proteins, which may interfere with the interaction with actin-regulatory interaction partners. Indeed, the alteration of the neuronal morphology in primary neuronal cultures upon overexpression of IRSp53 was blocked by co-expression with Shank1 (Soltau *et al.*, 2002; Sawallisch *et al.*, 2009).

Measuring the neuronal activity induced by different input signals via electrophysiological protocols showed normal basal synaptic transmission in IRSp53 deficient mice. However, a prominent increase in LTP at the Schaffer collateral-CA1 pyramidal (SC-CA1) synapse of the hippocampus was detected (Kim *et al.*, 2009; Sawallisch *et al.*, 2009). Whole cell recording

showed that specifically the NMDA receptor transmission is enhanced in IRSp53 ko mice (Kim *et al.*, 2009). This corresponds to biochemical analysis of the PSD protein composition, where in particular the amount of the NMDA receptor subunits GluN1, GluN2A and GluN2B was increased (Sawallisch *et al.*, 2009). Measurements by Kim *et al.* (2009) to analyse LTD did not show alterations in IRSp53 deficient mice. A presynaptic form of synaptic plasticity is the so-called paired-pulse facilitation (PPF) describing the probability of a presynaptic terminal to release neurotransmitters following an action potential. Kim *et al.* (2009) observed no changes in PPF in the field CA1 of the hippocampus. In contrast, Sawallisch *et al.* (2009) detected an enhancement of PPF in the dentate gyrus (DG) and CA1 field of the hippocampus.

The enhanced hippocampal LTP at the SC-CA1 synapses implies that the learning and memory of IRSp53 ko mice could be affected. In fact, IRSp53 deficient mice demonstrate severe impairments in hippocampal-based learning paradigms such as the contextual fear conditioning paradigm (Sawallisch *et al.*, 2009), the hidden-platform Morris water maze and the novel object recognition test (Kim *et al.*, 2009). Otherwise, in simple tests observing the motor coordination, motor activity, exploratory and anxiety related behaviour no differences between ko animals and wt littermates were recorded (Sawallisch *et al.*, 2009).

## 1.6 Objective of the study

The multidomain protein IRSp53 is a small synaptic protein that somehow impacts LTP and cognitive functions in simple learning tasks in the mouse model. Therefore, the central question is: How might IRSp53 affect the synaptic function in the CNS?

Experiences from studies in neuronal culture systems suggest that a critical amount of IRSp53 is required for the protein to fulfil its function. A suitable approach to test a reduction of IRSp53 in a physiological context was to analyse IRSp53 heterozygous (+/d) mice. First, the learning behaviour of IRSp53 +/d mice will be tested in simple learning task regarding a possible haploinsufficiency. Furthermore, I will investigate the composition of the PSD in the different forebrain regions cortex, hippocampus and striatum focusing on postsynaptic proteins that are essential for cognition. Taking into account that the synaptic dysfunction in IRSp53 ko mice correlates with an increased accumulation of NMDA receptors at the postsynapse, the NMDA receptor surface expression will be analysed. In addition, different signalling cascades activated following synaptic stimulation will be examined in acute hippocampal slices.

A persistent theme of the research on IRSp53 is: How is IRSp53 targeted to the synapse? Therefore, the influence of the four functional motifs of IRSp53 for the synaptic targeting will be determined. To gain insight into the mobility and translocation of wt IRSp53 fluorescent labelled IRSp53 will be expressed in hippocampal neurons and monitored in live-cell imaging experiments.

# 2 Material and Methods

Chemicals, consumables and technical equipment that were used in this thesis are listed in the appendix.

## 2.1 Standard molecular methods

Applied standard molecular biological methods were applied according to: “Molecular Cloning: a Laboratory Manual” (3rd Edition; Sambrook J, Russell DW; Cold Spring Harbor Laboratory Press, 2001). The enzymes used and the appropriate buffers as well as the commercial kits are specified in Table 1.

| Name | Source |
|---|---|
| Enzymes | |
| Phusion DNA Polymerase HF | Finnzyme, Espoo; Finland |
| Restriction enzymes | Thermo Scientific, Bonn, Germany |
| | NEB, Frankfurt am Main, Germany |
| T4 DNA Ligase | Roche Applied Science, Penzberg, Germany |
| Commercial buffers and kits | |
| Restriction enzyme buffers (10x) | Thermo Scientific, Bonn, Germany |
| | NEB, Frankfurt am Main, Germany |
| dNTPs | Quiagen, Hilden; Germany |
| Phusion HF Reaction buffer (5x) | Finnzyme, Espoo, Finland |
| NucleoBond® Xtra Midi Plasmid Kit | Macherey-Nagel, Düren, Germany |
| NucleoBond® PC buffers S1 to S3 | Macherey-Nagel, Düren, Germany |
| GeneJet PCR Purification Kit | Thermo Scientific, Bonn, Germany |
| GeneJet Gel Extraction Kit | Thermo Scientific, Bonn, Germany |
| BigDye Terminator Cycle Sequencing Kit | Applied Biosystems, Dresden, Germany |

Table 1 Enzymes, commercial buffers and kits.

***Transformation of competent E. coli***

Transformation defines the genetic alteration of bacteria by the transfer of naked plasmid DNA. One main method of transformation is chemical transformation, which combines a chemical treatment of bacteria to passively permeabilise the membrane with a heat-shock, which promotes the DNA uptake.

Plasmid DNA (1 µg) or ligation product (10 µl) was added to 100 µl of pre-thawed competent cells (1x $10^6$ cells) of the *E. coli* strain TOP10 (Invitrogen, Karlsruhe; Germany) and mixed by gently tapping the reaction tube. Afterwards, cells were incubated on ice for 20 min, followed by a heat-shock at 42°C for 45 sec. Cells were placed on ice for 2 additional min and then 200 µl of pre-warmed lysogeny broth (LB) medium (10 g/l Trypton, 5 g/l Yeast Extract, 5 g/l NaCl; pH 7.5) were added. Incubation was continued at 37°C for 30 to 60 min in a shaker at 350 revolutions per minute (rpm). Finally, the bacteria suspension was plated on selective LB-agar plates (15 g/l Agar, LB medium; pH 7.5 containing 50 µg/ml ampicillin or 100 µg/ml kanamycin) and incubated at 37°C overnight. Single colonies were picked for preparation of suspension cultures for plasmid DNA preparation.

***Plasmid DNA preparation***

Plasmid DNA was purified using the alkaline lysis procedure followed by desalting and concentration of the plasmid DNA by isopropanol precipitation.

Small-scale plasmid preparation was carried out by inoculating single colonies in 4 ml of selective LB medium containing the appropriate antibiotic which was incubated overnight at 37°C on a shaker. DNA Mini-preparation was then done by the use of NucleoBond® PC buffers S1 to S3 without using an anion exchange column. The bacteria were pelleted at 3000x g and resuspended in 100 µl buffer S1 of the NucleoBond® PC kit. Afterwards, 100 µl of buffer S2 were added and the tube was inverted several times. Next, 100 µl of buffer S3 were added and the tube was inverted numerous times. The precipitated genomic DNA and proteins were then separated from the plasmid DNA solution by centrifugation at 21,000x g for 30 min. Plasmid DNA was then precipitated, desalted and concentrated by isopropanol precipitation. Therefore, 2/3 units of volumes of pure isopropanol were added and the tube inverted several times. Thereafter, the flocculated DNA were pelleted at 5000x g and the DNA pellet was washed 3 times with 70% EtOH. Finally, the air-dried DNA pellet was dissolved in 50 µl of sterile water.

For Large-scale plasmid preparation, bacteria were cultured in a large volume (200 ml) and incubated at 37°C and 230 rpm in a shaker overnight. DNA preparation was then performed by using the NucleoBond® Xtra Midi Plasmid Kit following the manufacturers protocol. DNA was finally eluted in 500 µl of sterile water.

### *Restriction digestion of DNA*

Restriction enzymes are naturally occurring prokaryotic endonucleases that recognise specific sequences of 4 to 8 nucleotides and subsequently cleave double-stranded DNA (dsDNA) segments within or near this recognition site. These recognition sites are usually palindromic sequences and create either blunt or adhesive ends with 5'- or 3'-overhangs. Three types of restriction endonucleases exist. Type I and type III restriction endonucleases cut several nucleotides away from the recognition site, whereas endonucleases of type II cut within the recognition sites and were used for cloning.

A typical analytical restriction reaction consisted of 0.5 to 1 µg of DNA and 1U of restriction enzyme in the appropriate restriction buffer (according to manufactures instructions) within a total volume of 20 µl. For preparative digestions 5 µg DNA and 5 U of restriction enzyme and restriction buffer in 30 µl were used. All restriction reactions were incubated for 1 to 2 h at optimal temperatures for each enzyme (mainly 37°C). If required, enzymes were heat-inactivated after the digestion-step at 65°C for 10 min. Digestions were verified by agarose gel electrophoresis.

### *Agarose gel electrophoresis of DNA*

DNA fragments of different size can be separated by agarose gel electrophoresis. Here negatively charged DNA molecules migrates through an agarose matrix within an electric field. The relative migration rate of linear nuclear acids in an agarose matrix is reciprocally proportional to the logarithm of their molecular mass whereby longer molecules migrate slower than shorter ones.

Agarose gels of 1% in 1x TAE buffer (20 mM Tris, 10 mM Sodium acetate, 0.5 mM EDTA; pH 7.8) containing 0.5 µg/ml ethidium bromide (EtBr) were used to separate DNA fragments by electrophoresis at 150 V. The DNA samples were mixed with DNA sample buffer containing 3% Glycerin, 0.025% Bromphenol blue, 0.025% Xylene blue and 2.5 mM EDTA. 1 kilobases (kb) DNA size standard (Thermo Scientific, Bonn; Germany) allows an estimation of the size of the separated DNA fragments, which were visualised by EtBr that intercalates into DNA and fluoresces under UV-light.

### *Purification and concentration of DNA*

GeneJet PCR Purification Kit or GeneJet Gel Extraction Kit, which are based on an anion exchange column, were used following the manufacturers protocols to purify DNA fragments from enzymatic reactions or preparative agarose gels for cloning procedures. DNA was finally eluted in 20 to 40 µl of sterile water.

### *Ligation of DNA molecules*

The ligation is defined as the linking of two or more linear dsDNA fragments with compatible adhesive or blunt ends by creating a phosphodiester bond through a DNA ligase (5' phosphate end + 3' hydroxyl end) under ATP consumption.

A 20 µl reaction was prepared containing the vector and insert fragment in a molar ratio of approximately 1:1, 1U of the bacteriophage T4 DNA ligase per 1 pmol DNA, and ligation buffer containing 1 mM ATP. Ligation reactions were incubated at 16°C overnight.

### *Quantification of DNA concentration*

A rough estimation of DNA concentration was done in agarose gel separated fragment by comparing the intensity of EtBr-stained DNA fragments with a standard DNA size marker of defined DNA concentration.

Precise quantification of DNA was achieved by spectrophotometric quantification of absorption of ultraviolet light through DNA at an absorption peak of 260 nm ($OD_{260}$ measurement). Assuming that an optical density (OD) of 1 at 260 nm equals 50 µ g of dsDNA/ml, the dsDNA concentration can be calculated as follows:

dsDNA concentration [µg/µl] = $OD_{260}$ * 0.05 µg/µl * dilution factor.

Furthermore, the purity of the sample was analysed by OD measurement at 280 nm, which measures protein contamination. If the ratio of 260 nm/280 nm is lower than 1.8 the sample is contaminated with proteins. A ratio of 1.8 up to 2.0 indicates pure DNA.

### *Primer and Oligo design*

Specific primers with a maximal GC content of 60% for amplification of a particular gene or sequencing were designed under consideration of the following criteria: (1) More than 19 nucleotides had to align to the coding sequence of the particular gene. (2) For cloning procedures restriction enzyme recognition sites were added at the 5' end under consideration of the open reading frames. Furthermore, extra bases were attached to the 5' end depending on the restriction endonuclease as an anchoring point. The primers used are listed in Table 2.

| Name | Sequence (5' → 3') |
|---|---|
| Available primers in the lab | |
| EGFP1 fwd | GTC CGC CCT GAG CAA AGA CC |
| mRFP for | AAAGCTAGCATGGCCTCCTCCGAGGAC |
| CMV for | GCTAGCGATTACGCC |
| Re-Mut 708 for. | GGTGGAAAAGCAGTGCGCTGTGGCCAA |
| Re-Mut 708 rev. | TTGGCCACAGCGCACTGCTTTTCCACC |
| 4KzuE for. | CAAGTGTCAGGCTGAGCTGGAGGAGCTCCGCGAGGA GAGCCAAGGGAGTAAGAAC |
| 4KzuE rev. | GTTCTTACTCCCTTGGCTCTCCTCGCGGAGCTCCTCCA GCTCAGCCTGACACTTG |
| I268N for. | CAAGTCCAACCTGGTCAACTCAGATCCCATTCCTG |
| I286N rev. | CAGGAATGGGATCTGAGTTGACCAGGTTGGACTTG |
| I403P for. | CTTCAAGGAGGGCGACCTCCCCACGCTGCTAGTGCCTGAG |
| I403P rev. | CTCAGGCACTAGCAGCGTGGGGAGGTCGCCCTCCTTGAAG |
| FP/AA for. | CCAAGATGCGGGGCGCGTTCGCCTTCTCCTACACC |
| FP/AA rev. | GGTGTAGGAGAAGGCGAACGCGCCCCGCATCTTGG |
| V522G rev. | AAA GAA TTC TCA CCC TGT GGA CAC CAG CG |
| Designed primers | |
| Kaede-s | CGAGCTAGCATGGTGAGTGTGATT |
| Kaede-as | CATAGATCTGCCCTTGGCCTGACTC |
| SAP97_as | CAGGAGGAGGATTTGCCTGT |
| SAP97_1_s | CAGAGATTGAGAATGTCCACG |
| SAP97_2_s | GTAACCAAAATAATTGAAGGAGG |
| SAP97_3_s | GTCAGAGCCCTTTTTGATTACG |
| SAP97_4_s | CTATGAGGTGGATGGACGAG |
| SAP102_as | CTCCTGGGATGTGCTGGTTAC |
| SAP102_1_s | GAGCAGCTGCCATGGATGG |
| SAP102_2_s | CAGACACATGCTGGCTGAGG |
| SAP102_3_s | GGACAAGAGGATGCTATTTTGTC |

Table 2 Primers.

Oligos longer than 30 nucleotides (nt's) for the direct use in cloning (Table 3) were designed with respect to the open reading frames (ORF) of the succeeding coding sequences. A modified coding sequence of the *Thosea asigna* virus *2A-peptide* (Tang *et al.*, 2009) was inserted in-frame between the coding sequence of enhanced green fluorescent protein (EGFP) and IRSp53 using the restriction sites of the prokaryotic endonucleases BsrGI and BglII.

| Name | Sequence (5' → 3') |
|---|---|
| BsrGI-2A-BglII s | GTACAAGTCCGGACTCACTCGAGGATATCGGTCAAGGCCTCT |
| | CGAAGGCAGAGGAAGTCTTCTAACATGCGGTGACGTGGAGGA |
| | GAATCCCGGCCCTGCAG |
| BsrGI-2A-BglII as | GATCCTGCAGGGCCGGGATTCTCCTCCACGTCACCGCAT |
| | GTTAGAAGACTTCCTCTGCCTTCGAGAGGCCTTGACCGATA |
| | TCCTCGAGTGAGTCCGGACTT |

Table 3 Oligo nucleotides.

***Linker-annealing for oligos longer than 30 nucleotides***

Linker-annealing of oligos longer than 30 nt's (for sequence, see Table 3) was done by a slow decline of the temperature from 95°C to room temperature (RT) in a water bath to achieve an annealing of two compatible single stranded DNA fragments. Thence, an equimolar concentration of the appropriate single-stranded DNA (ssDNA) oligos (1 nmol of each) was added to the annealing buffer consisting of 0.5 M Tris HCl (pH 7.5) and 0.33 M $MgCl_2$.

***Polymerase chain reaction (PCR)***

The plasmid vector pKaede-PIST served as DNA template to amplify the coding sequence of the fluorescent protein Kaede in a thermocycler by using the "hot start" DNA polymerase Phusion with the two flanking primers pKaede-s and pKaede-as (for sequence of primers, see tabel 2). The reaction mix consisted of 2 ng of template DNA, 0.2 µM of each primer, 1 U of Phusion DNA polymerase in 1x Phusion buffer and 200 µM dNTPs (total volume of 50 µl). The PCR reaction followed the Finnzymes advertence and was adjusted as follows:

| | | | |
|---|---|---|---|
| Initial denaturation | 98 °C | 30 sec | |
| Denaturation | 98 °C | 10 sec | 40 cycles |
| Annealing | 58 °C | 30 sec | |
| Elongation | 72 °C | 20 sec | |
| Final Elongation | 72 °C | 5 min | |
| Storage | 4 °C | ∞ | |

***DNA sequencing***

DNA sequences of generated constructs were confirmed by ABI DNA sequencing according to Sanger's method of dideoxy-mediated chain termination with several specific primers (table 2). The sequencing reaction followed the instructions of BigDye Terminator Cycle Sequencing Kit. PCR reaction contained 1 µg of template DNA, 0.5 µM primer, 2 µl 5x sequencing buffer, 1 µl of

terminator-ready Big-Dye reaction mix and distilled water in a final volume of 10 µl. The PCR program was set up as follows:

| | | | |
|---|---|---|---|
| Initial denaturation | 94°C | 5 min | |
| Denaturation | 94°C | 30 sec | 30 cycles |
| Annealing | 55°C | 15 sec | |
| Elongation | 60°C | 4 min | |
| Storage | 4°C | ∞ | |

PCR products were precipitated by adding 25 µl of 100% ethanol (EtOH) and 3 M sodium acetate (NaAc) in a 22:1 ratio and pelleted by centrifuging at RT for 40 min at full speed in a tabletop centrifuge. The supernatant was discarded and the DNA pellet was washed once with 70% EtOH and air-dried for sequencing by the ABI 16-capillar sequencer (ABI PRISM 3500 Genetic analyser; Applied Biosystems, Darmstadt, Germany).

## 2.2 Standard cell biological and protein biochemical methods

Expression studies and testing of protein-protein interactions in non-neuronal cells were done using the Adenovirus 5 (Ad 5) transduced human embryonic kidney cells (HEK 293) (Graham & Smiley, 1977). The cells were cultured in DMEM (DMEM, 10% FCS, 1x penicillin/streptomycin, 2 mM L-Glutamin) and incubated at 37°C and 5% $CO_2$. The expression plasmids used for transfections are listed in Table 4.

| Name | Source/Origin |
|---|---|
| pCMV-Flag-C1 | Sigma-Aldrich, Taufkirchen, Germany |
| pCMV-Flag-IMD | cloned construct |
| pCMV-SAP90myc | Stefan Kindler, Hamburg, Germany |
| pCMV-SAP97myc | Stefan Kindler, Hamburg, Germany |
| pCMV-SAP102myc | Stefan Kindler, Hamburg, Germany |
| pcDNA3.1-ProSAP2 | Tobias Böckers, Ulm, Germany |
| pEGFP-C1 | Clontech, Mountain View, USA |
| pEGFP-mIRSp53 wt | AG Kreienkamp |
| pEGFP-mIRSp53 4KtoE | AG Kreienkamp |
| pEGFP-mIRSp53 I268N | AG Kreienkamp |

| | |
|---|---|
| pEGFP-mIRSp53 I403P | AG Kreienkamp |
| pEGFP-mIRSp53 V522G | AG Kreienkamp |
| pEGFP-2A-mIRSp53 wt | cloned construct |
| pEGFP-2A-mIRSp53 4KtoE | cloned construct |
| pEGFP-2A-mIRSp53 I268N | cloned construct |
| pEGFP-2A-mIRSp53 I403P | cloned construct |
| pEGFP-2A-mIRSp53 V522G | cloned construct |
| pEGFP-IMD | cloned construct |
| pEGFP-truncatedIMD | cloned construct |
| pKaede-PIST | AG Kreienkamp |
| pKaede-mIRSp53wt | cloned construct |
| pRFP-ProSAP2 | AG Kreienkamp |

Table 4 List of expression plasmids.

***Transfection of HEK293 cells***

Transfection of HEK 293 cells was carried out by the Calcium phosphate method, which is suitable for an efficient transfer of DNA into most mammalian cell lines (Graham & van der Eb, 1973). HEK 293 cells were plated at a density of 4x $10^6$ cells on 78.5 cm² culture dishes and transfected after 24 h at a confluency of 50 – 60%. The transfection mix consisted of 20 µg of DNA in total with the appropriate plasmid DNAs, 1 x BBS and 0.25 M $CaCl_2$ and autoclaved bidistilled $H_2O$ ($H_2O$ bidest.) in a total volume of 1ml. First, DNA and pre-warmed calcium chloride ($CaCl_2$) was filled up to 500 µl of pre-warmed $H_2O$ bidest. and mixed by vortexing followed by adding 500 µl of 2x pre-warmed BBS (50 mM BES, 280 mM NaCL, 1.5 mM $Na_2HPO_4$; pH 6.95). The transfection cocktail was mixed a second time by vortexing, incubated for 20 min at RT and added on the cells without changing the medium. The medium was exchanged after a maximal incubation time of 24 h at 37°C and 5% $CO_2$ (Thomas & Smart, 2005).

***Protein extraction***

In order to analyse protein expression levels, protein-protein interactions and protein localisation, various protein preparations were done and evaluated in immunoblots. Whole cell lysates were prepared from HK293 cells, whereas protein fractionation was performed using a HEK293 cell line stably expressing the somatostatin receptor type 5 (SSTR5) (C. Bauch, AG Kreienkamp, Germany).

Proteins extracts were prepared about 24 h after transfection of HEK293 cell. HEK cells were scraped from the culture dishes within the medium and transferred to a 15 ml Falcon tube followed by a centrifugation at 800x g for 3 min at RT. The supernatant was discarded.

Whole cell lysates were prepared by using radio immunoprecipitation assay (RIPA) buffer (50 mM Tris-HCl pH 7.4, 150 mM NaCl, 1% NP-40, 0.5% Sodium deoxycholat, 0.1% SDS, protease inhibitor tablets Mini Complete). Pelleted HEK293 cells were resuspended in RIPA lysis buffer and incubated for 15 min on ice followed by a centrifugation step at 10,000x g for 5 min at 4°C. The cell lysate were transferred into a new tube and stored at -80°C or sample buffer was added for storage at -20°C.

For protein fractionation, the pelleted HEK293 cell were pottered in 1 ml HEPES lysis buffer (25 mM HEPES pH 7.4, 150 mM NaCl, protease inhibitor tablets Mini Complete) followed by a centrifugation at 800x g for 5 min to remove cell debris and nuclei. The post-nuclear lysate was transferred to a new tube and membrane proteins were separated from the cytosolic proteins by centrifugation at 23,000x g for 30 min at 4°C. The membrane protein pellet was then resuspended in HEPES lysis buffer. The different protein fractions were stored at -80°C or sample buffer was added for storage at -20°C.

### *Immunoprecipitation by GFP-Trap*

Immunoprecipitation experiments allow to determine whether two proteins are in the same protein complex. The GFP-Trap (ChromoTek, Martinsried, Germany) consists of αGFP antibodies coupled to sepharose beads, which selectively enables the precipitation of GFP or GFP fusion proteins.

HEK293 cells were transfected by Calcium-phosphate transfection with the appropriate plasmid DNAs and cultured for at least 24h. Afterwards whole cell lysates were prepared using the RIPA buffer and an input sample was taken. The remaining protein lysate was added to the GFP-Trap (10 µl, washed twice with RIPA buffer) and incubated for at least 2h on a rotator at 4°C. Sepharose beads were pelleted by centrifugation at 1000x g at 4°C and the supernatant was then exchanged through fresh ice-cold RIPA buffer. This procedure was repeated 5 times and the pellet was finally, dissolved in 50 µl 1x Sample buffer.

### *Determination of the protein concentration*

Protein concentrations were determined using the *DC* Protein assay kit (BioRad, Munich, Germany). Here, $Cu^{2+}$ is reduced proportionally to the total protein concentration present in the solution to $Cu^{1+}$ that chelates with biocinchonic acid forming a purple-coloured product, absorbing light at a wavelength of 405 to 750 nm. The colorimetric change measured at 562 nm in a spectrophotometer correlates with total protein concentration. For each cell lysate, duplicates were measured following the BioRad manufacturers protocol. A bovine serum albumin (BSA) standard curve with defined protein concentrations was used to calibrate measurements.

***Western blot***

In a western blot experiment, denatured proteins are separated according to their size by sodium dodecyl sulfate polyacrylamid gel electrophoresis (SDS-Page) followed by a protein transfer on to a nitrocellulose membrane within an electrical field. Specific proteins can then be detected via immunological detection. Buffers and solutions sequentially needed are specified in Table 5:

| Name | Composition |
|---|---|
| PBS | 137 mM NaCl, 2.7 mM KCl, 1.4 mM $KH_2PO_4$, 4.3 mM $Na_2HPO_4$; pH 7.4 |
| PBS-T | PBS, 0.1 Tween20 |
| Running buffer (1x) | 25 mM Trizma base, 192 mM Glycine, 0.1% SDS |
| Sample buffer (5x) | 10% SDS, 50% Glycerine, 312.5 mM Trizma base, 0.5% Bromphenol blue, 10% 2-mercaptoethanol |
| Separating gel (e.g. 10%) | 4.1 ml $H_2O$, 3.3 ml Acrylamid/Bis, 2.5 ml 1.5 M Trizma base pH 8.8, 0.1 ml 10% SDS, 100 µ l APS, 10 µ l TEMED |
| Stacking gel (4%) | 6.1 ml $H_2O$, 1.3 ml Acrylamid/Bis, 2.5 ml 1 M Trizma base pH 6.8, 0.1 ml 10% SDS, 100 µ l APS, 10 µ l TEMED |
| TBS | 10 mM Trizma base pH 8.0, 150 mM NaCl |
| TBS-T | TBS, 0.1% Tween20 |
| Transfer buffer | 25 mM Trizma base, 192 mM Glycine, 20% Methanol, 0.05% SDS |

Table 5 Buffers and solutions for western blot.

SDS-page with 4% stacking gel layered on a 8% to 12% separating gel was prepared by using the BioRad Mini-Protean III System following the BioRad manual and placed in an electrophoresis chamber containing 1x SDS running buffer. Sample were mixed with SDS loading buffer and heated for 3 min at 96°C. The samples and a PageRule$^{TM}$ Prestained Protein Ladder (Thermo Scientific, Bonn; Germany) to estimation the protein size were loaded and the electrophoresis was carried out at 150 V and 400 mA until the bromphenol-blue-front reached the bottom of the separation gel.

Transfer on a nitrocellulose membrane was performed using the Mini Trans blot system. Therefore, a sandwich was assembled consisting of a sponge, two sheets of Whatman paper, the gel, nitrocellulose membrane, another two sheets of Whatman paper, and a second sponge (all components moistened in 1x Transfer buffer). This complex was then placed in a blotting

chamber filled with1x Transfer buffer and electro-transfer was done at 150 V and 400 mA for 2 h in an ice bath or at 30 V and 90 mA overnight at RT.

For immunological staining, the membrane was incubated with blocking solution for 30 min to prevent unspecific binding of the antibodies to the membrane. Blocking solution was then exchanged with the primary antibody solution (Table 6) and incubated overnight at 4°C. Subsequently, the membrane was washed 3 times with washing buffer for about 5 min each. Secondary antibody (α ms-HRP/rat-HRP/rb-HRP; Dianova, Hamburg, Germany) were added in a 1:3000 dilution in the appropriate washing buffer and were incubated for 45 min, followed by additional 3 wash steps of 5 min each. Finally, the membrane was moistened with ECL Plus western blot detection reagent (Thermo Scientific, Bonn, Germany) for 5 min. Chemiluminescence was recorded in a ChemiDoc™ XRS system (BioRad, Munich, Germany) and/or OPTIMAX X-Ray film processor (Protec, Oberstenfeld-Gronau, Germany).

| Primary antibody | Host | Dilution | Solution | Source |
|---|---|---|---|---|
| Tag's | | | | |
| α Flag | rb | 1:1000 | 5% Milk-TBST | Serum, AG Kreienkamp, Hamburg, Germany |
| α GFP | ms | 1:2000 | 5% Milk-TBST | Serum, AG Kreienkamp, Hamburg, Germany |
| | rat | 1:1000 | 5% Milk-TBST | Covance, Littleton, USA |
| α GST | rb | 1:4000 | 5% Milk-TBST | Serum, AG Kreienkamp, Hamburg, Germany |
| α 2A-peptide | rb | 1:500 | 5% Milk-TBST | Merck Millipore, Darmstadt, Germany |
| House keeping proteins | | | | |
| α β-Actin | ms | 1:1000 | 5% Milk-TBST | Abcam, Cambridge, UK |
| α GAPDH | ms | 1:1000 | 5% Milk-TBST | Merck Millipore, Darmstadt, Germany |
| Postsynaptic density proteins | | | | |
| α AMPAR1 | rb | 1:1000 | 5% Milk-TBST | Abcam, Cambridge, UK |
| α IRSp53 | rb | 1:5000 | 5% Milk-TBST | Serum, AG Kreienkamp, Hamburg, Germany |
| α NMDAR 2A | rb | 1:1000 | 1% BSA-TBST | NovusBiologicals, Littleton, USA |
| α NMDAR 2B | rb | 1:1000 | 1% BSA-TBST | NovusBiologicals, Littleton, USA |

| | | | | |
|---|---|---|---|---|
| α NMDAR 1 | ms | 1:1000 | 5% Milk-PBST | Merck Millipore, Darmstadt, Germany |
| | rb | 1:1000 | 5% Milk-PBST | Abcam, Cambridge, UK |
| α PSD95, cloneK28/43 (pan-MAGUK) | ms | 1:2000 | 5% Milk-TBST | Merck Millipore, Darmstadt, Germany |
| α PSD95, clone K28/86 | ms | 1:3000 | 5% Milk-TBST | Merck Millipore, Darmstadt, Germany |
| α SAP102 | ms | 1:500 | 5% Milk-PBST | Abcam, Cambridge, UK |
| α Shank(PDZ) Tag 90 (pan-Shank) | rb | 1:3000 | 5% Milk-TBST | Serum, AG Kreienkamp, Hamburg, Germany |
| α SynGAP | rb | 1:1000 | 5% Milk-TBST | Abcam, Cambridge, UK |
| Signalling pathways | | | | |
| α Akt1 | rb | 1:1000 | 1% BSA-TBST | Cell Signaling, Frankfurt am Main, Germany |
| α Phospho-Akt1 (Ser473) | rb | 1:1000 | 1% BSA-TBST | Cell Signaling, Frankfurt am Main, Germany |
| α CamKII | rb | 1:1000 | 5% Milk-PBST | Abcam, Cambridge, UK |
| α Phospho-CamKII (Thr286) | ms | 1:1000 | 5% Milk-PBST | Abcam, Cambridge, UK |
| α CREB | rb | 1:1000 | 1% BSA-TBST | Abcam, Cambridge, UK |
| α Phospho-CREB (Ser133) | rb | 1:1000 | 1% BSA-TBST | Cell Signaling, Frankfurt am Main, Germany |
| α p44/42 (ERK1/2) | rb | 1:1000 | 5% BSA-TBST | Cell Signaling, Frankfurt am Main, Germany |
| α Phospho-p44/42 (Thr202/Tyr204) | rb | 1:1000 | 5% BSA-TBST | Cell Signaling, Frankfurt am Main, Germany |

Table 6 Primary antibodies for western blot.

***Cdc42-Overlay assay***

The interaction of IRSp53 with the small G-protein Cdc42 was tested using a Cdc42-overlay assay with GDP- and GTP-loaded Cdc42.

Cell lysates of GFP-IRSp53 expressing HEK293 cells were blotted and the membranes were blocked with 5% milk-TBST overnight at 4°C. Recombinant purified Cdc42 tagged with glutathione-S-transferase (GST) was diluted into nucleotide binding buffer (200 mM Trizma base pH 7.5, 100 mM NaCl, 7.5 mM $MgCl_2$, 1 mM DTT, 0.1% Triton-X-100) in a concentration of 0.1 mg/ml in a total volume of 200 µl. The sample was then divided into two equal batches, of which one was

loaded with non-hydrolysable 2 mM GTPγS, and incubated for 1 h at RT. Cdc42 samples were then diluted in 1% milk-TBST to a concentration of 1 µg/ml. The blocking solution was exchanged by the Cdc42 containing solutions and incubated for 1 h at RT. Bound Cdc42 was then detected using an αGST antibody through chemiluminescence detection as described above.

## 2.3 Recombinant adeno-associated viral gene delivery system

The recombinant adeno-associated virus (rAAV) system used in this thesis was obtained from CellBiolabs (Heidelberg, Germany). Both, the AAV-1 and AAV-2 Helper Free Expression System, were used to produce rAAVs of mixed serotypes 1 and 2 that enable high infection efficiency via serotype 1 as well as a simple and efficient purification by serotype 2 (Zolotukhin *et al.*, 1999).

### *Production and harvesting of rAAVs*

HEK293T cells (18 plates, diameter of 10 cm) were seeded at a confluence of 60 to 70%. DNA from the helper plasmid, packaging vectors and the shuttle vector (Table 7) were co-transfected in an equal amount not exceeding 20 µg of total DNA/plate using calcium-phosphate transfection.

| Vector type | Name | Origin |
|---|---|---|
| Helper vector | pHelper vector | CellBiolabs, Heidelberg, Germany |
| Packaging vector | pAAV-RC1 | CellBiolabs, Heidelberg, Germany |
| | PAAV-RC2 | CellBiolabs, Heidelberg, Germany |
| Shuttle vector | pAAV-GFP | CellBiolabs, Heidelberg, Germany |
| | pAAV-GFP-2A-mIRSp53 wt | cloned construct |
| | pAAV-GFP-2A-mIRSp53 4KtoE | cloned construct |
| | pAAV-GFP-2A-mIRSp53 I268N | cloned construct |
| | pAAV-GFP-2A-mIRSp53 I403P | cloned construct |
| | pAAV-GFP-2A-mIRSp53 V522G | cloned construct |

Table 7 Viral vectors.

After 16 to 24h the culture medium was exchanged and cells were further incubated for 24 to 48 h. Cells were harvested with sterile 1x PBS, transferred into three 50 ml Falcons and centrifuged at 1000x g for 3 min. The supernatants were removed and each pellet was resuspended in 45 ml 20 mM Tris, 150 mM NaCl (pH 8.0). To degrade unpacked viral DNA, plasmid and chro-

mosomal DNA, 6.6 µl Benzonase (250 – 350 U/ml) were added. Then, NaDOC (pH 8.0) were added to a final concentration of 0.5% for cell lysis. The suspension was shaken 1 h at 37°C and centrifuged at 3000x g for 15 min. The virus containing supernatants were transferred into new 50 ml falcons and flash frozen in liquid nitrogen ($N_2$).

***Purification of rAAVs via Heparin column***

The supernatants containing the viral particles were thawed at 25°C, centrifuged at 3000 x g for 15 min and filtered through 0.4 µm Acrodisc Syringe Filters (Merck Millipore, Schwalbach, Germany). A HiTrap Heparin HP 1ml column (GE Healthcare, Munich, Germany) was equilibrated with 10 ml 150 mM NaCl/ 20 mM Tris (pH 8.0) using the perfusor pump Graseby 3400 (Smith Medical, Grasbrunn, Germany) at a flow rate of 1 ml/min. Afterwards, the supernatants were loaded onto the column, followed by 3 wash steps using 20 ml 100 mM NaCl/ 20 mM Tris (pH 8.0), 1 ml 200 mM NaCl/ 20 mM Tris (pH 8.0) and 1 ml 300 mM NaCl/ 20 mM Tris (pH 8.0). The virus was eluted at high salt concentrations with 1.5 ml 400 mM NaCl/ 20 mM Tris (pH 8.0), 3 ml 450 mM NaCl/ 20 mM Tris (pH 8.0) and 1.5 ml 500 mM NaCl/ 20 mM Tris (pH 8.0). Finally, rAAVs were desalted and concentrated by using the 100K Amicon Ultra concentrator (Merck Millipore, Schwalbach, Germany) with 1x PBS to a final volume of 400 to 500 µl. The virus was transferred into new Eppendorf-tubes, flash frozen with liquid $N_2$ and stored at -80 °C.

The purification of the virus was analysed by coomassie staining. Hence, samples of the different purification steps were loaded on an SDS-Page and proteins were detected by Roti-Blue coomassie staining (Roth, Karlsruhe, Germany).

***Virus titre determination by Fluorescence activated cell sorting (FACS)***

The infectious titres of the different virus preparations were determined by Fluorescence activated cell sorting (FACS) according to Kutner *et al.* (2009). Therefore, 5x $10^4$ HEK293 cells per well were plated in 24 well plates and infected with the virus using 3 different dilutions. Four days after infection, the cells were trypsinised and pelleted by centrifugation at 1000x g for 3 min. The pellets were washed two times with 1x PBS and resuspended in a final volume of 500 µl.

GFP positive HEK293 cells were measured with the FACS CantoII (BD Biosciences, Heidelberg, Germany) and evaluated using the BD FACSDiva™ software. Infectious viral titre (TU/ml) was then calculated as follows:

TU/ml = (Plated cells*% GFP positive cells*dilution*1000)/ µl used for infection.

## 2.4 Preparation of neuronal cultures, brain regions and acute slices

### *Animals*

Animals were kept in the breeding facility of the University hospital Hamburg-Eppendorf according to the guidelines of the German law on animal welfare. The mice strains used were the wt strain C57Bl/6J and the B6.129.P2-*Baiap2*$^{Gt(XG757)Byg}$/Hhtg ko strain.

### *Genotyping of IRSp53 deficient mice*

Genotyping of the B6.129.P2-*Baiap2*$^{Gt(XG757)Byg}$/Hhtg ko mice were done by the use of the DirectPCR® Lysis Reagent Tail (peqlab, Erlangen, Germany). Tails of 0.2 to 0.5 cm length were digested in 50 µl DirectPCR Lysis Reagent containing 0.4 mg/ml Proteinase K (Sigma-Aldrich, Taufkirchen, Germany) in a thermomixer at 55°C and 800 rpm overnight. Proteinase K was then inactivated by incubation of the lysates at 85°C for 45 min.

The resulting DNA solution was analysed by PCR amplification of the wt allele and/or the mutant allele using the Taq DNA polymerase (Qiagen, Hilden, Germany). Three different primer sets (Table 8) were selected to determine if mice were heterozygous or homozygous for the mutant allele. The reaction mix consisted of 1.5 µl of the DNA solution, 0.2 µM of each primer, 50 µM $MgCl_2$, 1 U of Taq DNA polymerase in 1 x PCR buffer and 200 µM dNTPs in a total volume of 20 µl. PCR conditions were as follows:

| | | | |
|---|---|---|---|
| Initial denaturation | 94°C | 5 min | |
| Denaturation | 94°C | 30 sec | 35 cycles |
| Annealing | 56°C | 30 sec | |
| Elongation | 72°C | 1 min | |
| Storage | 4°C | ∞ | |

| Primer set | Name | Sequence (5' → 3') |
|---|---|---|
| 1 | IRSp53-Exon3-s | CAGGGCTCTAAGGAACTTGG |
| | IRSp53-WT-as | GAGACAGCCCACTAGGGTGAG |
| | IRSp53-KO-as | GCCAAGGCCATACAAGTGTTG |
| 2 | IRSwt-s | GCTCTAAGGAACTTGGTAAGAC |
| | IRSwt-as | CATAGGCCCTTTATATCTGCC |
| 3 | IRSko-s | CCAACTATGTAGGAGGAAGG |
| | IRSko-as | CTATACGAACGGTAGGATCC |

Table 8 Primer sets for Genotyping.

The PCR products were analysed by agarose gel electrophoresis using the 100 basepairs (bp) ladder (Thermo Scientific, Bonn, Germany) as molecular size marker.

### *Preparation and cultivation of primary hippocampal and cortical neurons of E16.5*

The preparation followed the protocol “Rat Hippocampal Neurons in Low-Density culture” described by Banker & Goslin (2002) with some changes.

*Preparation of the glass or plastic surface:*

Sterile culture plates with or without cover slips were coated with 1mg/ml Poly-L-Lysine (PLL) hydrobromide (Sigma-Aldrich, Darmstadt, Germany) overnight and washed 3 times with sterile water. Furthermore, the surfaces were coated a second time with 1 µg/ml Laminin (Roche, Mannheim, Germany) for at least 2h followed by 3 wash steps with sterile 1x PBS. The plates were filled with culture medium (High glucose DMEM, 1x FCS, 220 µM L-glutamine, 1x penicillin/streptomycin)

*Dissection of the hippocampus or cortex of E16.5 embryos:*

Timed pregnant mice were killed through a cervical dislocation after anesthesia by $CO_2$. The abdomen was disinfected with 70% ethanol and the skin was cut. In a second step the abdominal wall was cut through, and the uterus with the embryos was excised and placed in a bacteriological 10 cm plate containing ice cold 1x PBS. The embryos were removed from the uterus and the allantois. The embryos were decapitated and the heads transferred into fresh ice cold 1x PBS. Heads were kept in position with forceps to cut the skin and the skull in a caudal to rostral direction along the midline. Most of the skin and skull covering the cortex was removed and the brain was taken out by moving a second forceps caudally, beginning carefully at the olfactory bulbs, separating the brain from cranial nerves. To separate the cerebral hemispheres, brainstem was grasped and hemispheres cut apart with a scalpel. The meninges were peeled away, and the hemispheres placed with their inner/medial side up to cut out the hippocampus, leaving behind primarily the cortex. The hippocampi or cortices were transferred to sterile 1x PBS and kept on ice until all brains were dissected.

*Trypsinisation and plating:*

The volume of 1x PBS in which the hippocampi or cortices were collected was brought up to 5 ml. Then 500 µl of 2.5% trypsin (Gibco Invitrogen, Darmstadt, Germany) were added for a number of 5 dissected embryos. After incubation at 37°C for 15 min (hippocampi) or 30 min (cortex) the trypsin solution was carefully removed and exchanged through pre-warmed HBSS (10 mM HEPES in 1x HBSS, pH 7.4) three times. Cells were dissociated with a regular Pasteur pipette, then with a fire-polished Pasteur pipette in a final volume of 2 ml HBSS. Cell number was determined by means of a Neubauer chamber (Brand, Wertheim, Germany) and plated in the desired

concentration dependent on the application (Table 9). The cultures were incubated for approximately 4h in an incubator (HERA cell 150, Heraeus, Thermo Scientific, Bonn; Germany) at a temperature of 37°C and a $CO_2$ content of 5%. The plating medium was exchanged to Neurobasal medium after 4h (Neurobasal, 1x B27, 220 µM L-glutamine, 1x penicillin/streptomycin) and 1/3 of the medium was substituted every 5 days.

| Culture dishes | Application | Seeded cells |
|---|---|---|
| 6 well plate | Biochemistry | 700,000 cells/well |
| 24 well plate | ICC | 30,000 cells/well |
| µ-Dish $^{35mm, high}$ | Live-cell imaging | 100,000 cells |

Table 9 Number of cells plated, dependent on the application.

***Preparation of specific brain regions***

Mice of an age of P60 to P90 were killed through cervical dislocation after anaesthesia by $CO_2$ and the head was cut off. After removing the scalp, the skullcap was cut in a caudal to rostral direction along the midline. The skullcap was removed and the brain was taken out by moving a bent anatomical forceps caudally, beginning at the olfactory bulbs, separating the brain from cranial nerves. The brain was transferred into ice cold 1x PBS. To separate the cerebral hemispheres, brainstem was grasped and hemispheres were cut apart with a scalpel. The hemispheres were placed with their inner/medial side up to cut out the hippocampus. The striatum was separated from the cortex using surgical forceps. Finally, the different brain regions were transferred into new Eppendorf-tubes and flash frozen with liquid $N_2$.

***Preparation of acute hippocampal slices***

P21 to P35 old mice were terminally anesthetised by an intraperetoneal injection of a mixture of Ketamin (12 mg/ml) and Rompun (1.6 mg/ml) dissolved in 0.9% Saline dependent on their body weight (12 ml/kg). Animals were decapitated and the scalp followed by the skullcap was cut through in a caudal to rostral direction along the midline. The skullcap was removed and the brain was taken out by moving a bent anatomical forceps caudally, beginning at the olfactory bulbs, separating the brain from cranial nerves. The brain was transferred into slicing buffer (25 mM HEPES in 1x HBSS, pH7.4). To separate the cerebral hemispheres, brainstem was grasped and hemispheres were cut apart with a scalpel. Then, the hemispheres were glued to a tissue chopper (Stoelting, Dublin, Ireland) facing up the hippocampi and were cut into 300 µm thick slices. The sliced hemispheres were transferred back into fresh slicing medium to carefully separate the hippocampal slice from each other with the help of a bi-ocular. Finally, the separated slices were transferred into holders containing a net at the bottom for further treatments.

***Perfusion of IRSp53-deficient mice and preparation of coronal brain slices***

P90 to P100 old mice were terminally anesthetised by an intraperetoneal injection of a mixture of Ketamin (12 mg/ml) and Rompun (1.6 mg/ml) solved in 0.9% Saline dependent on their body weight (12 ml/kg). The mouse was fixed in the supine position and the heart was exposed. A blunt cannula was inserted into the left cardiac ventricle and the circulatory system was cleaned with 0.9% physiological saline followed by 50 ml 4% PFA solved in 1x PBS. Then, the brain was removed as described above and stored in 2% PFA solution for 24 h. Thin 50 µm coronal brain slices were prepared using the LeicaVT1000S (Leica, Wetzlar, Germany). The brain slices were stored in 1x PBS at 4°C until further treatments.

## 2.5 Analysis of cultured primary neurons and specific brain regions

***Transfection of primary hippocampal neurons***

Primary neurons were transfected at 13 days in vitro (DIV) using Lipofectamin®2000 Reagent (Invitrogen, Karlsruhe, Germany) following the manufactory advertence with some changes. Prior transfection neurons were incubated for 30 min in Neurobasal medium lacking the B27 supplement (NB−). In the meantime, the transfection mix was prepared. Therefore, NB− was either mixed with Lipofectamin®2000 Reagent, vortexed carefully and mixed with the appropriate plasmid DNA (Table 10, information specified per well). Both mixtures were incubated for 5 min at RT, then combined in an 1:1 ratio and incubated for an additional 20 min at RT. The DNA-reagent complex was then added to the cells and incubated at 37°C and 5% $CO_2$ for 1 h. Then, the transfection mix was removed and cells were washed 3 times with NB− and cultured again for at least 24 h in conditioned Neurobasal medium, which was removed prior transfection and stored at 37°C and 5% $CO_2$.

| Plate | Plasmid | [c] DNA | Lipofectamin®2000 | $V_{Ges}$ NB− |
|---|---|---|---|---|
| 24 well plate | pEGFP-mIRSp53* | 500 ng | 2 µl | 300 µl |
| µ-Dish$^{35\ mm,\ high}$ | pEGFP-mIRSp53* | 500 ng | 4 µl | 600 µl |
| | pKaede-mIRSp53wt | 1 µg | 4 µl | 600 µl |
| | pRFP-ProSAP2 | 2 µg | 4 µl | 600 µl |

Table 10 Specification of Lipofectamin®2000 Reagent based transfection of primary neurons.

### *Immunocytochemistry (ICC) of primary hippocampal neurons*

Immunocytochemistry is a suitable method to analyse the subcellular localisations of proteins as well as the co-localisations of two proteins.

Transfected primary neurons were fixed at 14 DIV with 4% PFA solved in 1x PBS for 15 min at RT. The cover slips were washed 3 times with 1x PBS and then transferred to a humidified chamber. Afterwards, coverslips were incubated in blocking solution, consisting of 1x PBS, 5x neural goat serum (NGS, Gibco Invirtogen, Karlsruhe, Germany), 1% BSA (Sigma-Aldrich, Darmstadt, Germany) and 0.5% Triton-X-100, for 45 min at RT. Blocking solution was exchanged by the primary antibody solution consisting of 1x PBS, 5x NGS and 0.5% Triton-X-100 with the appropriate primary antibody (Table 11), followed by incubation overnight at 4°C. The cover slips were then washed four times with 1x PBS for 10 min, followed by incubation with the appropriate secondary antibody or toxin (Table 11) diluted in 1x PBS, 5% NGS and 1% BSA for at least 3 h at RT. Then, DAPI (4',6-Diamidino-2-phenylindol, 1:10,000 dilution in 1x PBS; Sigma-Aldrich, Taufkirchen, Germany) which labels the nucleus, was added for 10 min, followed by 3 wash steps with 1x PBS for 10 min each at room temperature. Finally, the cover slips were washed with distilled water and fixed on an object slide with aqua poly/mount (Polyscience, Eppelheim, Germany).

| | Host | Dilution | Source |
|---|---|---|---|
| Primary antibody | | | |
| α GFP-Alexa488 | ms | 1:400 | Sigma-Aldrich, Darmstadt, Germany |
| α Shank1 (prestige) | rb | 1:500 | Sigma-Aldrich, Darmstadt, Germany |
| α IRSp53 | rb | 1:100 | affinity purified serum |
| Secondary Antibody | | | |
| α rb-Cy3 | go | 1:500 | Dianova, Hamburg, Germany |
| Toxin | | | |
| Texas-Red X Phalloidin | | 1:500 | Invitrogen, Karlsruhe, Germany |

Table 11 Antibodies and toxin used for immunocytochemistry.

Neurons were analysed using the Leica TCS SP5 confocal laser-scanning microscope with the LaicaLAS software (Leica, Wetzlar, Germany). Co-localisations were evaluated counting multiplexed fluorescence signals on two dendrites on a 100 µm distance using the software ImageJ (NIH, Maryland, USA).

### *Live-cell imaging of primary hippocampal neurons*

Primary hippocampal neurons were plated on µ-Dish$^{35\ mm,\ high}$ (preparation see section 2.4) suitable for live-cell imaging and transfected at 13 DIV (details see page 36). Directly before

starting the imaging the neuronal medium was exchanged with pre-warmed (37°C) artificial cerebrospinal fluid (ACSF) oxygenised with 95% $O_2$ and 5% $CO_2$. Live-cell imaging was performed using the Improvision LiveCell Spinning Disk Microscope (PerkinElmer, Rodgau, Germany) containing an environmental chamber with temperature, humidity as well as $CO_2$ control and the software Velocity 6 (PerkinElmer, Rodgau, Germany).

### *Preparation of the postsynaptic density (PSD) of specific brain regions*

Preparation of the PSD was performed after the protocol described in Coba *et al.* (2009) with some modifications.

Frozen hippocampus, cortex and striatum (preparation see section 2.4) were thawed, pottered in buffer P1 (10 mM HEPES pH7.4, 2 mM EDTA, 5 mM $Na_3VO_4$, 30 mM NaF, 20 mM β-glycerol phosphate and protease inhibitor tablets Mini Complete) and centrifuged for 5 min at 800x g at 4°C. A post-nuclear lysate sample was taken from the supernatant. The remaining supernatant was transferred into a new tube and centrifuged again at 10,000x g at 4°C for 15 min. The supernatant was discarded and the pellet resuspended in buffer P2 (50 mM HEPES pH7.4, 2 mM EDTA, 2 mM EGTA, 5 mM $Na_3VO_4$, 30 mM NaF, 20 mM β-glycerol phosphate, 1% Triton-X-100 and protease inhibitor tablets Mini Complete). Afterwards, the suspended pellet was centrifuged a third time at 23,000x g for 80 min at 4°C. The pellet containing the PSD was resuspended in buffer P3 (50 mM Tris pH9.0, 5 mM $Na_3VO_4$, 30 mM NaF, 20 mM β-glycerol phosphate, 1% sodium deoxycholate and protease inhibitor tablets Mini Complete) and transferred into a new tube for storage at -80°C.

### *Cell-surface biotinylation of primary cortical neurons and acute hippocampal slices*

Cell-surface biotinylation enables a relative quantification of the surface expression of membrane proteins. Thus, cell-surface proteins were labelled with the membrane impermeable reagent Sulfo-NHS-SS-Biotin (Thermo Scientific, Bonn, Germany), followed by precipitation with EZview™ Red Streptavidin Affinity Gel (Thermo Scientific, Bonn, Germany).

*Cell-surface biotinylation of primary cortical neurons:*

Primary cortical neurons (preparation see section 2.4) were infected with rAAVs at 2 DIV and biotinylated at 7 and 12 DIV. Cells were washed twice with 1x HBSS (Gibco Invitrogen, Karlsruhe, Germany) on ice followed by 20 min incubation with 1 mg/ml Sulfo-NHS-SS-Biotin solved in 1x HBSS on a shaker at 4°C. Surplus material was washed away 3 times with 5 mM Tris (pH7.4) diluted in 1x HBSS and whole cell lysates were prepared using 400 µl RIPA buffer (see section 2.2). Biotin labelled proteins were precipitated from 75% of the post-nuclear lysate added to 30 µl of the Streptavidin Affinity Gel and incubated for at least 3 h at 4°C on a rotator. The

Streptavidin agarose were pelleted by centrifugation at 1000x g at 4°C for 1 min, washed 5 times with ice-cold RIPA buffer and the pellet was finally dissolved in 50 µl 1x Sample buffer. Relative surface protein expressions were analysed by western blot (see section 2.2) loading equal volumes and blotting each sample two times.

*Cell-surface biotinylation of acute slices:*

Acute slices (preparation see section 2.4) were transferred for 3 h into pre-warmed (37°C) artificial cerebrospinal fluid (ACSF) oxygenised with 95% $O_2$ and 5% $CO_2$. Afterwards, the slices were washed 2 times 5 min each with 1x HBSS on a shaker followed by 30 min biotinylation at 4°C using 1 mg/ml Sulfo-NHS-SS-Biotin dissolved in 1x HBSS. Excess biotin was removed by washing 3 times for 5 min each with 5 mM Tris (pH7.4) diluted in 1x HBSS and the slices were transferred into new Eppendorf-tubes and flash frozen in liquid $N_2$. The tissue were pottered in 400 µl RIPA buffer (see section 2.2) and incubated for 15 min on ice. Biotin labeled proteins were precipitated from 50% of the tissue lysate using 40 µl of the Streptavidin Affinity Gel by incubating overnight on a rotator at 4°C. The Streptavidin agarose were pelleted by centrifugation at 1000x g at 4°C for 1 min, washed 5 times with ice-cold RIPA buffer and the pellet was finally solved in 60 µl 1x Sample buffer. Each experiment consisted of 6 slices from one mouse per genotype. Three slices were used for one preparation and thence duplicates were obtained for each genotype. Relative surface protein expressions were analysed by western blot (see section 2.2) loading equal volumes and blotting each sample two times.

### *β-Galactosidase staining of coronal brain slices*

Coronal brain slices of IRSp53$^{+/d}$ mice (preparation see section 2.4) were incubated in 0.01% sodium deoxycholate and 0.02% NP-40 solved in 1x PBS for 10 min at RT. Then, slices were washed in 1x PBS for 10 min and bathed into the X-Gal staining solution (5 mM $K_3Fe(CN)_6$, 5 mM $K_4Fe(CN)_6$, 2 mM $MgCl_2$ and 500 µg/ml X-Gal) for at least 1 h at 37°C. Slices were washed again in 1x PBS for 5 min each and threaded on a slide. After 24 h drying time slices were covered using PolyMount. Imaging was done using the Improvision LiveCell Spinning Disk Microscope and the software Velocity 6.

### *Immunohistochemistry (IHC) of coronal brain slices – free floating*

Coronal brain slices of the IRSp53 deficient mouse line (preparation see section 2.4) were washed 3 times in 1x PBS for 10 min and then bathed in the blocking solution consisting of 1x PBS, 10x NGS, 0.3% BSA and 0.3% Triton-X-100 for 30 min at RT on a shaker. The slices were transferred into primary antibody solution (1x PBS, 1x NGS, 0.2% BSA and 0.3% Triton-X-100) with the primary antibody rabbit α phosopho-CREB(Ser133) in a 1:1000 dilution. After incubation overnight at 4°C on a shaker, the slices were washed 3 times with 1x PBS for 10 min, followed

by incubation in the secondary antibody solution (1x PBS, 1x NGS, 0.2% BSA and 0.3% Triton-X-100 with the secondary antibody α rabbit-Alexa488) for 2 hours at RT on a shaker. Then, DAPI was added for 15 min, followed by 3 wash steps with 1x PBS for 10 min each at room temperature. Finally, the slices were threaded on a slide and fixed with aqua poly/mount. Imaging was done using the Improvision LiveCell Spinning Disk Microscope and the software Velocity 6.

## 2.6 Analysis of signalling pathways in the hippocampus

### *Slice recovery and chemical stimulation*

Slices were prepared as described in section 2.4 and transferred into pre-warmed (37°C) ACSF oxygenised with 95% $O_2$ and 5% $CO_2$. The slices were allowed to recover for 4 to 5 h until stimulations occurred. Dependent on the stimulation protocol the ACSF (120 mM NaCl, 26 mM $NaHCO_3$, 1 mM $NaH_2PO_4$, 2.5 mM KCl, 2.5 mM $CaCl_2$, 10 mM D-glucose, pH 7.4) contained different $MgSO_4$ concentrations (chemical LTP: 2 mM $MgSO_4$, chemical LTD induction: 1 mM $MgSO_4$) during the recovery time. The stimulants were diluted in oxygenated ACSF, whereas Forskolin and Rolipram stimulation were carried out in modified ACSF containing no $MgSO_4$. All stimulants were obtained from Trocris Biosciences (Bristol, UK).

| Chemicals | [c] | Duration | Reference |
|---|---|---|---|
| Rolipam & | 0.1 µM | 30 min | Otmakhov *et al.* (2004) |
| Forskolin | 50 µM | | |
| Bicuculine & | 50 µM | 30 min | Dietrich *et al.* (2008) |
| 4-AP | 2.5 mM | | |
| (RS)-DHPG | 100 µM | 5 min | Osterweil *et al.* (2010) |

Table 12 Stimulation protocols for acute slices.

Each experiment consisted of 8 to 12 slices from one mouse per genotype, whereas duplicates were prepared for the non-stimulated control as well as the stimulated slices. Chemical stimulation protocols are listed in Table 12.

### *Protein extraction*

The slices were transferred into Eppendorf-tubes and flash frozen in liquid $N_2$. Afterwards, the slices were pottered with RIPA buffer (see section 2.3) containing PhosSTOP (Roche, Mannheim, Germany), 1 µl/ml Benzonase (250 – 350 U/ml; Novagen, Darmstadt, Germany), pH 8 and incubated on ice for 1 h. The cell lysate was then centrifuged at 10,000x g for 8 min at 4°C and

the supernatant was transferred into a new tube and stored at -80°C or Lämmli buffer was added for storage at -20°C. Samples were analysed by western blot (see section 2.2) loading equal protein amounts.

## 2.7 Behavioural analysis of IRSp53 deficient mice

Behavioural tests were carried out with P60 to P90 old genotyped male mice. The mice were kept according to the guidelines of the German law on animal welfare. The animals had food and water ad libitum and were habituated 4 weeks to a switched 12 h light-dark cycle. The male mice were housed separately one week before behavioural testings. Males were experimentally naïve and the experiments were carried out in their night phase/ active phase.

***Elevated Plus Maze***

The Elevated plus maze (EPM) was used to test anxiety-related behaviour and designed according to Walf & Frye (2007). The testing arena is as a plus shaped arena elevated 75 cm from the floor with four 30 cm long and 5 cm wide arms, linked by a 5 $cm^2$ centre. Two opposing arms were bordered through a 2 mm rim (open arms), whereas the other two arms were limited by 15 cm high walls (closed arms). To monitor the animals a vertical infrared-sensitive camera was placed above the centre. The mouse was placed into the centre facing an open arm and observed for 5 min. The EPM was cleaned with Kleenex and water after each mouse.

The following parameters were assessed: open arm entries, closed arm entries (all four paws had to be on one arm), total crossovers (sum of open and closed arm entries), latency of first entry into an open arm, time spent in the open arms and number of rearings.

***Puzzle box***

The puzzle box analyses the ability to solve problems coupled to a positive cue based on the principle of operant conditioning. Furthermore, motor coordination and exploratory behaviour can be investigated based on the complexity of the different tasks. The puzzle box and the testing protocol was performed according to Ben Abdallah *et al.* (2011).

The box consists of a plexiglas box divided into two equal compartments. A dark “goal” compartment closed with a lid contained fresh sawdust and home cage-like materials (sawdust, serviette and food) and a brightly illuminated (100 lux) “open” white compartment. A barrier of

different features separated the two compartments: door, underpass, sawdust filled underpass and underpass closed with a plug, which made it possible to enter the goal compartment.

The testing took place in a dark room illuminated with infrared light in which the animals were placed for at least 30 min prior to the test to get used to the experiment room. The box was positioned on top of a table, which made it possible to observe the mouse without direct eye contact. At the start of each trial, the mouse was placed in the light compartment with its head facing the wall, at the opposite end from the goal. Trial duration varied between 3 and 4 min depending on the task difficulty and the intervals between the trials were regularly 1 min (Figure 4). At the end of each trial the mouse was kept in the dark goal compartment for approximately 30 sec and afterwards returned to its home cage. If mice were unable to solve the task by themselves the task was displayed by the experimenter and the mouse guided into the goal compartment. Cleaning between trials was done with kleenex and water.

The performance was assessed measuring the latency to solve the task and to reach the goal compartment. Furthermore, the latency was measured when the animal fulfilled the task but not entering the goal compartment (first try).

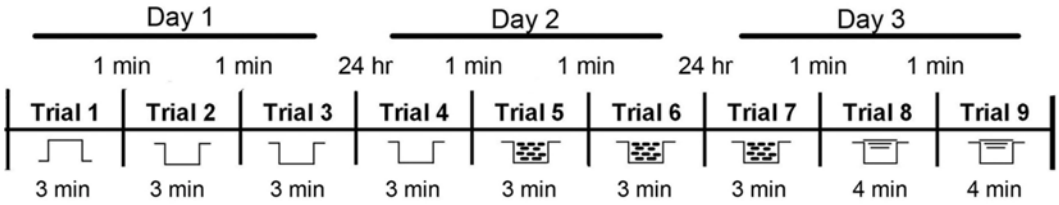


**Figure 4 Schematic representation of the Puzzle box paradigm.**

### *Contextual fear conditioning*

The contextual fear conditioning paradigm investigates memory formation based on classical conditioning. Hence, mice had to associate an unconditioned stimulus (foot shock) within a context. Contextual fear conditioning was performed as described by Sawallisch *et al.* (2009).

Mice were conditioned in a chamber (23.5 $cm^2$) with a stainless grid floor framed by high transparent plexiglas walls (19.5 cm). The chamber was illuminated with white light (10 lux) and the animals were monitored by a modified Mouse-E-Motion system (Infra-e-motion, Hamburg, Germany), automatically measuring the activity, and by video camera. Mice were placed in the chamber for 4 min and conditioned with three foot shocks (250 µA, 1 sec) at 120, 160 and 200 sec. Immediately after the conditioning, mice were returned back to their home cage for 24 h. In the recall trial the animals were placed back into the chamber/context without any foot shocks for 3 min (Figure 5). Cleaning between mice was done with kleenex and water.

The learning effect was measured by calculating the percentage of time spent immobile (freezing) for at least 1 sec. Furthermore, the number of rearings in the recall phase were counted.

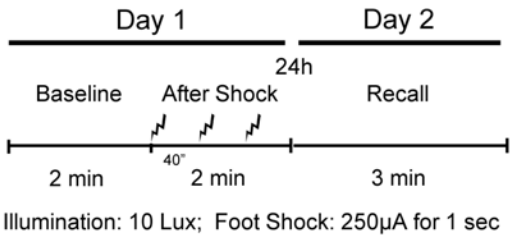


**Figure 5 Schematic representation of the Contextual fear-conditioning paradigm.**

## 2.8 Statistics

The data collected in the different experiments were statistically evaluated using the software Graphpad Prism 6.0 (GraphPad Software, La Jolla, USA). The significance was defined as $p \leq 0.05$. The statistical tests and sample sizes used are specified in the Figure legends. Unless otherwise indicated, all values in the Figures are presented as mean ± SE.

# 3 Results

## 3.1 Analysis of IRSp53 expression in IRSp53 heterozygous (+/d) animals

The main goal of the present study was to further investigate the functional role of IRSp53 in the CNS of mice. For analysis of a possible gene dosage effect, IRSp53 was reduced in a physiological context by analysing IRSp53 heterozygous (+/d) mice.

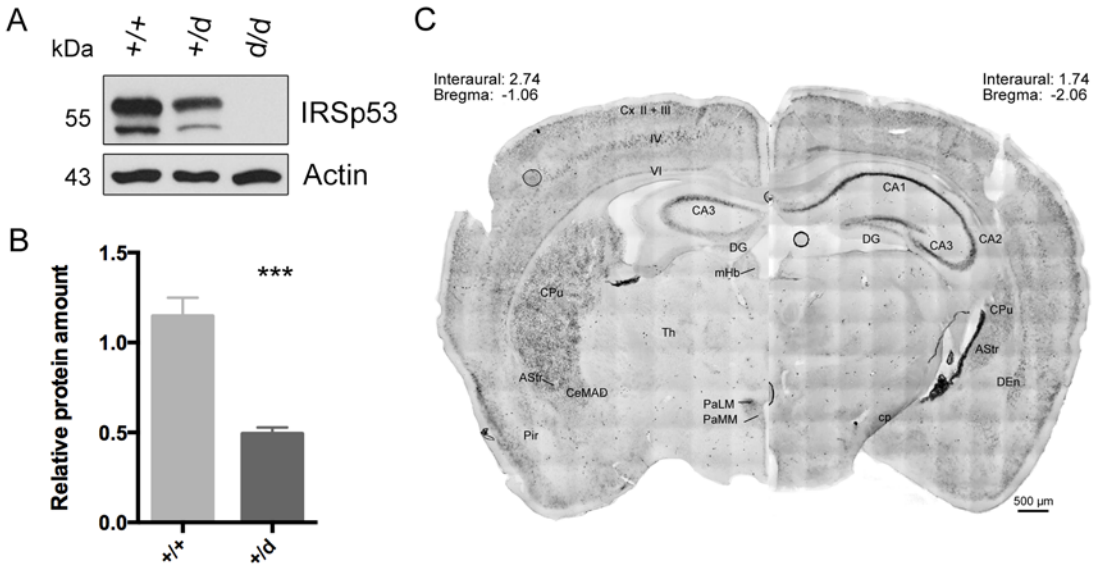


**Figure 6 IRSp53 expression in IRSp53 heterozygous (+/d) mice.** [A] Tissue lysates of the hippocampus from the different genotypes were analysed by western blotting using the antibodies indicated. [B] Quantification demonstrates a 50% reduction of IRSp53 in heterozygous mice compared to wt littermates (n = 10; Two-tailed unpaired Student's t-test: $p < 0.0001$). [C] A β-galactosidase staining of coronal brain sections shows strong expression of IRSp53 in the cortex (Cx = cerebral cortex, cp = basal cerebral peduncle, DEn = dorsal endopiriform nucleus, Pir = piriform cortex), hippocampus (CA1/2/3 = field CA1/2/3 of hippocampus, DG = dentate gyrus) and striatum (CPu = caudate putamen, AStr = amygdalstriatal transmission area), but also scattered expression in other brain regions such as the amygdala (CeMAD = central amygdaloid nucleus), thalamic (mHB = medial habenular nucleus, Th = thalamus) and hypothalamic (PaLM = lateral paraventricular hypothalamic nucleus, PaMM = medial paraventricular hypothalamic nucleus) brain regions.

Therefore, tissue lysates of the hippocampus were analysed by western blotting. Relative protein amounts were normalised against the housekeeping protein β-actin and further standardised to wt protein levels. IRSp53 expression levels are reduced by about 50% suggesting no com-

pensatory response due to the lack of one allele coding for IRSp53 (Figure 6 A, B). However, the IRSp53 ko mice were generated using the embryonic stem cell line XG757 from BayGenomics Consortium (http://baygenomics.ucsf.edu) (Sawallisch *et al.*, 2009), which results in the expression of a truncated version of IRSp53 containing the first 73 aa of the IMD fused to Neo/β-Gal (tr.IMD/Neo/β-Gal) under control of the endogenous IRSp53 promoter. By β-galactosidase staining of coronal brain slices the IRSp53 expression pattern was analysed (Figure 6 C) and shows a strong expression especially in the cortex, hippocampus and striatum. Also scattered IRSp53 expression was found in other brain regions such as in thalamic and hypothalamic brain regions as well as in the central amygdala.

## 3.2 Behavioural analysis of IRSp53 +/d and d/d mice

Previous behavioural experiments of IRSp53 deficient mice exhibited a severe learning deficit in three memory-based tests, the novel object recognition, the Morris water maze (Kim *et al.*, 2009) and the contextual fear-conditioning paradigm. By assessing the motor activity and coordination, as well as exploratory behaviour, no differences compared to wt littermates were observed (Sawallisch *et al.*, 2009). In a testing battery, I examined the behaviour of RSp53 +/d and d/d male mice compared to wt littermates. Therefore, previously applied test as well as new paradigms were chosen. First, the innate anxiety was observed in the elevated-plus maze (EPM). This was followed by a memory-based learning approach addressing problem solving motivated through an aversive cue. Finally, the contextual fear conditioning in which IRSp53 deficient mice performed badly was repeated including the IRSp53 +/d mice.

Male mice were accustomed to a switched day/night cycle for four to five weeks prior to testing, which allowed the observation of the animals in their active night phase. The testing battery started by measuring the innate anxiety in an EPM. This maze is elevated from the floor and consists of four plus shaped arms with two opposing closed arms (CA) and two opposing open arms (OA) linked by a 5 $cm^2$ centre. Mice were placed at the centre and monitored for five minutes and the following parameters were acquired: number of closed arm and open arm entries, latency to enter an open arm and the number of rearings (Figure 7). IRSp53 +/d and d/d mice showed no altered responses in the elevated plus maze compared to wt littermates.

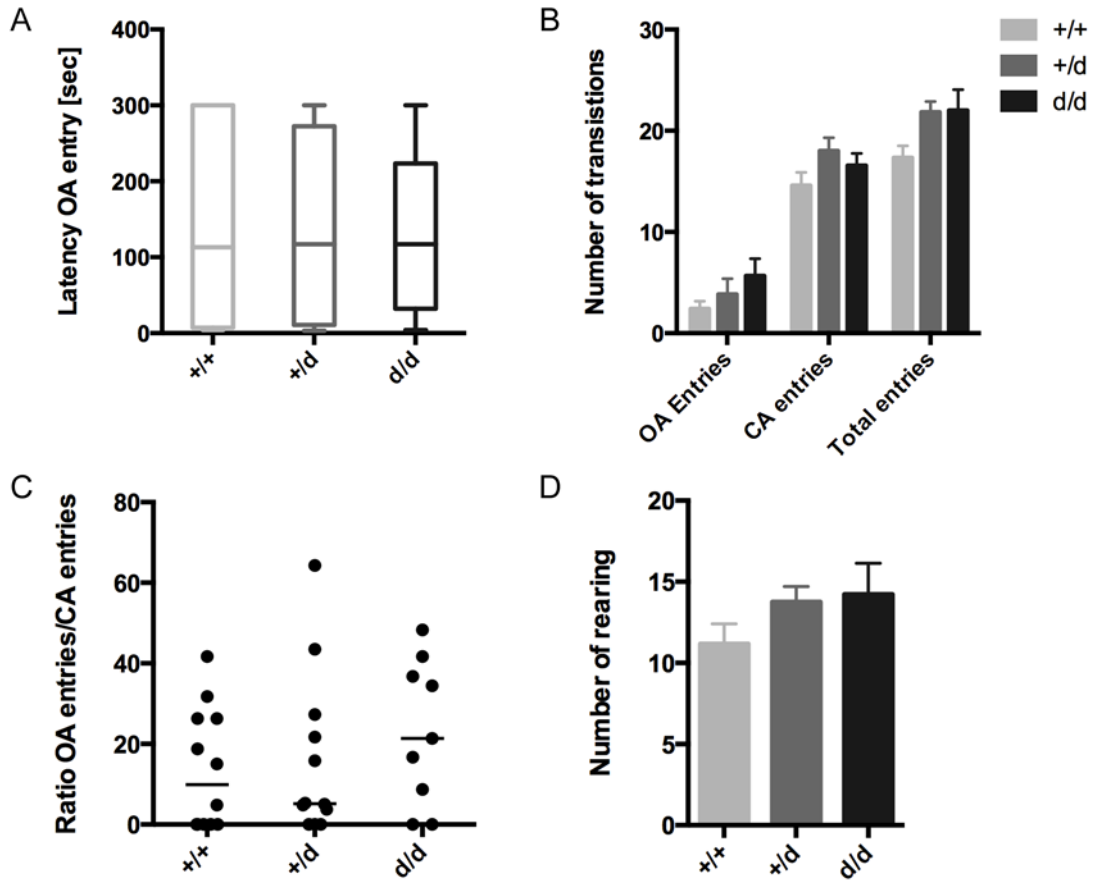


**Figure 7 Testing of innate anxiety of wt, IRSp53 +/d and d/d mice in the Elevated-plus maze.** [A] Latency to enter the open arms (OA), [B] the number of transitions between the open arms and closed arms (CA), as well as [C] the ratio between the open and closed arms entries show no differences between +/d and d/d animals compared to their wt littermates. [D] Counting of the rearings demonstrates also no differences for all three genotypes (n +/+ = 12, n +/d = 12, n d/d = 10).

As IRSp53 deficient mice performed badly in the fear-conditioning assay, which includes a significant fear component, the puzzle box was chosen as an additional test, which does not use painful stimuli as motivation to learn. This test assesses memory formation based on the motivation to reach a home cage area by solving problems of increasing difficulty in an aversive environment (Ben Abdallah *et al.*, 2011). The testing area consists of two compartments linked by a pass, one brightly white illuminated compartment (aversive environment) and one dark compartment containing home cage material. The experimental paradigm involves four different tasks distributed on three consecutive days (Figure 8 A). Day 1 consists of a habituation phase to the puzzle box in which mice had to solve two simple tasks, first passing a door and second to crawl through an underpass to reach the home cage area. On days two and three mice needed to repeat the last task from the day before followed by 2 trials of a new task. On day 2 the animals had to remove sawdust, which blocked the underpass, and on day 3 they had to actively lift out a plug to get access to the goal compartment. Learning was then measured by recoding the

latency to reach the home cage area. If the problem was not solved, the trial was cancelled after a duration of 3 min for trial 1 to 7 and of 4 min for trial 8 and 9.

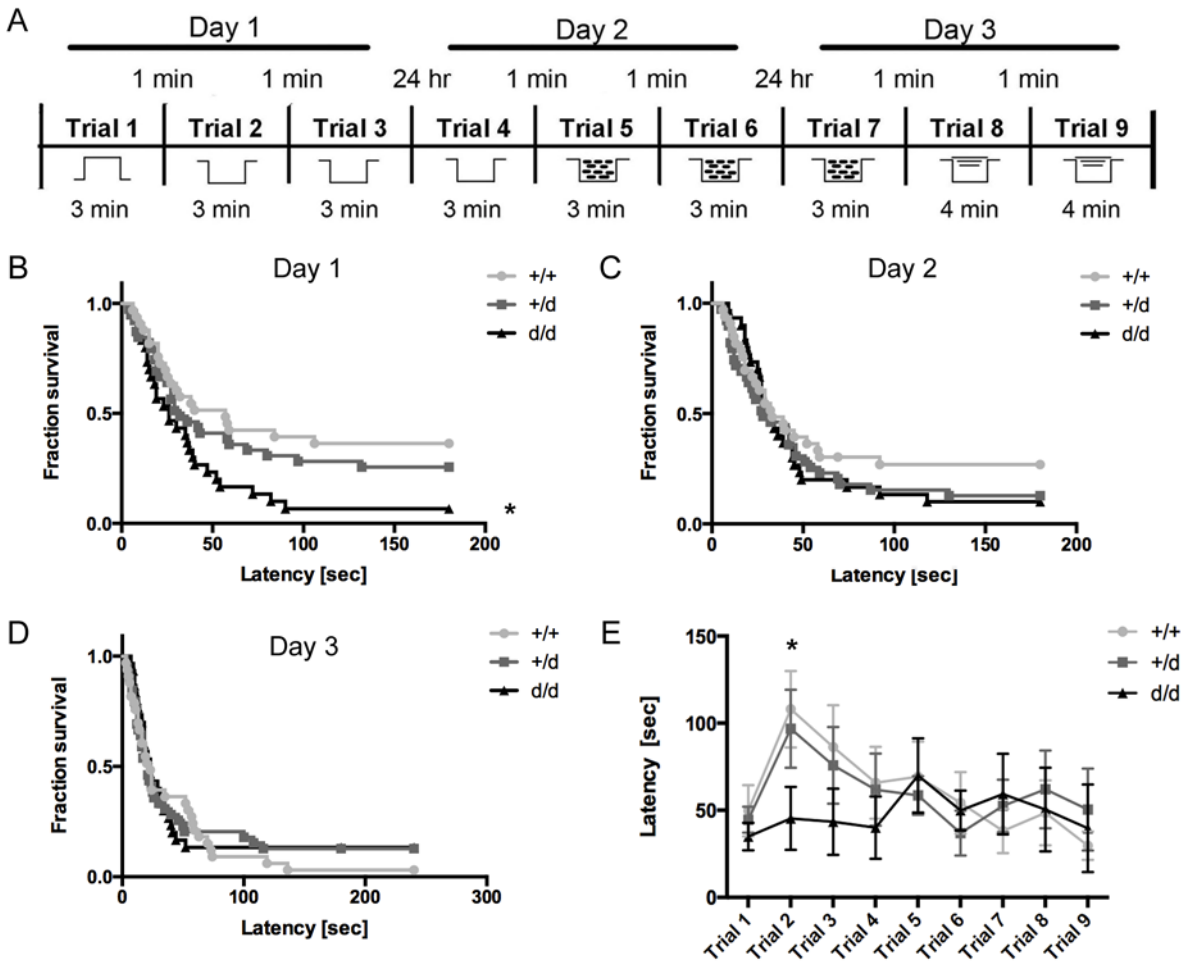


**Figure 8 Analysis of a learning impairment of mice in a puzzle box due to a reduction or loss of IRSp53.** [A] Scheme of the puzzle box assay; animals have to escape from a brightly lit compartment into their home cage area during 9 consecutive trials within 3 days. The path to the home cage area changes three times with increasing difficulty. [B, C, D] Latencies to reach the home cage area were statistically evaluated by a survival analysis. [B] On day 1 IRSp53 ko animals solve the task faster than their wt and +/d littermates (n +/+ = 11, n +/d = 13, n d/d = 11; Log rank (Mantel Cox) test: d/d p = 0.0144). [C, D] On day 2 and 3 performances demonstrate no differences between all three genotypes. [E] Analysis of the trial performances depict a genotype difference specifically at trial 2 on day 1 in which the ko animals reach faster the goal compartment than their wt and +/d littermates (Two-way ANOVA: d/d p = 0.0469).

In this test, IRSp53 +/d and d/d animals learn as efficient as wt littermates but IRSp53 ko mice demonstrate a faster escape into the goal compartment at trial 2 in the habituation phase. A detailed analysis of trial 2 reveals a significant genotype difference. However, all genotypes show similar performances when comparing the latency for the first approach (first try), meaning solving the task but not entering the goal zone. This implies that IRSp53 deficient mice escape faster to their home cage and do not explore the novel environment (Figure 9).

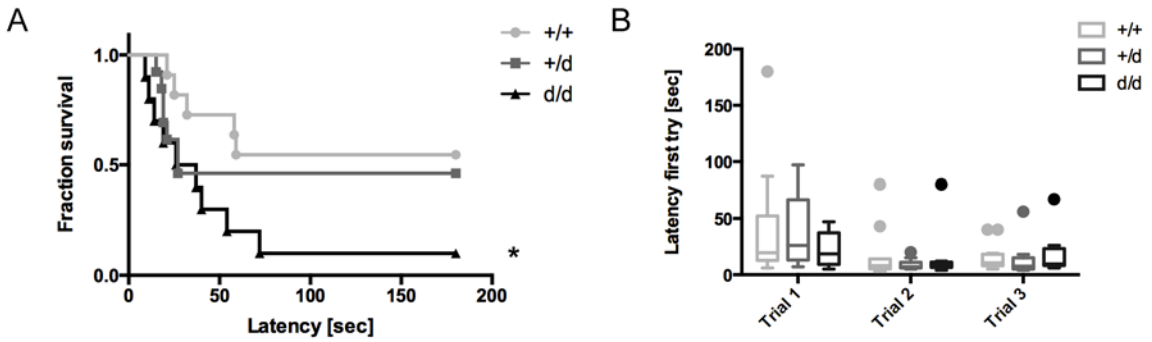


**Figure 9 Performance of the IRSp53 mice in the puzzle box at day 1, a part of the habituation phase.** [A] Latencies to reach the home cage area at trial 2 on day 1 demonstrate a faster escape of the IRSp53 ko mice compared to their wt and +/d littermates (n +/+ = 11, n +/d = 13, n d/d = 11; Log rank test for trends: d/d p = 0.026). [B] However, evaluation of the observed latency to reach the goal zone but not entering it (first try) exhibits no differences between all three genotypes.

Finally, the animals were investigated in contextual fear conditioning assessing the ability to learn the association of a context coupled to a nociceptive stimulus (Figure 10). For that, the animals were placed in a chamber with a metal grid. Animals were allowed to explore the new environment, followed by three mild electric foot shocks. After 24 h, mice were reintroduced in the conditioning chamber and the learning effect was measured as the time spent immobile (freezing). Interestingly, both the IRSp53 +/d and d/d animals exhibit markedly reduced freezing compared to wt littermates. Considering the learning effect within a group, wt mice show a strong memory in the recall as expected. IRSp53 +/d mice demonstrate moderate learning as well, whereas IRSp53 deficient mice fail to do so. Narrow observation of the animals during the recall phase reveals a conspicuous rearing behaviour of the IRSp53 +/d and d/d mice, which appears more as a prominent flight instinct. However, by counting the number of rearings no genotype differences were detectable.

In summary, it can be stated that there is no distinction in the innate anxiety between the different genotypes. Furthermore, tests directed at the cognitive ability to remember a location and to solve problems in an aversive environment exhibit no learning impairments in IRSp53 +/d and d/d animals. Remarkably, in behavioural experiments examining fear-evoked learning not only IRSp53 deficient, but also heterozygous mice display a severe learning impairment.

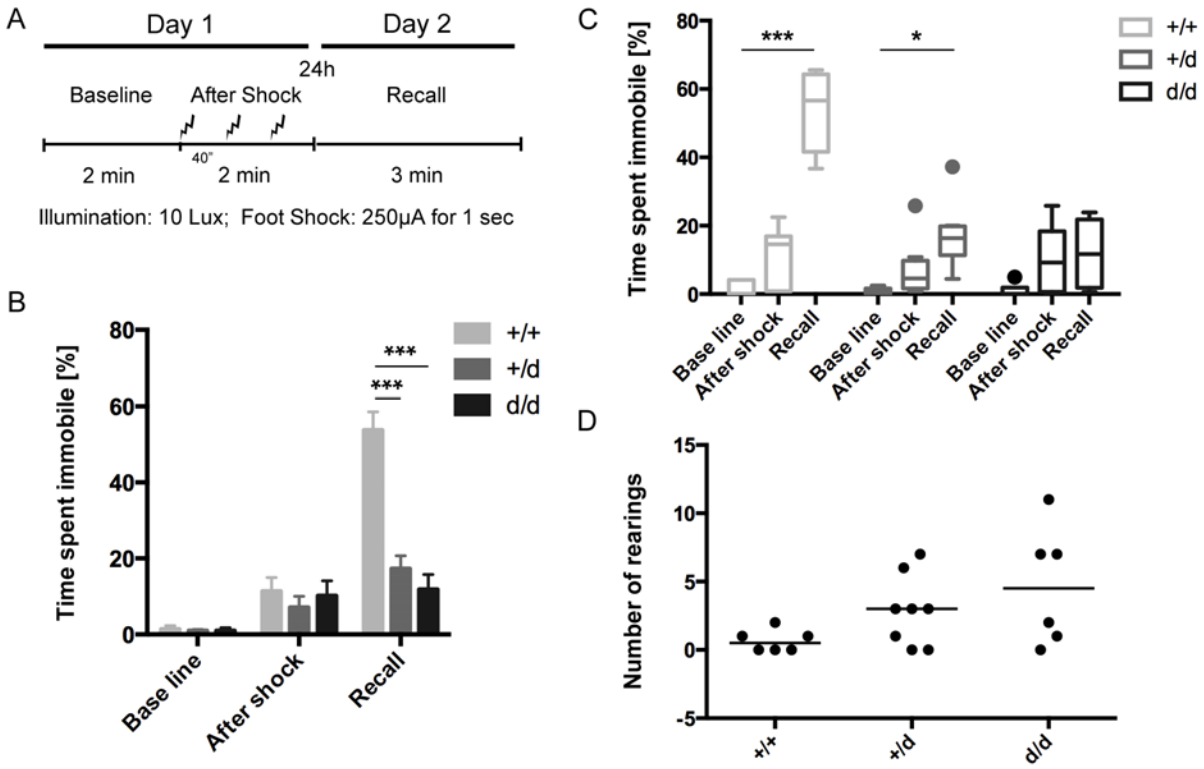


**Figure 10 Contextual fear conditioning of wt, IRSp53 +/d and d/d animals.** [A] Scheme for the contextual fear-conditioning assay; animals were habituated to a new cage for two minutes before receiving three foot shocks in 40 second intervals. After 24 hours the animals were reintroduced into the conditioning chamber without further electrical shocks. [B] The time spent immobile ('freezing') was recorded before (Base line), in between and immediately after foot shocks (After shock) and on the next day (Recall). Both IRSp53 +/d and d/d mice exhibit significantly reduced freezing behaviour upon recall compared to their wt littermates (n +/+ = 6, n +/d = 8, n d/d = 6; Two-way ANOVA: +/d $p < 0.0001$, d/d $p < 0.0001$). [C] Analysis of the data with respect to the ability of the animals to memorise the context associated with the painful stimuli demonstrate genotype differences. Though freezing is reduced in +/d animals, they spend more time freezing than their d/d littermates (Two-way ANOVA: +/+ $p < 0.0001$, +/d $p = 0.0330$). [D] Counting of the rearings during the recall phase demonstrates enhanced but not significant rearing behaviour of IRSp53 +/d and d/d animals.

## 3.3 Exclusion of a dominant-negative effect

The observation that IRSp53 +/d animals perform as poorly as IRSp53 deficient mice in the contextual fear conditioning leads to the consideration that: (1) The phenotype in +/d mice arises due to an IRSp53 haploinsufficiency, meaning the amount of IRSp53 available is not enough. (2) The tr.IMD/Neo/β-Gal fusion expressed from the mutant allele acts in a dominant-negative manner. As it is known that the IMDs of IRSp53 can dimerise (Millard *et al.*, 2005), it appeares possible that the remaining truncated IMD could be targeted to synapses and integrate into the helical bundle of the IMD of non-mutated IRSp53, thereby inhibiting its function.

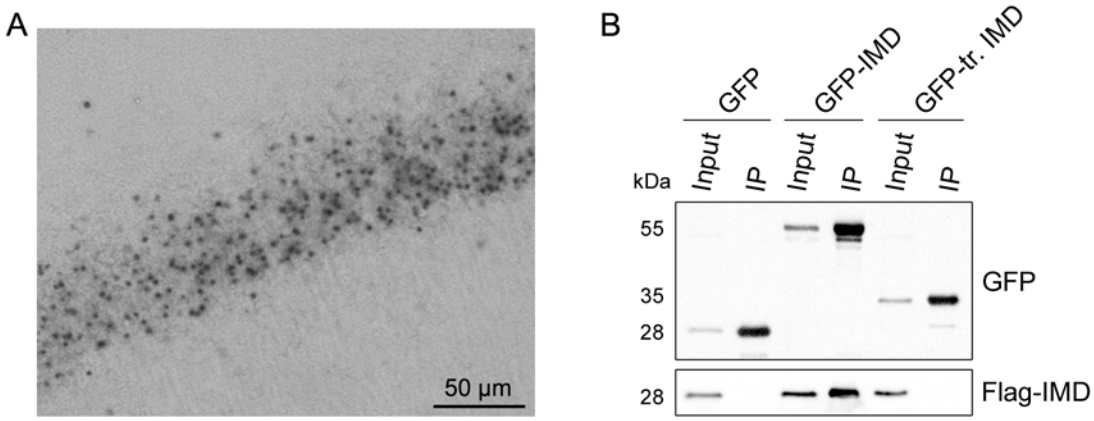


**Figure 11 Exclusion of a dominant-negative effect of the remaining truncated IRSp53 protein product onto non-mutated IRSp53.** [A] β-galactosidase staining of the CA1 region of the hippocampus from a coronal brain section reveals a somatic location of the residual IRSp53 fragment fused to the selection cassette for the gene targeting. [B] HEK293 cells were transfected with constructs coding for Flag tagged full length IM domain (aa 1 – 243) GFP, GFP fused to full length IM domain or fused the truncated IM domain (aa 1 – 73, the residual IRSp53 fragment expressed in the IRSp53 deficient mouse line). After cell lysis, GFP tagged proteins were immunoprecipitated by GFP-trap. Immunoprecipitation (IP) of the Flag-IMD with the different GFP tagged constructs were analysed by western blot using the antibodies indicated. Full-length IM-domain, but not the truncated version, interacts with the Flag-IMD.

Histological staining of brains of IRSp53 +/d mice indicates a restriction of the tr.IMD/β-Gal/Neo fusion protein to the neuronal cell bodies and no localisation in the dendrites or postsynaptic sites (Figure 11 A). Furthermore it was tested, whether the truncated IMD is able to dimerise with the full length IMD. Therefore, full length flag-tagged IMD and either full lengths IMD (1 – 243 aa) or the truncated IMD (1 – 73 aa) tagged with GFP were co-expressed in HEK cells and analysed with respect to an intermolecular interaction by immunoprecipitation (Figure 11 B). Here, I observed an efficient dimerisation of the full length IMDs. However, the truncated IMD does not interact with the isolated IMD and thus a dominant-negative effect caused by the truncated protein can be excluded.

## 3.4 Postsynaptic levels of IRSp53 in different forebrain regions

Sawallisch *et al.* (2009) demonstrated that IRSp53 is enriched at the postsynapse by PSD fractionation of whole brain lysates. Here, postsynaptic accumulation of IRSp53 in the brain regions with the highest expression levels (cortex, hippocampus and striatum) was investigated. Therefore, post-nuclear lysates (pnl) and PSD fractions (psd) of wt and IRSp53 +/d mice were prepared and analysed by western blot. Relative protein amounts were quantified, normalised to the housekeeping protein β-actin and further standardised to wt protein levels (Figure 12).

In cortex and striatum IRSp53 is significantly reduced in the pnl as well as in the PSD samples derived from heterozygous animals. In contrast, hippocampal IRSp53 amounts in the PSD of IRSp53 haploinsufficient mice reach almost wt levels, although pnl levels are significantly reduced. Thus the ratio psd/pnl, which reflects the relative enrichment, is significantly increased.

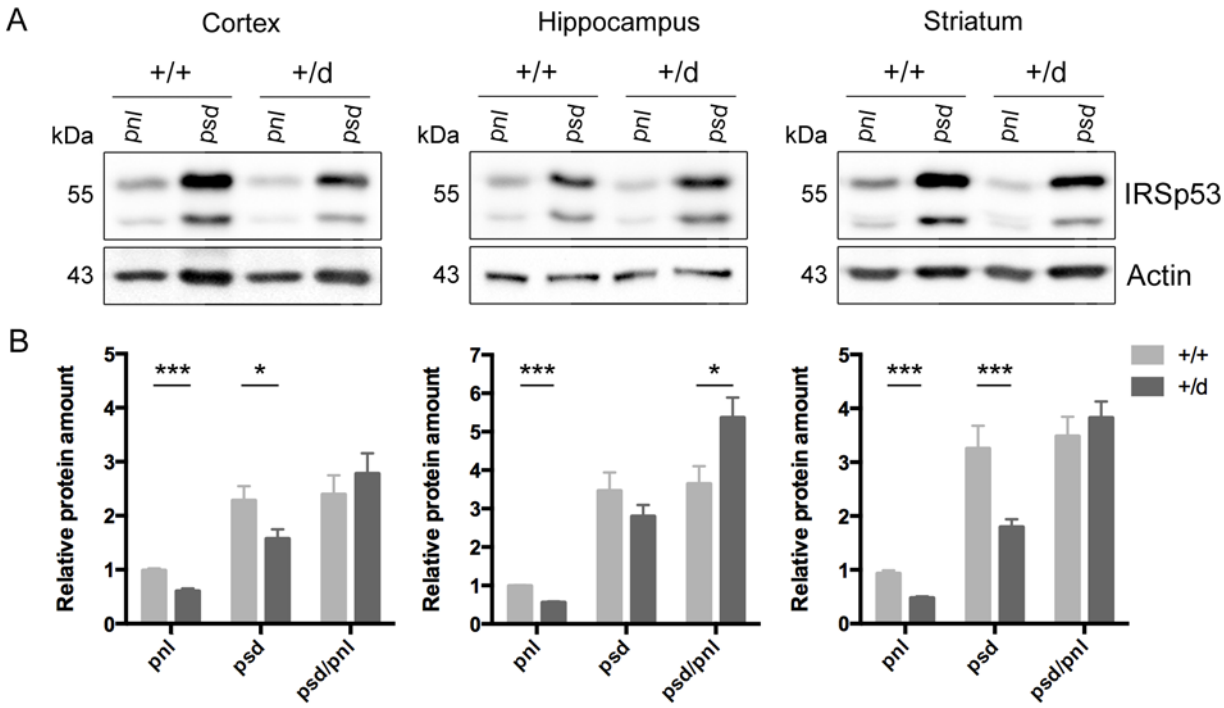


**Figure 12 Postsynaptic expression levels of IRSp53 in different forebrain regions of IRSp53 haploinsufficient mice.** [A] Post-nuclear lysates (pnl) and PSD fractions (psd) of the cortex, hippocampus and striatum from wt and IRSp53 +/d mice were analysed by western blot using the antibodies indicated. [B] Quantification of cortical IRSp53 protein levels demonstrates a significant reduction of IRSp53 in the pnl and psd of heterozygous mice compared to wt littermates (n = 8; Multiple t-test: pnl $p < 0.0001$, psd $p = 0.03108$). Evaluation of hippocampal IRSp53 protein levels shows a significant decrease of IRSp53 in the pnl of +/d mice, but achieves almost wt levels in the psd (n = 10; Multiple t-test: pnl $p < 0.0001$, ratio psd/pnl $p < 0.0001$). In the striatum quantification of IRSp53 demonstrates a significant reduction of IRSp53 in the pnl and psd of IRSp53 haploinsufficient mice (n = 4; Multiple t-test: pnl $p < 0.0001$, psd $p < 0.0001$).

## 3.5 Identification of the functional domains required for synaptic targeting of IRSp53

The strength of the enrichment of IRSp53 to the postsynapse varies depending on the brain region. So, which functional domains are necessary for the synaptic targeting? IRSp53 consists of four distinct functional motifs: the IM domain (IMD), the CRIB domain (CRIB), SH3 domain (SH3) and the PDZ ligand (PDZL). Published data using deletion constructs showed that the IM

and CRIB domain as well as the PDZ ligand motif contribute to synaptic localization (Hori *et al.*, 2005). However, deletion constructs may lead to misfolded protein products. A study by Choi *et al.* (2005) analysed the contribution of the SH3 domain and the PDZL using missense mutations and showed that both domains are important for the postsynaptic localisation of IRSp53. To clarify these contradictions, IRSp53 constructs were designed where the function of each single domain is disturbed by missense mutations (Figure 13 A). The conversion of four lysins (K) to glutamate (E) in the IM domain described by Saarikangas *et al.* (2009) interferes with lipid binding without affecting the protein folding. Binding of GTP-bound Cdc42 to the central CRIB domain can be disrupted by an exchange of the isoleucine (I) to asparagine (N) at the position 268 (Govind *et al.*, 2001). The binding of the SH3 domain to prolin-rich sequences (PPPP-motif) can be inactivated through an isoleucine to prolin (P) exchange at position 403 (Choi *et al.*, 2005). Finally, binding of PDZ domains by a C-terminal PDZ ligand motif can be impeded by C-terminal valin (V) to glycin (G) mutation (Kornau *et al.*, 1995) at position 521 of IRSp53.

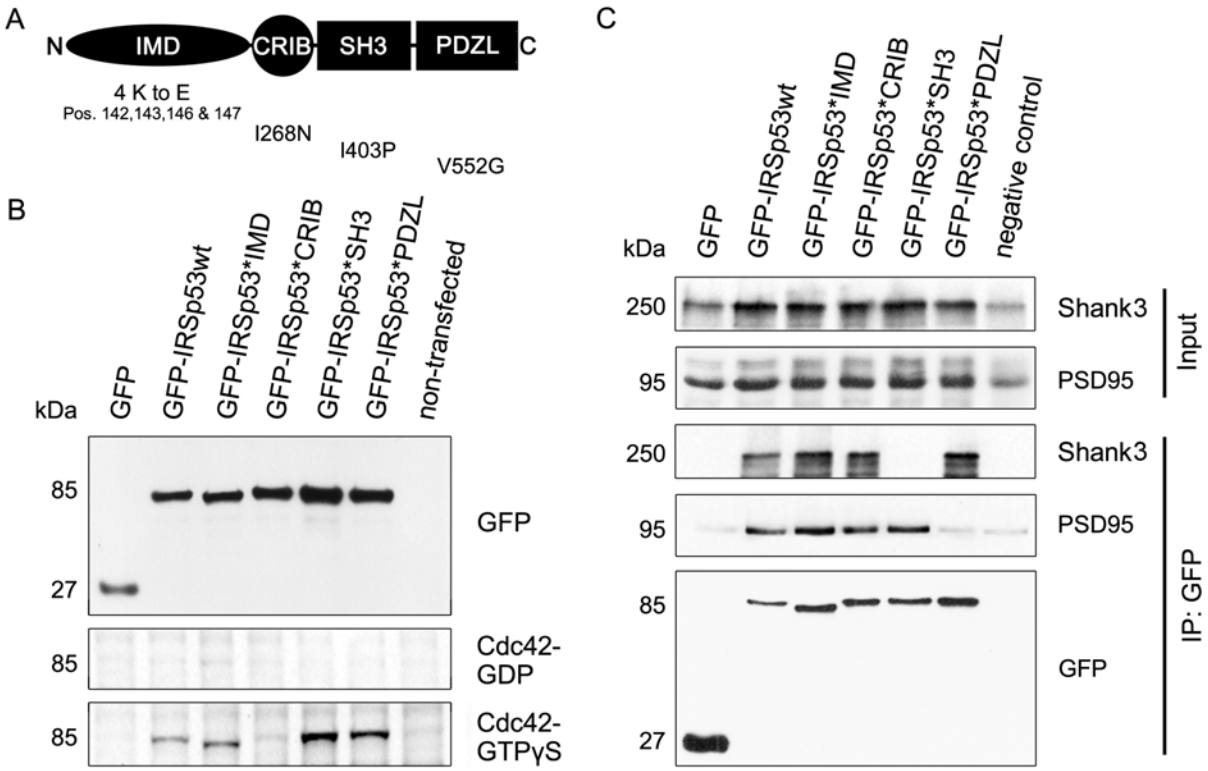


**Figure 13 Validation of IRSp53 missense mutations that neutralise single functional domains.** [A] Domain structure of IRSp53. Individual domains of IRSp53 were disrupted by missense mutations as indicated. [B, C] IRSp53 mutant constructs were expressed in HEK293 cells and analysed for an interaction with their binding partners. [B] Binding of active Cdc42 was verified in a Cdc42 overlay assay; binding is selectively lost in the IRSp53*CRIB mutant. [C] Binding of Shank3 and PSD95 was analysed by co-immunoprecipitation. The SH3 mutant of IRSp53 prohibited Shank3 binding, whereas mutating the PDZL selectively lost PSD95 binding.

GFP-tagged wt and mutant IRSp53 constructs were expressed in HEK293 cells and analysed in their functionality (Figure 13 and 14). Binding of GTP-bound Cdc42 was assessed by an overlay assay using bacterially expressed GST-Cdc42 in the absence or presence of GTPγS, a non-

hydrolysable GTP analogue (Figure 13 B). The I268N mutant of IRSp53 failed to bind active Cdc42 as expected. Binding of the postsynaptic interaction partners Shank3 and PSD95 was verified by co-expression in HEK293 cells followed by co-immunoprecipitation using the GFP-trap (Figure 13 C). As expected, binding of Shank3 to the SH3 domain was selectively abolished by the I403P mutation. Binding of PSD95 was selectively lost by the PDZL mutation V521G.

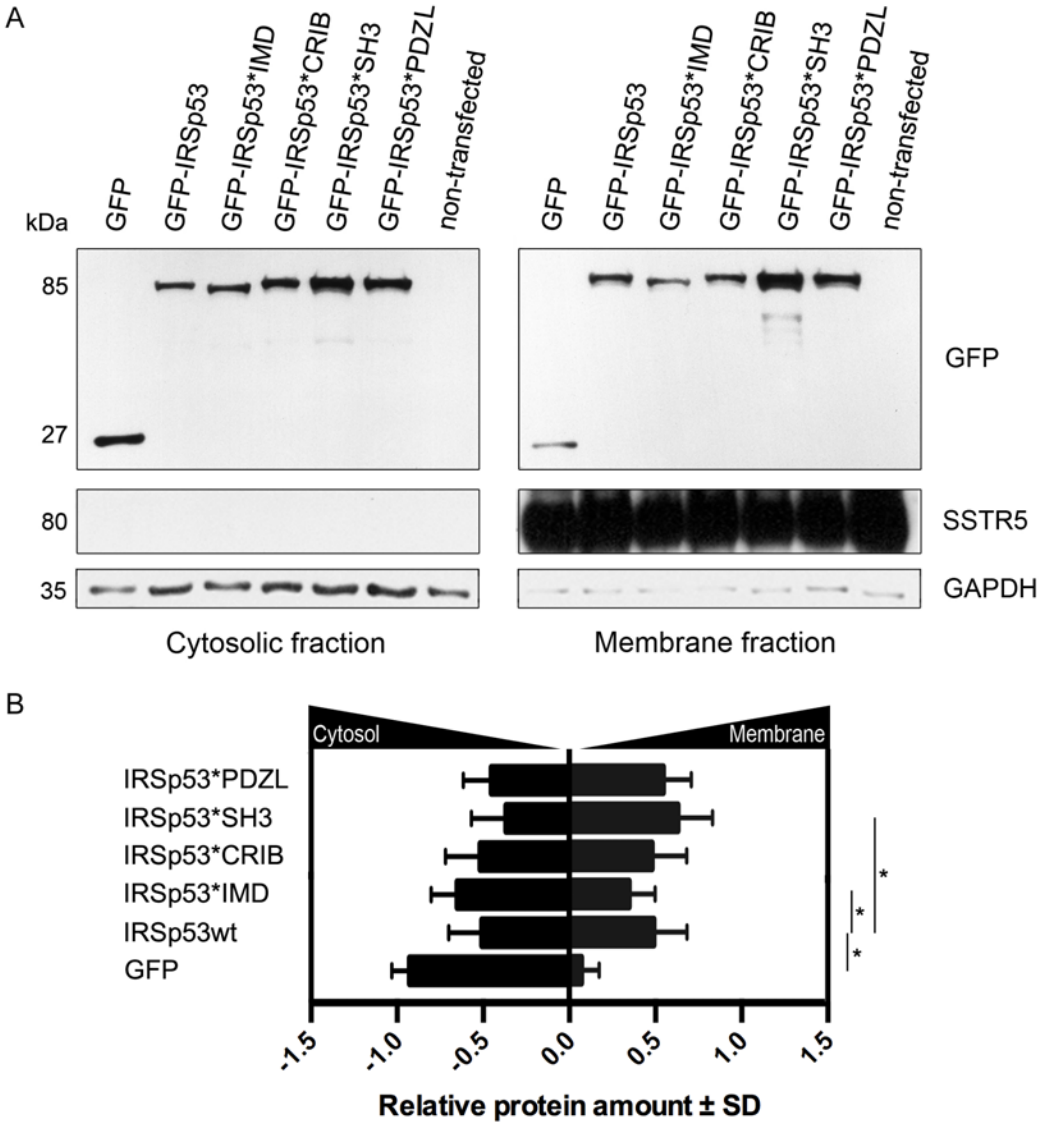


**Figure 14 Cell fractionation to verify IRSp53 IMD deactivation.** [A] GFP tagged wt and mutant IRSp53 constructs were expressed in a SSTR5 stable expressing HEK293 cell line; membrane and cytosolic fractions were prepared and analysed by western blot using the antibodies indicated. [B] The relative IRSp53 amount of the mutant variants were normalised against wt IRSp53 in the different fractions. Then the shift from the cytosolic to the membrane fraction was quantified between wt and mutant IRSp53 (cytosolic fraction is shown as negative values and membrane fraction as positive values). The IMD mutant is preferentially cytosolic, whereas the SH3 mutant is more enriched in the membrane fraction (n = 6, Multiple t-test: GFP p = 0.00048, GFP-IRSp53*IMD p = 0.00168, GFP-IRSp53*SH3 p = 0.0060).

Lipid binding mediated by the IM domain was evaluated as the association of GFP-tagged wt and mutant IRSp53 to cellular membranes of HEK293 cells, which express the transmembrane

protein SSTR5 (Figure 14). Membrane fractions and cytosolic fractions were separated by centrifugation and analysed by western blot. Successful fractionation was then controlled by SSTR5 staining for the membrane fraction and staining for the cytosolic protein GAPDH. Then the shift from the cytosolic to the membrane fraction was compared between wt and mutant IRSp53. The GFP control and the IMD mutant are significantly shifted to the cytosolic fraction as predicted. Interestingly, the SH3 domain mutant exhibits a shift to the membrane fraction, suggesting that the association with the membrane increases.

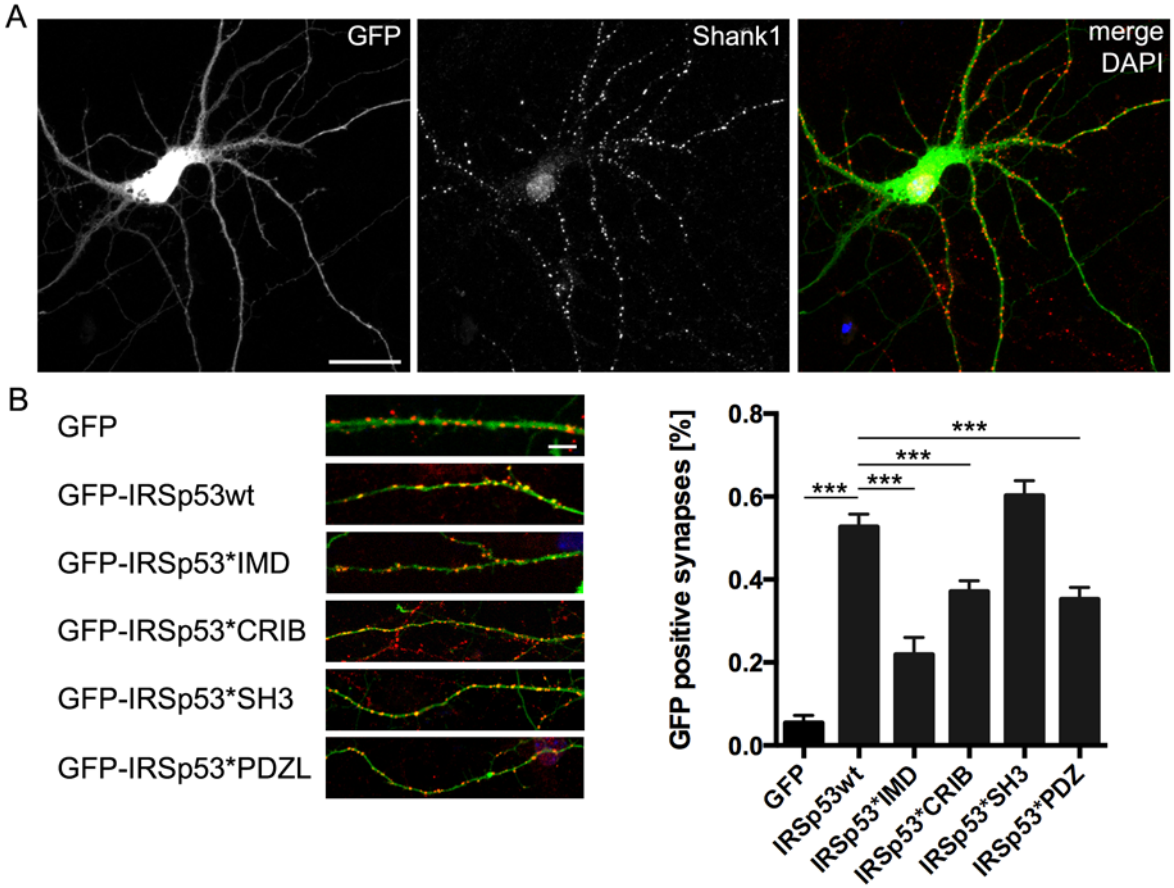


**Figure 15 Synaptic targeting of GFP-tagged wt and mutant IRSp53.** Immunocytochemistry of primary hippocampal neurons, transfected with GFP tagged IRSp53 wt and mutants. Neurons were transfected at 13 DIV, fixed with 4% PFA at 14 DIV and stained with specific antibodies against GFP and endogenous Shank1. [A] Representative confocal image of a primary hippocampal neuron stained for GFP and Shank1. [B] Representative confocal images of Shank1 positive dendrites expressing GFP, GFP tagged IRSp53 wt or mutant variants. [C] Quantification of GFP positive Shank1 clusters reveal 3 functional domains of IRSp53 that are important for the synaptic targeting (n = 5, analysed cells ≥ 10; One-way ANOVA: GFP $p < 0.0001$, IRSp53*IMD < 0.0001, IRSp53*CRIB $p = 0.0004$, IRSp53*PDZ $p = 0.0001$). Scale bar: A = 25 µm, B = 10 µm.

The IRSp53 wt expression constructs were transfected at 13 DIV into primary hippocampal neurons to evaluate co-localisation of the wt and mutant IRSp53 variants with the endogenous postsynaptic protein Shank1, a reliable marker of the PSD (Kreienkamp, 2008) (Figure 15). Therefore, the transfected neurons were fixed at 14 DIV and immunostained for GFP as well as against the endogenous Shank1 and imaged by confocal microscopy. For each construct at least

10 cells with two different dendrites of a length of about 100 µm chosen from 5 independent experiments were analysed. The percentages of GFP positive Shank1 clusters were quantified.

In neurons expressing GFP-tagged wt IRSp53 approximately 55% of the Shank 1 clusters are positive for GFP, whereas almost no Shank1 clusters are positive for GFP in the control transfection. The number of GFP positive Shank1 clusters is lowered by 20% upon mutation of either the CRIB domain or the PDZL of IRSp53. The most prominent loss of synaptic targeting is achieved by mutation of the lipid binding IMD with a decrease of about 35%. However, inactivation of the SH3 domain does not lead to any synaptic targeting defect. Thus, the IM and CRIB domain as well as the PDZ ligand motif of IRSp53 are required for their efficient postsynaptic targeting.

## 3.6 Postsynaptic targeting of IRSp53 in PSD95 deficient mice

The role of the PDZ ligand motif according to postsynaptic targeting of IRSp53 was further elucidated analysing the accumulation of IRSp53 in the PSD of PSD95 deficient mice (provided by Seth Grant and Marcelo Coba; Edinburgh, UK).

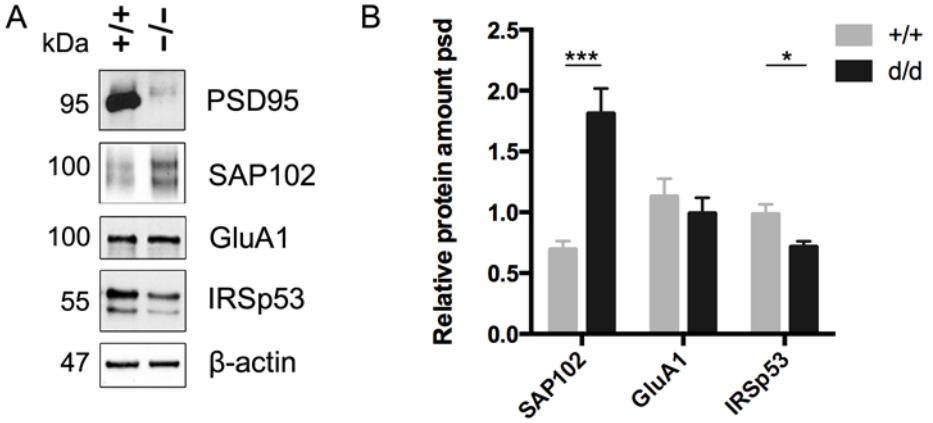


**Figure 16 Quantification of IRSp53 expression levels in the PSD of PSD95 deficient animals.** [A] PSD fractions (psd) of PSD95 deficient mice were analysed by western blot using the indicated antibodies. [B] Quantification of the protein levels demonstrates a significant increase of SAP102 and a slight but significant decrease of IRSp53 in the psd of PSD95 ko mice compared to wt littermates (n = 4; Two-way Repeated-measurement ANOVA: SAP102 $p < 0.0001$, IRSp53 $p = 0{,}0483$), whereas GluA1 is unaffected.

PSD fractions derived from the whole brain of wt and PSD95 deficient mice were analysed by western blot. Relative protein amounts were normalised to the housekeeping protein β-actin and further standardised to wt protein levels (Figure 16). The postsynaptic targeting of IRSp53 declines by roughly 30%, whereas GluA1 accumulation is unaffected by loss of PSD95. However, the reduction of IRSp53 in the PSD of PSD95 null-mice is lower than expected. As SAP102 is known to be up-regulated if PSD95 is lost (Cuthbert *et al.*, 2007), the protein level of SAP102

was analysed. Indeed, the protein amount of SAP102 demonstrates a marked increase in the PSD of PSD95 ko mice.

This leads to the question whether SAP102 interacts with IRSp53. Analysis of protein-protein interactions of the different PSD95 family members SAP102 and SAP97 with GFP-tagged IRSp53 was performed by co-immunoprecipitation using GFP-trap (Figure 17). HEK293 cells were co-transfected with vectors coding for GFP-tagged IRSp53 and the different PSD95 family members. After cell lysis, GFP tagged proteins were immunoprecipitated by GFP-trap and input and precipitate (IP) samples were analysed by western blot. The blot demonstrates that SAP102 interacts with IRSp53 comparable to PSD95. In contrast, co-precipitation of SAP97 with IRSp53 is weak. Accordingly, the PDZ domain mediated interaction of PSD95 with IRSp53 is necessary for postsynaptic targeting of IRSp53 and SAP102 might partially compensate for the loss of PSD95 in PSD95 ko animals in this respect.

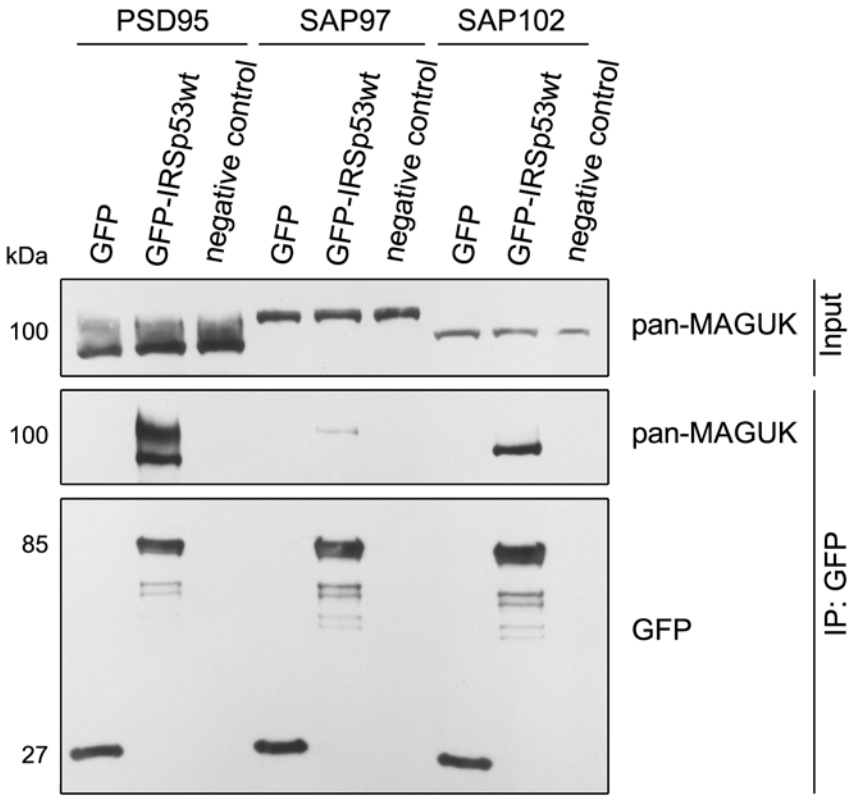


**Figure 17 Interaction of IRSp53 with different SAP/PSD95 family members.** HEK293 cells were transfected with constructs coding for GFP and GFP-tagged IRSp53, myc-tagged SAP102, SAP97 as well as PSD95. After cell lysis, GFP fusion proteins were immunoprecipitated by GFP-trap, input and precipitate (IP) samples were analysed by western blot using the indicated antibodies. Co-immunoprecipitation of the different SAP protein family members shows a strong interaction of IRSp53 with SAP102 and PSD95, but only a weak interaction with SAP97.

## 3.7 Investigation of the mobility of IRSp53 in living hippocampal neurons

The previous experiments suggest that three functional domains of IRSp53 are important for the synaptic targeting. However, experiments analysing fixed neurons do not reflect the dynamic of a protein in a living cell. Thus, the next step was to analyse the mobility of IRSp53 in live-cell imaging experiments. On the one hand, IRSp53 could be actively directed to the postsynapse through a motor protein driven transport. On the other hand, IRSp53 could be transported by a slow mechanism to the synapse where it is anchored by its postsynaptic binding partners. To gain insight into the transport mode, the photoconvertable fluorescent protein Kaede was chosen as a fluorescent tag for IRSp53. Kaede is a green fluorescent protein, which is irreversible converted to a red fluorescence after irradiation with UV-light (Ando *et al.*, 2002) and thus enables the observation of a distinct population of IRSp53 within the neuron. *Kaede* was cloned to *IRSp53* cDNA and cells expressing the green fluorescent Kaede protein fused to IRSp53 were irradiated with a brief 405 nm laser pulse (laser power: 12%, repeated irradiation in 40 cycles for 1 sec each) at defined regions of interest. This leads to an almost complete conversion of green to red fluorescence and allows the selective observation of the red fluorescence by live-cell imaging. Preliminary tests in HEK293 cells showed distinct membrane localisation as well as diffuse distribution in the cytosol of Kaede-IRSp53 (Figure 18). A limitation of Kaede is its ability to form oligomers, which could disturb the correct cellular distribution of IRSp53. But no artificial Kaede-IRSp53 oligomers were seen. Observation over a period of 5 minutes demonstrates high mobility of red fluorescent IRSp53. Cytosolic IRSp53 diffuses fast and partially accumulates at the PM. Moreover, membrane-associated IRSp53 seems to dissociate and migrate to the other side of the cell where it re-associates again at the PM.

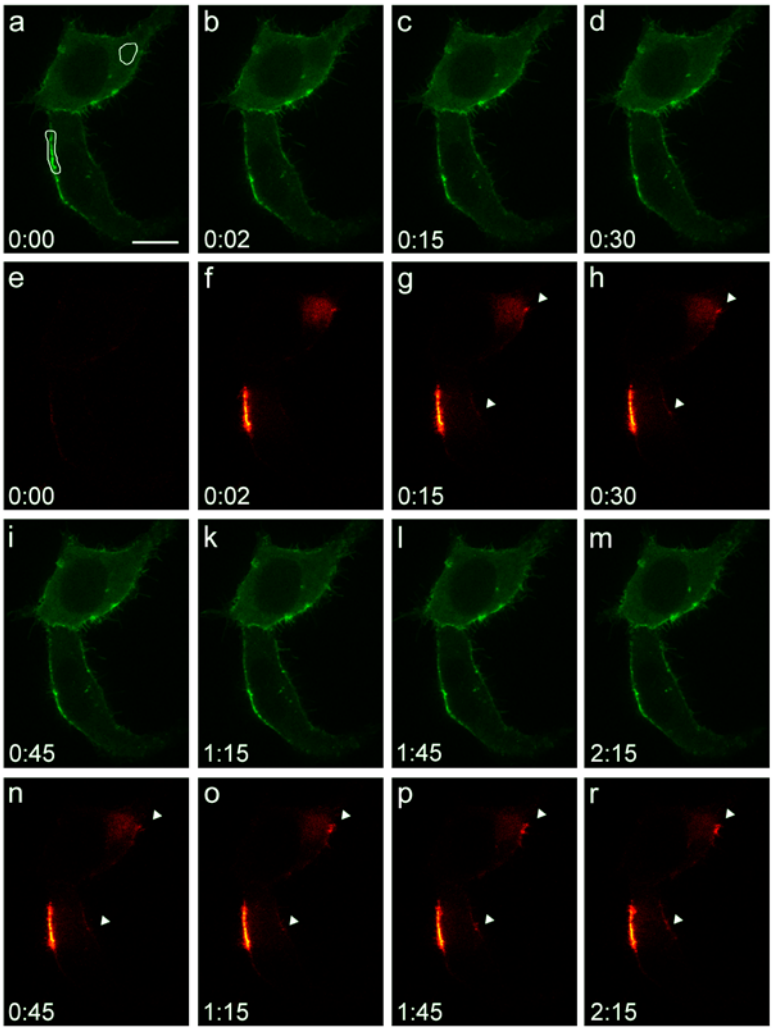


**Figure 18 Tracking of the mobility of IRSp53 in HEK293 cells using the photoconvertable fluorescent protein Kaede.** HEK293 cells expressing a Kaede-IRSp53 fusion were subjected to live-cell imaging using settings for green (a-d, i-m) and red (e-h, n-r) fluorescence. After an initial image was taken at time 0, the areas indicated by white circles were irradiated using a 405 nm laser to convert green into red fluorescence. During the observation time red fluorescent IRSp53 displays high mobility, as a part accumulates at the membrane as well as membrane-associated IRSp53 seems to migrate to the other side of the cell (indicated by white arrows). Scale bar: 20 µm.

But how mobile is IRSp53 in living hippocampal neurons? Initially, the co-localisation of either the Kaede-IRSp53 fusion or GFP-tagged IRSp53 with mRFP-Shank3 was verified (Figure 19). Both IRSp53 fusion proteins overlap nicely with the postsynaptic marker mRFP-Shank3. A remarkably difference is seen in the fluorescence intensity between the Kaede- and GFP-tagged IRSp53. The fluorescent signal of the Kaede-IRSp53 fusion is low compared to the fluorescent signal of the GFP tagged IRSp53, which might reflect different expression levels. A diffuse cytosolic localisation is visible in neurons expressing GFP-IRSp53.

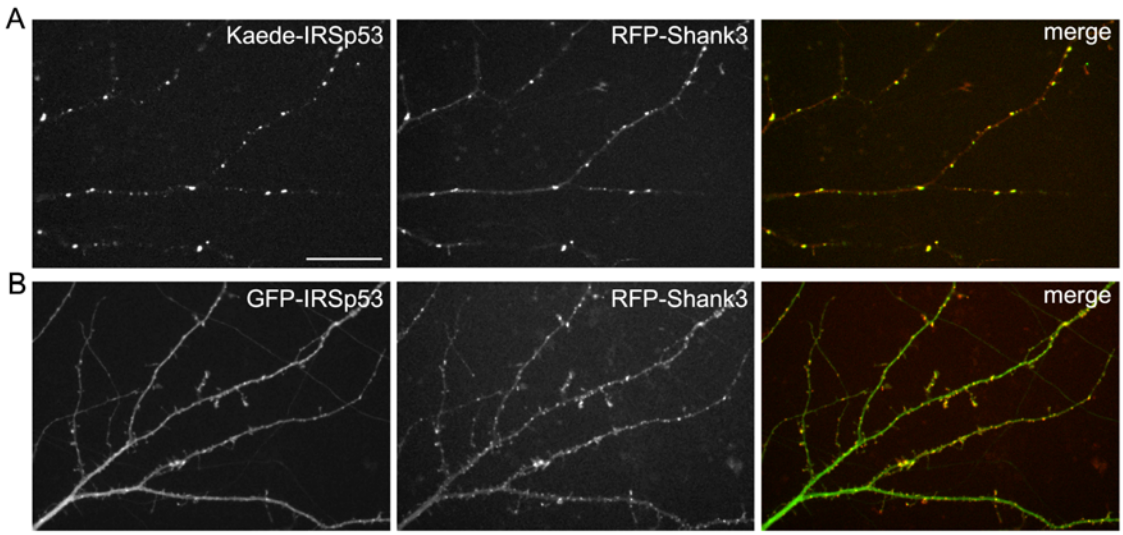


**Figure 19 Co-localisation of Kaede- and GFP-tagged RSp53 with Shank3 in living primary hippocampal neurons.** Living primary hippocampal neurons transfected at 13 DIV with RFP-ProSAP2 (RFP-Shank3) and Kaede-IRSp53 or GFP-IRSp53 were imaged at 14 DIV. [A] Kaede-IRSp53 co-localises with the postsynaptic mRFP-Shank3. [B] GFP-tagged IRSp53 co-localises with mRFP-Shank3. Scale bar: 20 µm.

Primary hippocampal neurons, transfected at 13 DIV with Kaede-tagged IRSp53, were analysed by live-cell imaging at 14 DIV. A suitable dendrite was monitored over a period of at least 5 min after conversion of green to red fluorescence. Due to low cytosolic Kaede-IRSp53 fluorescence signals only the mobility of IRSp53 accumulated at synapses was investigated. Tracking of red fluorescent IRSp53 exhibits almost no movement of IRSp53 anchored at synapses (Figure 20). During the observations a high mobility of green fluorescent Kaede-tagged IRSp53 was visible within thick dendrites. Because of the weak fluorescent signal of the diffuse cytosolic Kaede-IRSp53 the experiments were repeated expressing GFP-tagged IRSp53. There again, no movement of either cytosolic or synaptic IRSp53 was visible.

Hori *et al.* (2005) observed that IRSp53 is targeted to synapses under NMDA receptor stimulation. They describe that neurons were stimulated for 3 min with NMDA and glycin followed by fixation with 4% PFA. Through immunocytochemical staining of overexpressed IRSp53 and endogenous PSD95 the percentage of IRSp53 positive PSD95 clusters was determined (Hori *et al*., 2005). Based on these findings, the mobility of IRSp53 was observed upon NMDA receptor stimulation. Hence, neurons expressing the GFP-IRSp53 fusion protein were stimulated with 50 µM NMDA and 10 µM glycin in oxygenated ACSF and green fluorescent IRSp53 was tracked (Figure 21). At these conditions, no alteration of the synaptic IRSp53 signal was detectable after NMDA receptor stimulation. Moreover, cytosolic IRSp53 does not show altered mobility or accumulation at dendritic sites after addition of the stimulants. Nevertheless, the dendrites start to swell after approximately 3 minutes, which indicates the beginning of neuronal cell death. Thus, I could not reproduce here the NMDA receptor dependent translocation of IRSp53 to postsynaptic sites.

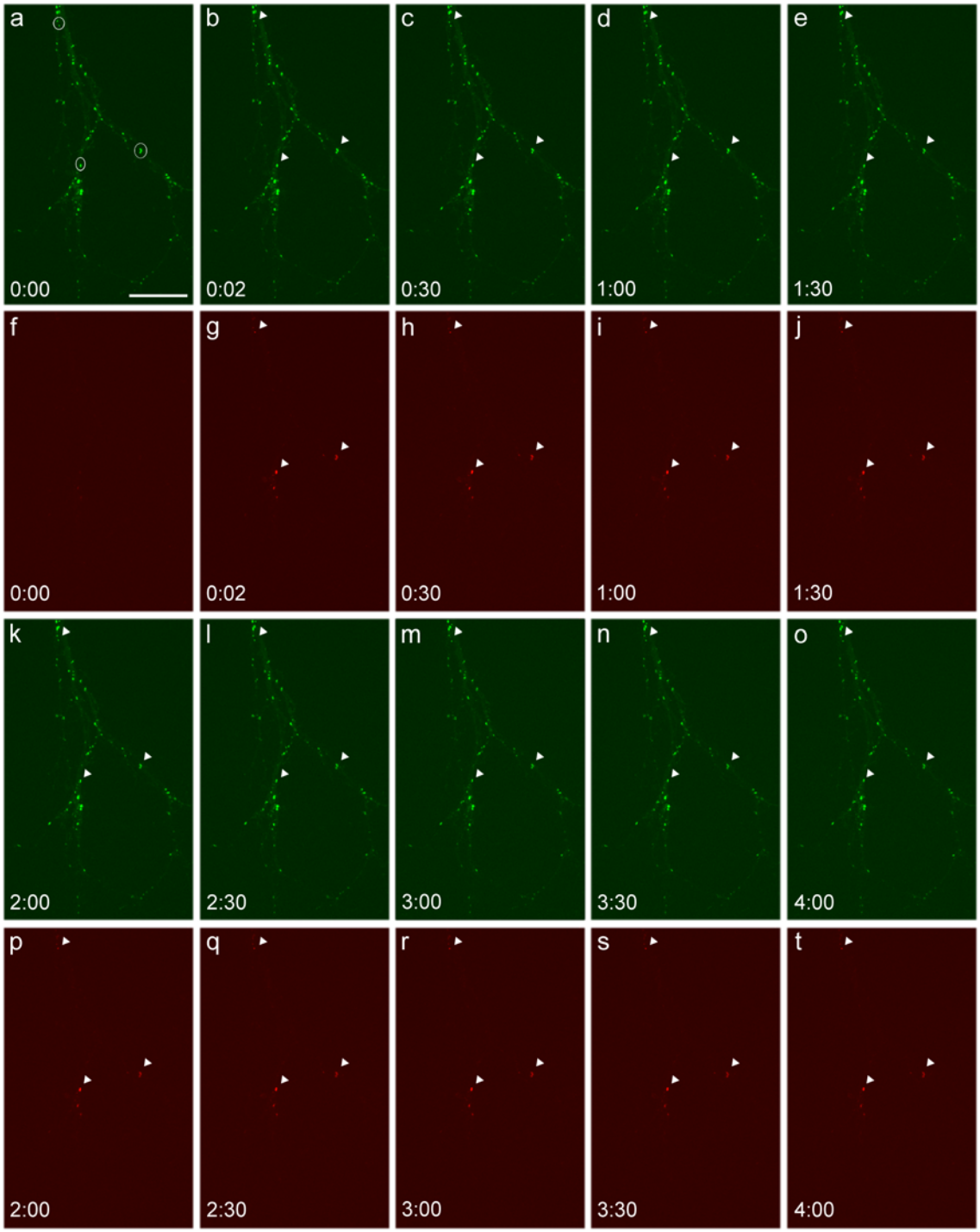


**Figure 20 Live-cell imaging of Kaede-tagged IRSp53 in primary hippocampal neurons.** Live-cell imaging at 14 DIV of primary hippocampal neurons, transfected at 13 DIV with a vector coding for Kaede-tagged IRSp53. Neurons expressing Kaede-IRSp53 fusion were subjected to live-cell imaging using settings for green (a-e, k-o) and red (f-j, p-t) fluorescence. After an initial image was taken at time 0, three areas indicated by white circles were irradiated using a 405 nm laser for a fluorescence conversion from green to red. Monitoring of red fluorescent IRSp53 over the time exhibits almost no mobility of IRSp53 accumulated at synapses (indicated by white arrows). Scale bar: 20 µm.

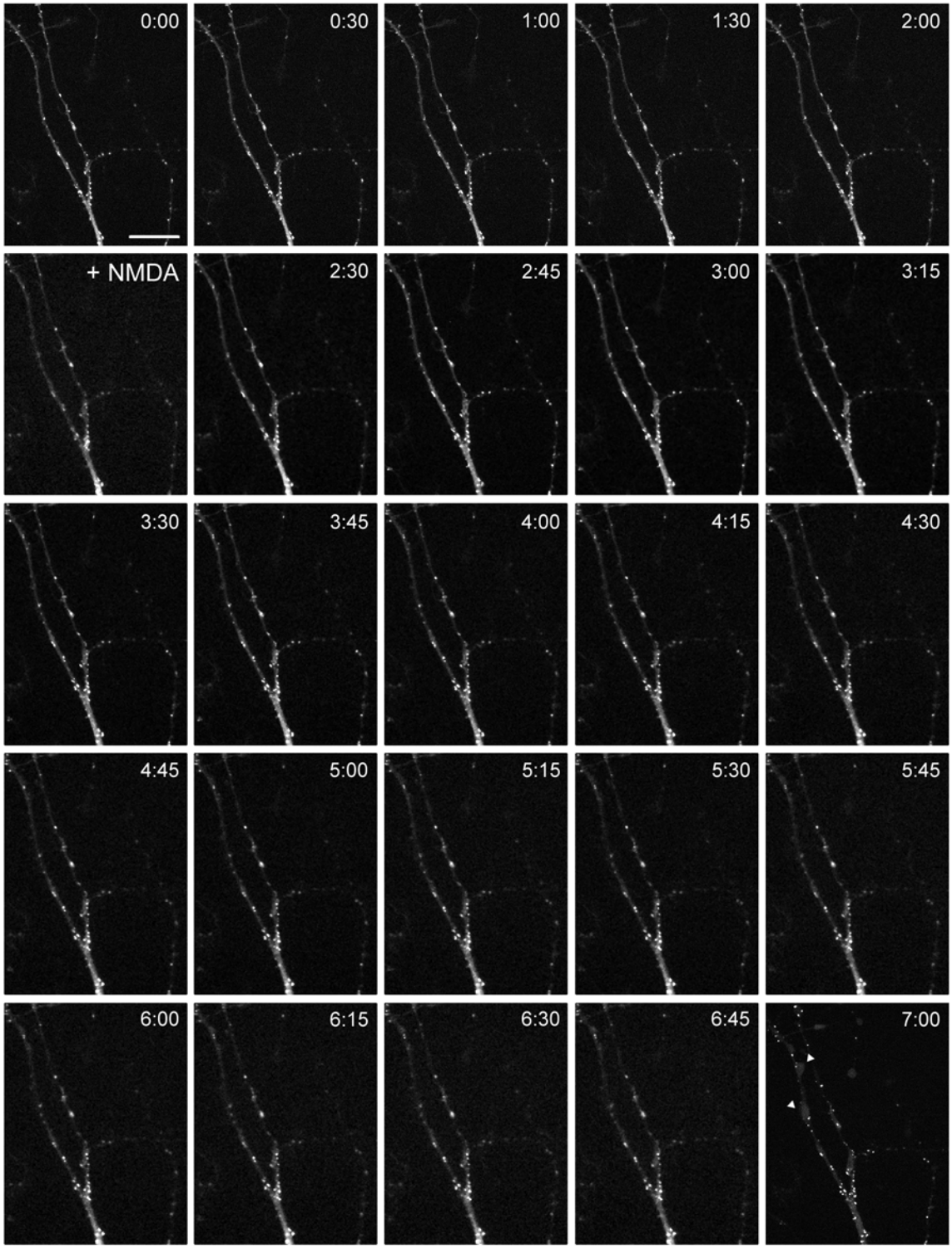


**Figure 21 Live-cell imaging of GFP-tagged IRSp53 in primary hippocampal neurons following NMDA stimulation.** Live-cell imaging of primary hippocampal neurons at 14 DIV, transfected at 13 DIV with a vector coding for GFP-tagged IRSp53. Neurons expressing GFP-IRSp53 fusion were subjected to live-cell imaging monitoring green fluorescence prior and after addition of 50 µM NMDA and 10 µM glycine (as indicated). Almost no movement of IRSp53 accumulated at synapses prior and after NMDA receptor stimulation was observed. However, swelling of dendrites (indicated by white arrows) was clearly seen starting after about 3 min. Scale bar: 20 µm.

## 3.8 Analysis of an altered PSD composition in different forebrain regions of IRSp53 haploinsufficient and deficient mice

Alterations in the composition of the PSD have been observed in IRSp53 null-mice. In particular an increase in the NMDA receptor subunits GluN1, GluN2A and GluN2B as well as Densin-180 in the PSD derived from the whole brain was detected (Sawallisch *et al.* 2009). However, NMDA receptor amounts in whole brain and hippocampal tissue lysates were unchanged (Kim *et al.*, 2009). To analyse this in further detail, I analysed 5 representative postsynaptic proteins known to be involved in cognition according to their postsynaptic targeting in the cortex, hippocampus and striatum of wt, IRSp53 +/d and d/d mice. The proteins analysed are the NMDA receptor subunit GluN1, the AMPA receptor subunit GluA1, members of the Shank protein family, PSD95 and SynGAP.

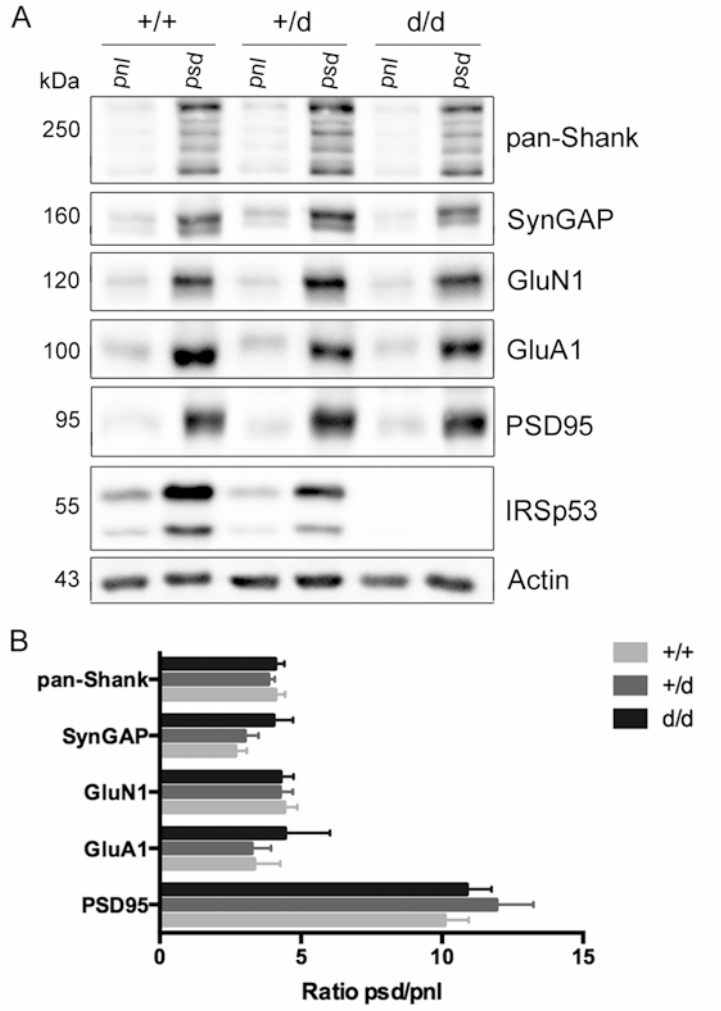


**Figure 22 Postsynaptic accumulation of selected PSD proteins in the cortex of wt, IRSp53 hapoinsufficient and deficient mice.** [A] Post-nuclear lysates (pnl) and PSD fractions (psd) of the cortex from the different genotypes were analysed by western blot using the antibodies indicated. [B] Quantification of the different analysed proteins demonstrates no differences in their postsynaptic enrichment (ratio psd/pnl) in the cortex of IRSp53 +/d and d/d mice compared to wt littermates (n = 8).

Cortical PSDs show no changes of enrichment factors (ratio psd/pnl) of the postsynaptic proteins investigated comparing all three genotypes (Figure 22). Both the total protein amount (pnl fraction) and the relative accumulation in the PSD fraction were unaltered.

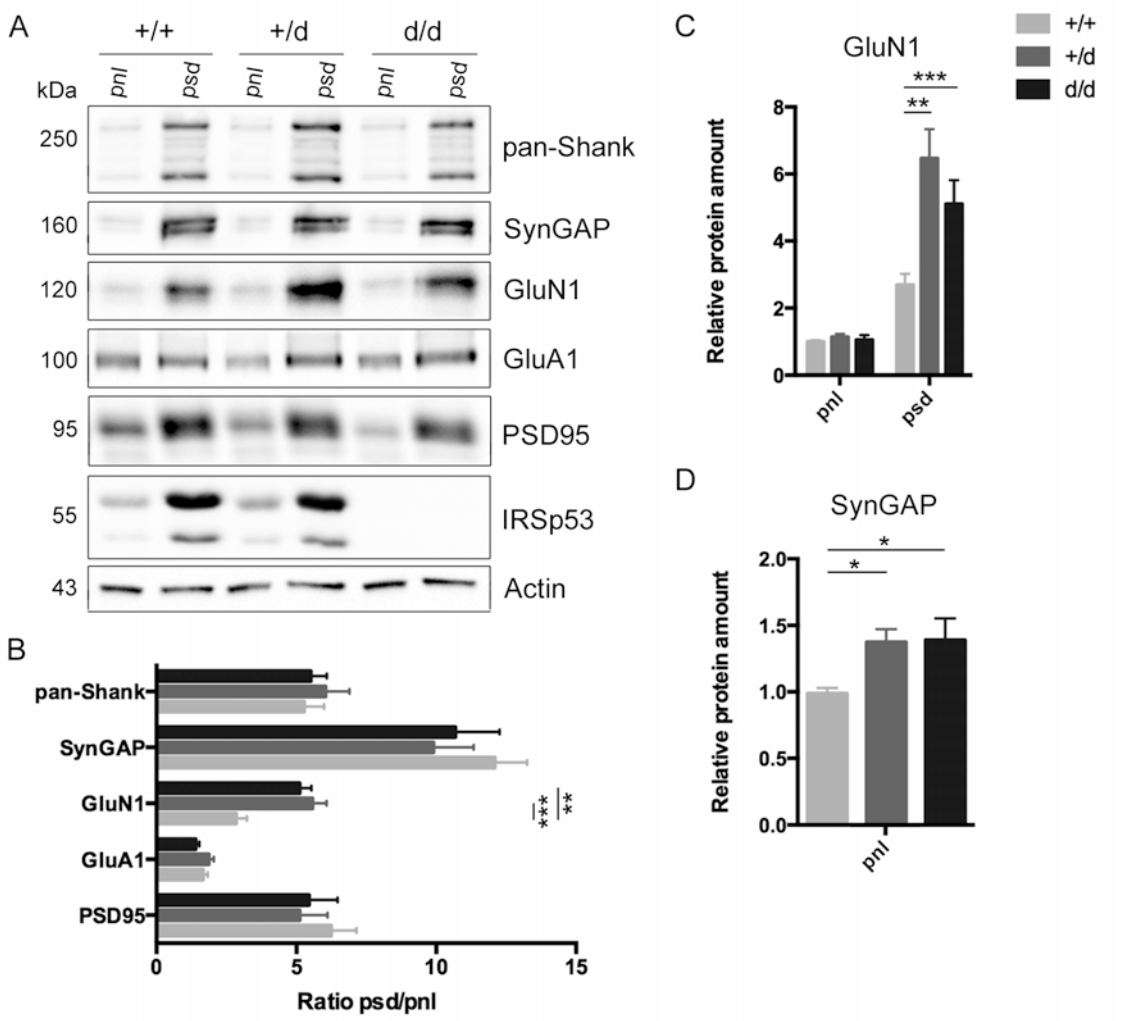


**Figure 23 Postsynaptic accumulation of selected PSD proteins in the hippocampus of wt, IRSp53 haploinsufficient and deficient mice.** [A] Post-nuclear lysates (pnl) and PSD fractions (psd) of the hippocampus from the different genotypes were analysed by western blot using the antibodies indicated. [B] Quantification shows a significant increase in the synaptic enrichment (ratio psd/pnl) of GluN1 in IRSp53 +/d and d/d mice compared to wt littermates (n = 10; Two-way ANOVA: +/d $p < 0.0002$, d/d $p = 0.0022$). All other analysed postsynaptic proteins exhibit no differences in their enrichment. [C] Detailed evaluation of hippocampal GluN1 protein levels in pnl and PSD fractions (psd) from the different genotypes. GluN1 protein levels show a significant increase only in the psd fraction and not in the pnl (Two-way ANOVA: psd +/d $p < 0.0001$ and d/d $p = 0.0012$). [D] Detailed quantification of the pnl of hippocampal SynGAP protein levels depicts a significant increase in IRSp53 +/d and d/d mice compared to wt littermates (Mutipe t-test: pnl +/d $p = 0.0435$ and d/d $p = 0.0302$).

PSD fractionation of the hippocampus (Figure 23) shows no changes in the synaptic accumulation of GluA1, the Shank proteins, PSD95 and SynGAP. However, postsynaptic enrichment of the NMDA receptor subunit GluN1 is significantly increased in IRSp53 haploinsufficient and deficient mice to levels up to 200%, while the pnl levels remain constant. The GluN1 protein levels in the PSD increases significantly for both +/d and d/d IRSp53 mice to levels up to 200%. This indicates an altered subcellular distribution of NMDA receptors in IRSp53 +/d and d/d mice. Interestingly, the relative protein amount of SynGAP rises to about 140% in the pnl in IRSp53

haploinsufficient and deficient mice compared to wt littermates, whereas PSD levels and the psd/pnl ratio are unaffected.

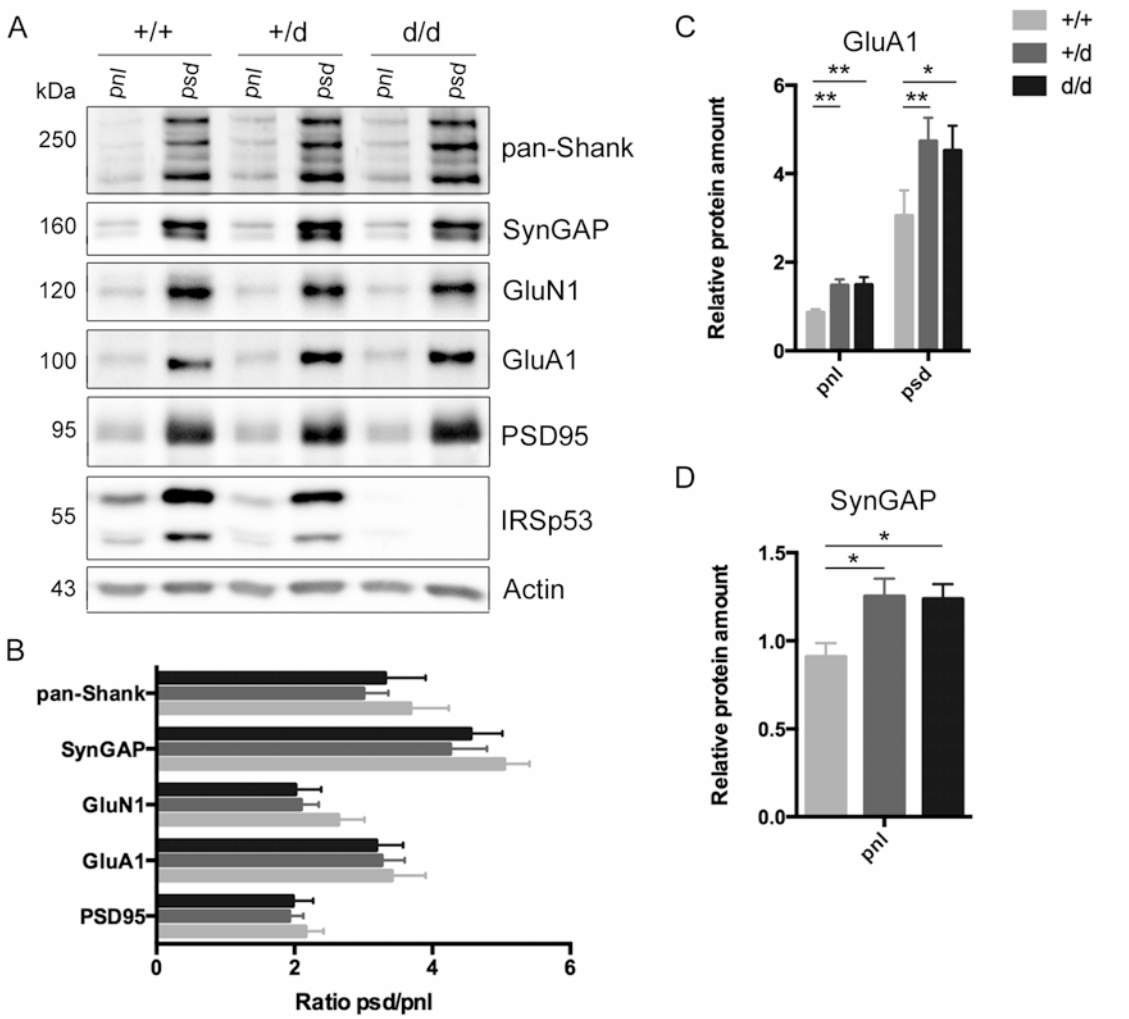


**Figure 24 Postsynaptic accumulation of selected PSD proteins in the striatum of wt, IRSp53 haploinsufficient and deficient mice.** [A] Post-nuclear lysates (pnl) and PSD fractions (psd) of the striatum from the different genotypes were analysed by western blot using the antibodies indicated. [B] Quantitative analysis demonstrates no differences in the postsynaptic enrichment (psd/pnl) of the different analysed proteins in the striatum of IRSp53 +/d and d/d mice compared to wt littermates (n = 4). [C] Detailed evaluations of the pnl and PSD of striatal GluA1 protein levels exhibit a significant increase in both cases of IRSp53 +/d and d/d mice (Two-way ANOVA: pnl +/d $p = 0.0018$ and d/d $p = 0.0019$, psd +/d $p < 0.0094$ and d/d $p = 0.0028$). [D] Detailed quantification of the striatal pnl of IRSp53 +/d and d/d mice demonstrates a significant increase of the protein SynGAP compared to wt littermates (Two-tailed unpaired t-test: pnl +/d $p = 0.0298$ and d/d $p = 0.0168$).

Striatal PSD preparations reveal no changes in postsynaptic enrichment (ratio psd/pnl) of the investigated proteins comparing all three genotypes (Figure 24). Remarkably, evaluation of the relative pnl and psd protein levels of GluA1 shows a ≈ 60% significant increase in both IRSp53 +/d and d/d mice. It appears therefore that the GluA1 containing AMPA receptor levels are increased at excitatory synapses in the striatum due to the reduction or loss of IRSp53. As observed for the hippocampus, SynGAP levels rise up to 130% in the pnl in IRSp53 +/d and d/d mice compared to wt littermates, but PSD levels and the enrichment factors are unchanged.

The NMDA receptor consists of 4 subunits: two obligatory GluN1 subunits and two receptors modulatory GluN2 subunits. Two major GluN2 isoforms are GluN2A and GluN2B affecting the kinetics of the NMDA receptors (Dingledine *et al.*, 1999; Sanz-Clemente *et al.*, 2013). In this respect it is important to know whether the GluN2A and GluN2B levels are altered in the PSD of the forebrain regions examined. Therefore, PSDs from the cortex, hippocampus and striatum of wt, IRSp53 +/d and d/d mice were analysed by western blot using subunit specific antibodies. Relative protein amounts were normalised against the housekeeping protein β-actin and further standardised to wt protein levels (Figure 25).

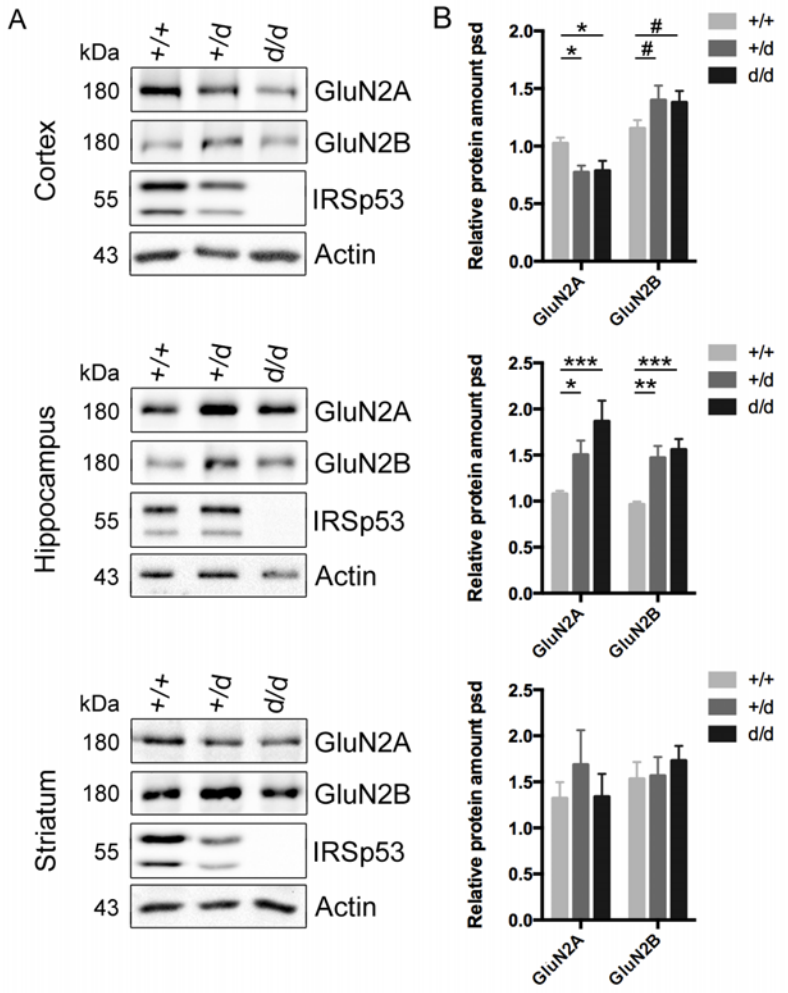


**Figure 25 Analysis of the NMDA receptor subunits in the PSD of different forebrain regions of wt, IRSp53 haploinsufficient and deficient mice.** [A] NMDA receptor subunits in the PSD of the cortex, hippocampus and striatum from the different genotypes were analysed by western blot using the antibodies indicated. [B] Quantitative analysis of cortical NMDA receptor subunit composition demonstrates a significant reduction of the subunit GluN2A, but an increase of GluN2B in IRSp53 +/d and d/d mice compared to wt littermates (n = 8; Two-way ANOVA: GluN2A +/d p = 0.0215 and d/d p = 0.0331, GluN2B +/d p = 0.0614 and d/d p = 0.0929). In the hippocampus GluN2A and GluN2B protein levels show a significant increase in IRSp53 +/d and d/d animals (n = 10; Two-way ANOVA: GluN2A +/d p = 0.0219 and d/d p < 0.0001, GluN2B +/d p = 0.0037 and d/d p = 0.0003). Quantification of striatal GluN2A and GluN2B protein levels demonstrates no differences between all genotypes (n = 4).

In the cortex of IRSp53 haploinsufficient and deficient mice the GluN2A subunit decreases significantly to roughly 80% compared to wt mice, whereas the GluN2B subunit of both genotypes is increased to roughly 130%. A different situation emerges in the hippocampus. Here, the levels of GluN2A and GluN2B increase significantly as already observed for GluN1 to levels of about 150% in both IRSp53 +/d and d/d animals. Quantification of the striatal NMDA receptor subunit composition exhibits no differences between all genotypes.

In summary it can be said, that the postsynaptic composition is not altered in the cortex, but significant changes are observed in the hippocampus and striatum with respect to ionotropic glutamate receptor subunits. On the one hand, NMDA receptors represented by the subunit GluN1 are increased in the hippocampal PSD while pnl levels remain constant. On the other hand, in the striatum the GluA1 containing AMPA receptors are increased in the pnl and PSD fraction. Moreover, in both brain regions the total amount of SynGAP was enhanced, but no changes were found in the PSD. The analysis of the NMDA receptor composition in the PSD derived from the cortex, hippocampus and striatum reveals a more differentiated picture. In the cortex, GluN2A containing NMDA receptors are apparently exchanged by GluN2B containing NMDA receptors of IRSp53 +/d and d/d mice compared to wt littermates. On the contrary, in the hippocampus all investigated NMDA receptor subunits increase and subsequently the number of NMDA receptors located at the postsynapse must be enhanced.

## 3.9 Analysis of glutamate receptor surface expression

An increased NMDA receptor amount in the PSD of the hippocampus raises the question whether the NMDA receptor targeting to the cell surface is changed. In mature neurons the NMDA receptors are stabilised at the PSD by PSD95 (Roche et al., 2001). IRSp53 and the NMDA receptor bind to the same PDZ domain of PSD95 (Konrau *et al.*, 1995; Soltau *et al.*, 2004). Thus IRSp53 could occupy the PDZ domain of PSD95, thereby preventing the NMDA receptor stabilisation at the PSD. If this is the case, IRSp53 overexpression in wt primary cortical cultures should result in a reduced NMDA receptor localisation at the surface. As transfection methods for neuronal cultures are inefficient and do not allow biochemical studies, I attempted gene delivery into neurons by a recombinant adeno-associated virus (rAAV) system. To selectively label receptors located at the surface the method of cell surface biotinylation adopted from Roche *et al.* (2001) was applied using PM impermeable biotin reagent.

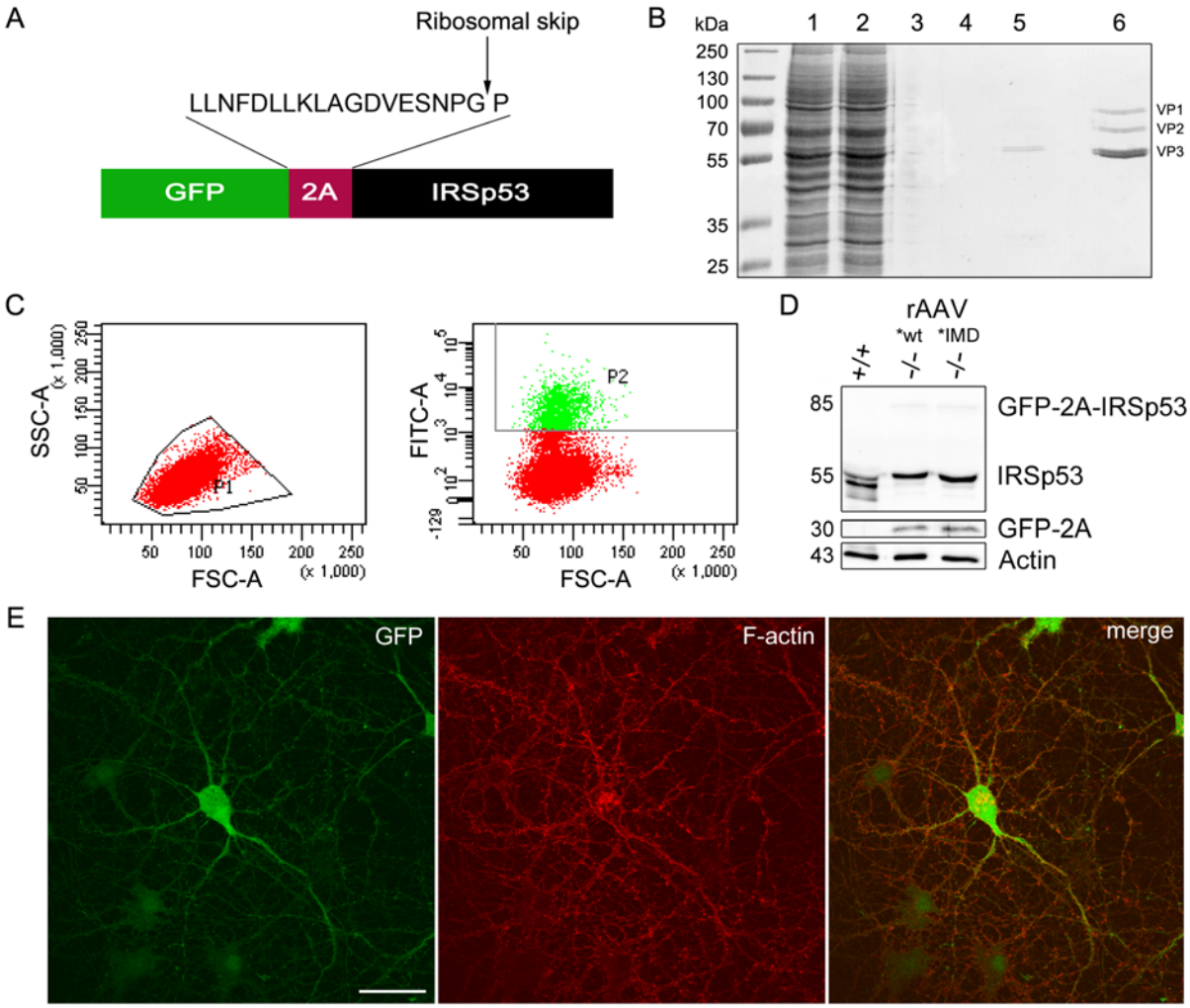


**Figure 26 Establishment of rAAV-mediated expression of IRSp53.** [A] Scheme of the coding sequence of the rAAV based expression construct. The coding sequence of GFP is fused to cDNA coding for the *Thosea asigna* viral 2A peptide, followed by the *IRSp53* cDNA. The 2A peptide induces a ribosomal skip mechanism, resulting in the expression of a GFP-2A peptide fusion and IRSp53, which differs from the native protein only by an N-terminal prolin residue. [B] Coomassie stained SDS-Page of fractions obtained during purification of viral particles from HEK293T cells lysates (lane 1, 2) after several washing steps (lane 3, 4) and elution by a salt gradient (lane 5). Finally, viral particles were desalted and concentrated (lane 6). The position of the viral capsid proteins (VP1 – 3) is indicated. [C] Infectious titre was quantified by FACS analysis; HEK293 cells were infected with rAAV and the number of GFP positive cells (P2) were counted compared to the total cell population (P1). [D] Western blot analysis of rAAV infected hippocampal slices of IRSp53 deficient mice compared to slices of wt animals. IRSp53 levels of wt slices are comparable to those in rAAV infected ko slices (both wt and IMD mutant). Both the recombinant IRSp53 and the GFP-2A peptide fusion are produced at the predicted molecular weights, indicating efficient pseudo-termination at the 2A peptide sequence. [E] Primary hippocampal neurons infected at 2 DIV with rAAV coding for GFP-2A peptide and IRSp53 were fixed at 14 DIV and stained against F-actin by the toxin Phalloidin labelled with TRIC. Endogenous GFP fluorescence demonstrates efficient infection of hippocampal neurons by rAAVs of mixed serotype 1and 2. Scale bar: 30 µm.

Initially, IRSp53 constructs were designed allowing the expression of two separate proteins from one open reading frame (ORF) to either express GFP as a fluorescent marker and an almost native IRSp53. This can be achieved by the use of the viral 2A peptide tool that induces a

ribosomal skip mechanism (Donnelly *et al.*, 2001). In this study, I used the *2A peptide*-coding sequence from the *Thosea asigna* virus (Pringle *et al.*, 1999; Tang *et al.*, 2009) inserted between the cDNA coding for the GFP and the IRSp53. This chimeric ORF results in the expression of a GFP-2A peptide fusion and IRSp53, which differs from the native protein only by a N-terminal prolin residue (Figure 26 A). The *GFP-2A-IRSp53* gene cassette was then transferred into a rAAV-shuttle vector necessary for viral production. Viral production was performed in HEK293T cells by co-transfection of the rAAV-shuttle vector with the helper vector and the two packaging vectors encoding the capsid proteins for serotype 1 and 2 using calcium-phosphate transfection. A mixed serotype 1 and 2 was used because of an efficient and easy purification with heparin columns enabled by serotype 2 and a high transduction efficiency of various cell types through serotype 1 (Burger *et al.*, 2004; Burova & Ioffe, 2005; Osten *et al.*, 2007). Successful heparin column based purification followed by a rAAV particle concentration was documented by SDS-Page followed by Coomassie staining (Figure 26 B). The infectious titre was determined by FACS analysis, allowing for the control of the expression levels in different experiments as well as between different virus preparations (Figure 26 C). Preliminary tests in hippocampal slices and primary neurons demonstrate efficient pseudo-termination (Figure 26 D) and neuronal infection (Figure 26 E).

Using the established rAAV based gene delivery system, a weak but uniform overexpression detectable by GFP was achieved transducing primary cortical neurons at 2 DIV. NMDA and AMPA receptor surface expression was then analysed by cell surface biotinylation of premature neurons at 7 DIV and mature neurons at 12 DIV adopted from Roche *et al.* (2001) (Figure 27). Therefore, cell surface receptors were biotinylated with PM impermeable biotin reagent, followed by precipitations from cell lysates using streptavidin agarose. Input and precipitate samples were analysed by western blot. On the one hand, the relative receptor amount in the input was calculated through normalisation against β -actin and further standardisation to the GFP control experiment. On the other hand, relative surface expression was evaluated by calculating the ratio between the precipitate and the input. At 7 DIV the relative receptor amount of GluN1 increases significantly whereas the surface localisation significantly drops down from 50% to approximately 30% in IRSp53 overexpressing neurons compared to the GFP control. GluA1 containing AMPA receptors are not affected. At 12 DIV the total cellular amount of both GluN1 and GluA1 following IRSp53 overexpression adjusts to levels of the GFP control experiment. However, the surface expression of GluN1 and GluA1 significantly declines in mature neurons overexpressing IRSp53.

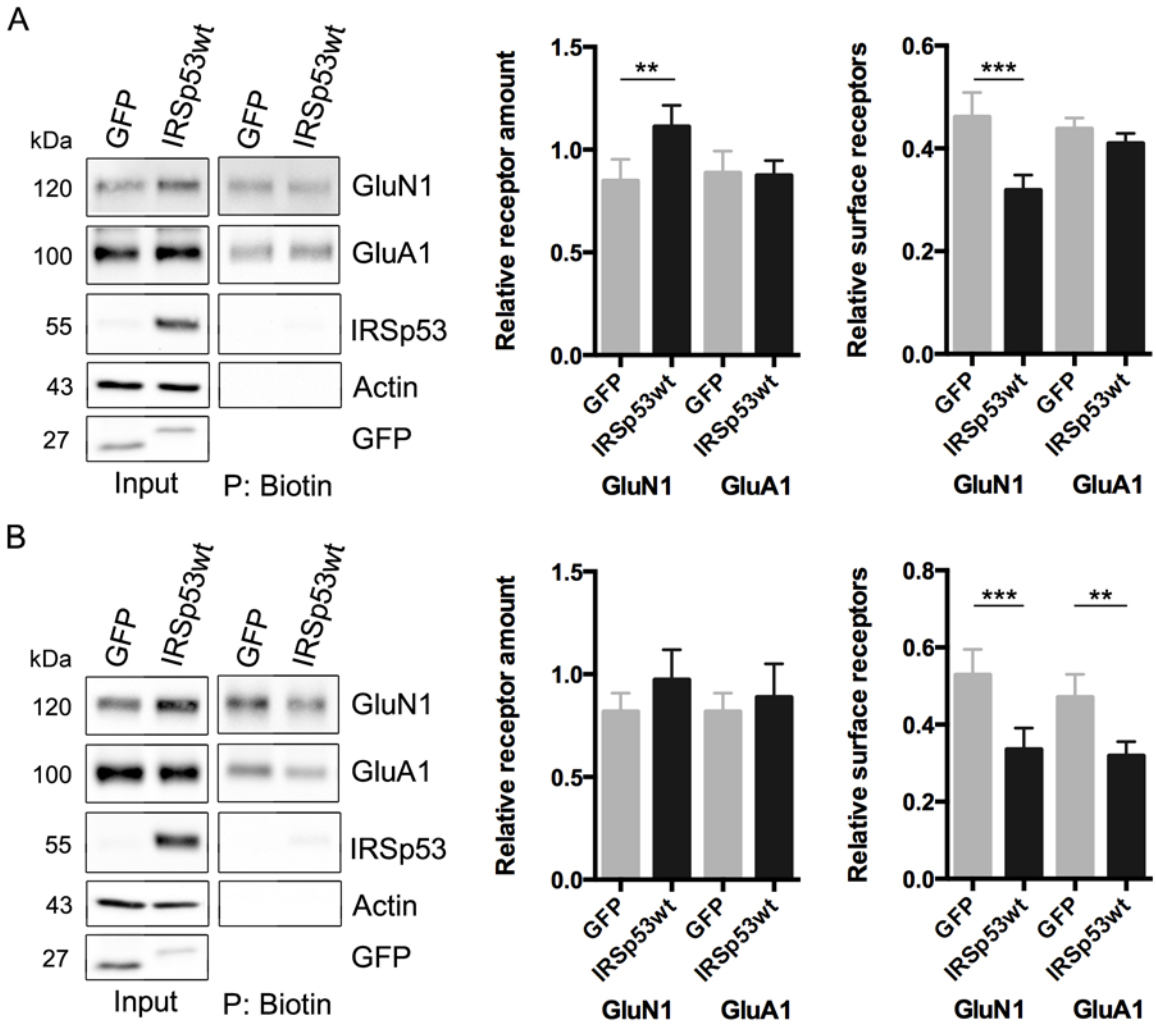


**Figure 27 Surface expression of NMDA and AMPA receptors after IRSp53 overexpression in primary cortical neurons.** Primary cortical neurons were infected at 2 DIV with rAAV coding for GFP or GFP-2A-IRSp53wt. Cell surface receptors were biotinylated either [A] at 7 DIV or [B] at 12 DIV. After cell lysis the biotin labelled proteins were precipitated by streptavidin agarose. Input and precipitate (P) were analysed by western blot using the antibodies indicated. [A, B] Relative surface expression was evaluated by calculating the ratio between the precipitate and the input. [A] Quantitative analysis of the 7 DIV data shows for GluN1 a significant increase of the total receptor amount in the input and a significant decrease at the cell surface after overexpression of IRSp53, whereas GluA1 containing receptors are unaltered (n = 7, Two-way Repeated-measurement ANOVA: input p = 0.0083, IP p = 0.0005). [B] Quantification of the 12 DIV data shows no changes of the NMDA and AMPA receptor amounts in the inputs, but a decreased surface expression for both following IRSp53 overexpression (n = 7, Two-way Repeated-measurement ANOVA: GluN1 p = 0.0008, GluA1 p = 0.0067).

In a next step, I examined whether a specific domain of IRSp53 is responsible for the described changes. NMDA and AMPA receptor surface expression was evaluated by cell surface biotinylation of immature neurons at 7 DIV (Figure 28) overexpressing wt and mutant IRSp53 as described above. The increase in the amount of total cellular GluN1 achieved by overexpression of wt IRSp53 was also observed when individual domains of IRSp53 are disrupted. The relative GluN1 surface expression remains constant at ≈ 30% for the IM and CRIB domain mutation as

already seen for the overexpression of wt IRSp53. Interestingly, the surface levels are decreased further to about 25% when IRSp53*SH3 and IRSp53*PDZ mutants are overexpressed. Surprisingly, by overexpressing IRSp53, where the IMD, SH3 domain or PDZL is inactivated, relative surface receptor amount decreases significantly for GluA1 containing AMPA receptors. Nevertheless, GluA1 input levels remain constant.

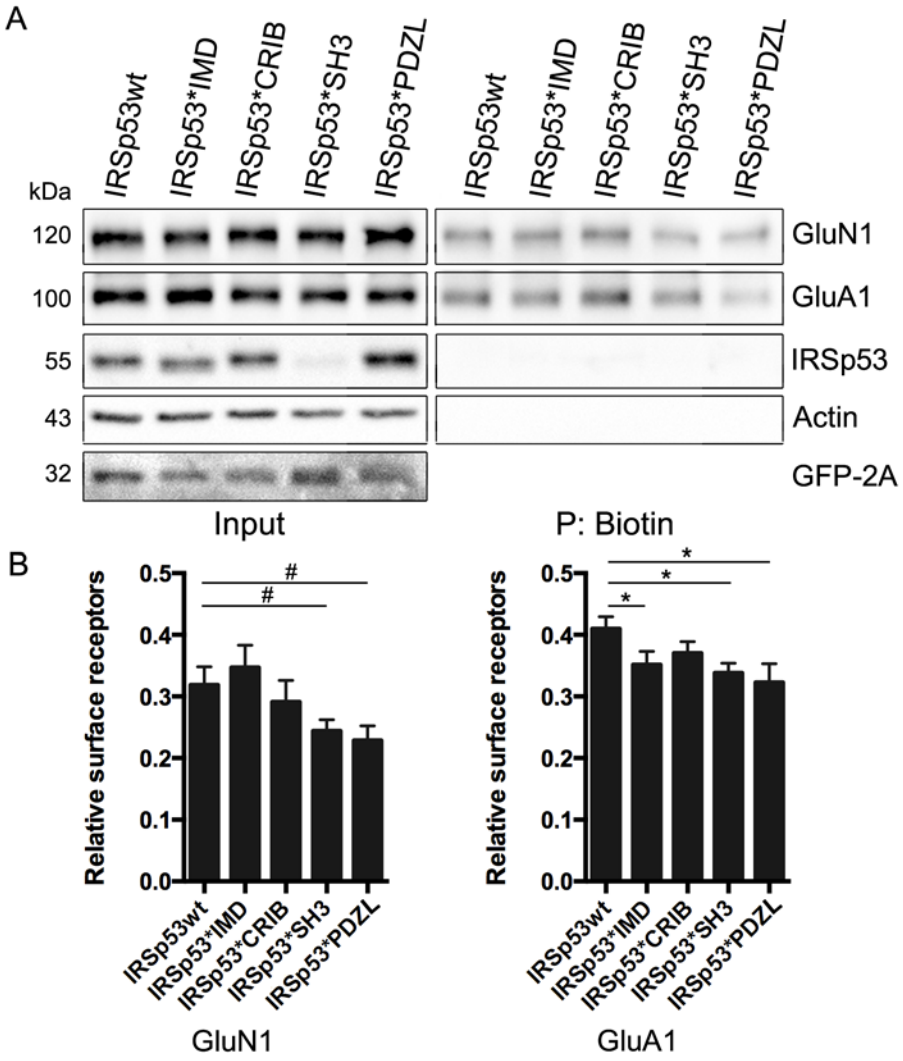


**Figure 28 Surface expression of NMDA and AMPA receptors of immature primary cortical neurons after overexpression of wt and mutant IRSp53.** [A] Primary cortical neurons were infected at 2 DIV with rAAVs coding for GFP-2A- and IRSp53wt or IRSp53 mutants. Cell surface receptors were biotinylated at 7 DIV and after cell lysis the biotin labelled receptors were precipitated by streptavidin agarose. Input and precipitate (P) were analysed by western blot using the antibodies indicated. The IRSp53 antibody fails to recognise the IRSp53*SH3 mutant; for explanation see text. [B] Relative surface expression was evaluated by calculating the ratio between the precipitate and the input. Quantification of the relative surface receptor amount shows no significant differences for GluN1 surface expression but a tendency for a decline in the GluN1 surface expression due to an inactivation of the SH3 domain and the PDZL (n = 7, One-way Repeated-measurement ANOVA: IRSp53*SH3 p = 0.0659, IRSp53*PDZ p = 0.0690). GluA1 surface expression is reduced for IRSp53 mutants of the IM and SH3 domain as well as for the PDZ binding motif compared to wt IRSp53 (n = 7, One-way Repeated-measurement ANOVA: IRSp53*IMD p = 0.0393, IRSp53*SH3 p = 0.0309, IRSp53*PDZ p = 0.0275).

Overexpression of the IRSp53*SH3 mutant could not be verified using the IRSp53 antibody (see Figure 28 A). This antibody was raised against the SH3 domain of IRSp53 for immunisation and thus failed to detect IRSp53*SH3. To exclude a lack of expression of the *IRSp53*SH3* mutant construct, GFP-tagged IRSp53 fusions of wt and I403P mutant were expressed in HEK293 cells and after cell lysis detected either by a GFP or the IRSp53 antibody in an immunoblot. The GFP-tagged IRSp53*SH3 mutant is detected by an antibody against GFP at the correct molecular weight but not by the antibody against IRSp53. Thus, the IRSp53*SH3 mutant can be expressed efficiently, but the anti-IRSp53 antibody fails to bind to the mutated SH3 domain of IRSp53 (data not shown).

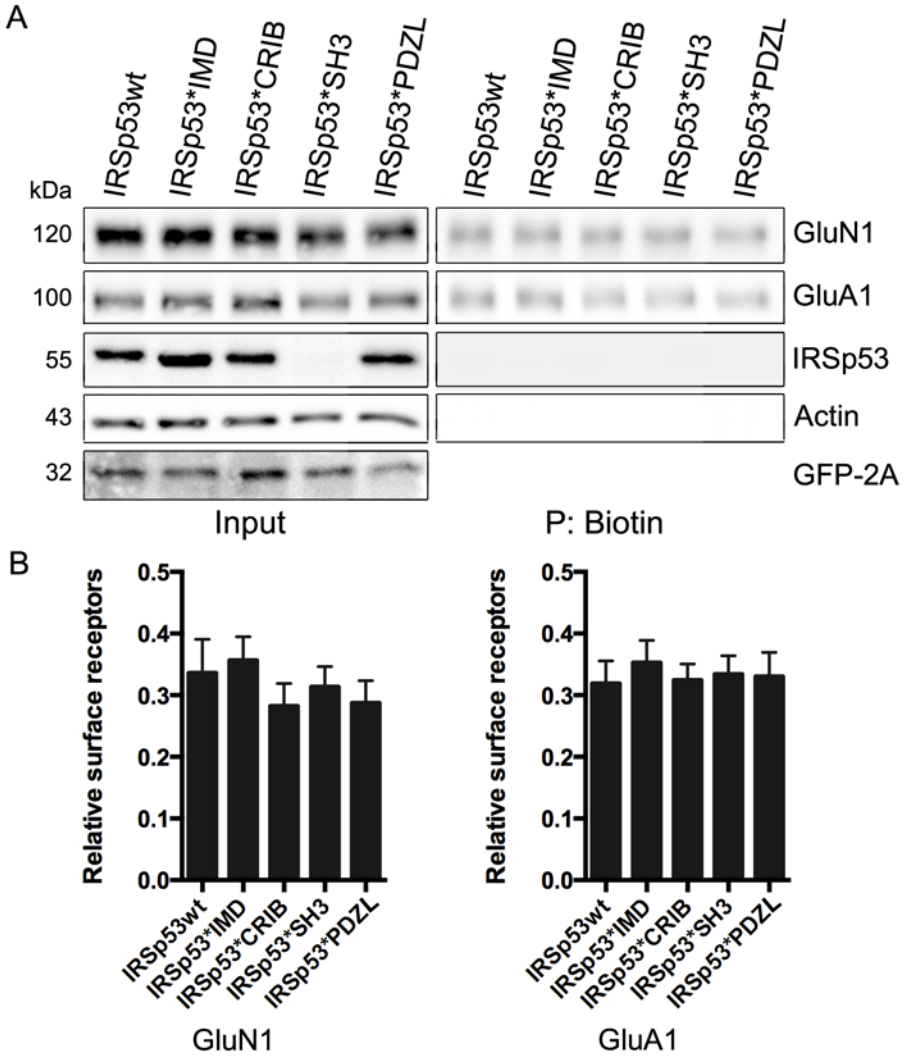


**Figure 29 Surface expression of NMDA and AMPA receptors of mature primary cortical neurons after overexpression of wt and mutant IRSp53.** [A] Primary cortical neurons were infected at 2 DIV with rAAVs coding for GFP-2A- and IRSp53wt or IRSp53 mutants. Cell surface receptors were biotinylated at 12 DIV and after cell lysis the biotin labelled receptors were precipitated by streptavidin agarose. Input and precipitate (P) were analysed by western blot using the antibodies indicated. [B] Relative surface expression was evaluated by calculating the ratio between the precipitate and the input. Quantification of the relative surface receptor amount shows no differences for both GluN1 and GluA1 comparing cells expressing wt IRSp53 and the mutant variants (n = 7).

Almost mature primary neurons (12 DIV) overexpressing the IRSp53 mutant constructs show neither differences in the relative receptor amount nor in the surface localisation of both GluN1 and GluA1 compared to cells overexpressing wt IRSp53 (Figure 29). Thus, the decreased surface expression of NMDA and AMPA receptors observed for wt IRSp53 overexpression compared to the GFP control cannot be attributed to a particular domain.

In conclusion, overexpressing IRSp53 in developing primary neurons alters the total number of NMDA receptors as well as their surface expression. In almost mature cultured neurons the total receptor amount of NMDA and AMPA receptors remains unchanged while the surface expression is reduced for both. However, these effects cannot be assigned to a specific functional domain of IRSp53.

Vice versa, the NMDA and AMAR receptor surface expression was investigated in the context of IRSp53 haploinsufficiency and deficiency (Figure 30). For this purpose, the cell surface biotinylation method was adapted to acute hippocampal slices. Prior to cell surface biotinylation the acute slices were allowed to rest in oxygenated ACSF for approximately 4 h, which is necessary for recovery of the metabolic state (Osterweil *et al.*, 2010). Here, no alterations in the surface expression of NMDA receptors and GluA1 containing AMRA receptors were detectable. Thus, the reduction or depletion of IRSp53 does not affect the surface expression of the NMDA receptors.

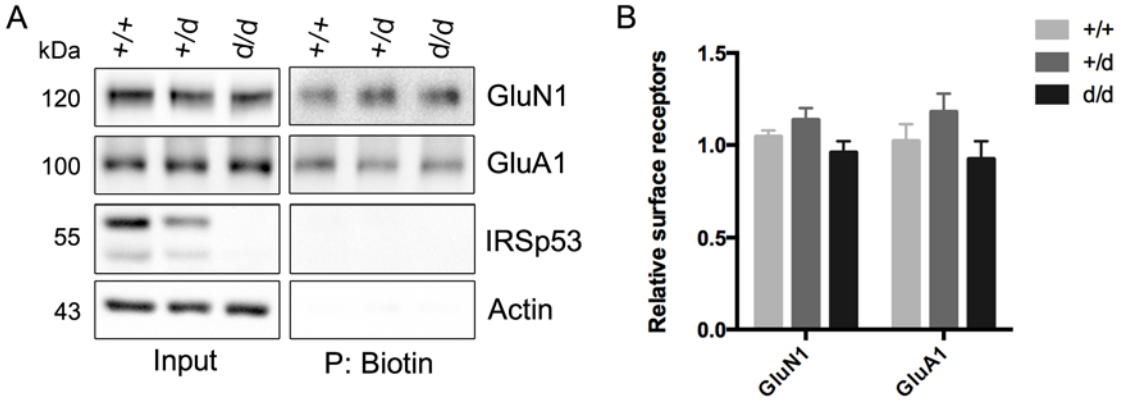


**Figure 30 Surface expression of NMDA and AMPA receptors in acute slices of wt, IRSp53 haploinsufficient and deficient mice.** [A] Acute hippocampal slices of P30 to P35 old mice were prepared and incubated in oxygenated ACSF for 4 hours. Afterwards, cell surface receptors were biotinylated and after tissue lysis the biotin labelled receptors were precipitated by streptavidin agarose. Input and precipitate (P) were analysed by western blot using the antibodies indicated. [B] Relative surface expression was evaluated by calculating the ratio of the precipitate and the input. Quantification of the relative surface receptor amount shows no differences for both, GluN1 and GluA1, comparing IRSp53 +/d and d/d mice with wt littermates (n = 4).

## 3.10 Screening of different signalling pathways activated by postsynaptic glutamate receptors

Electrophysiological studies revealed an enhanced NMDA-receptor dependent LTP in the hippocampus of IRSp53 deficient mice (Kim *et al.*, 2009 and Sawallisch *et al.*, 2009). LTP entails the most favoured model to explain the mechanism to improve synaptic function important for memory formation in the hippocampus. This requires the activation or deactivation of different signalling pathways. Several kinases are phosphorylated following LTP induction and a closer look into the phosphorylation pattern of such kinases may provide an insight into signalling pathways affected due to the loss of IRSp53.

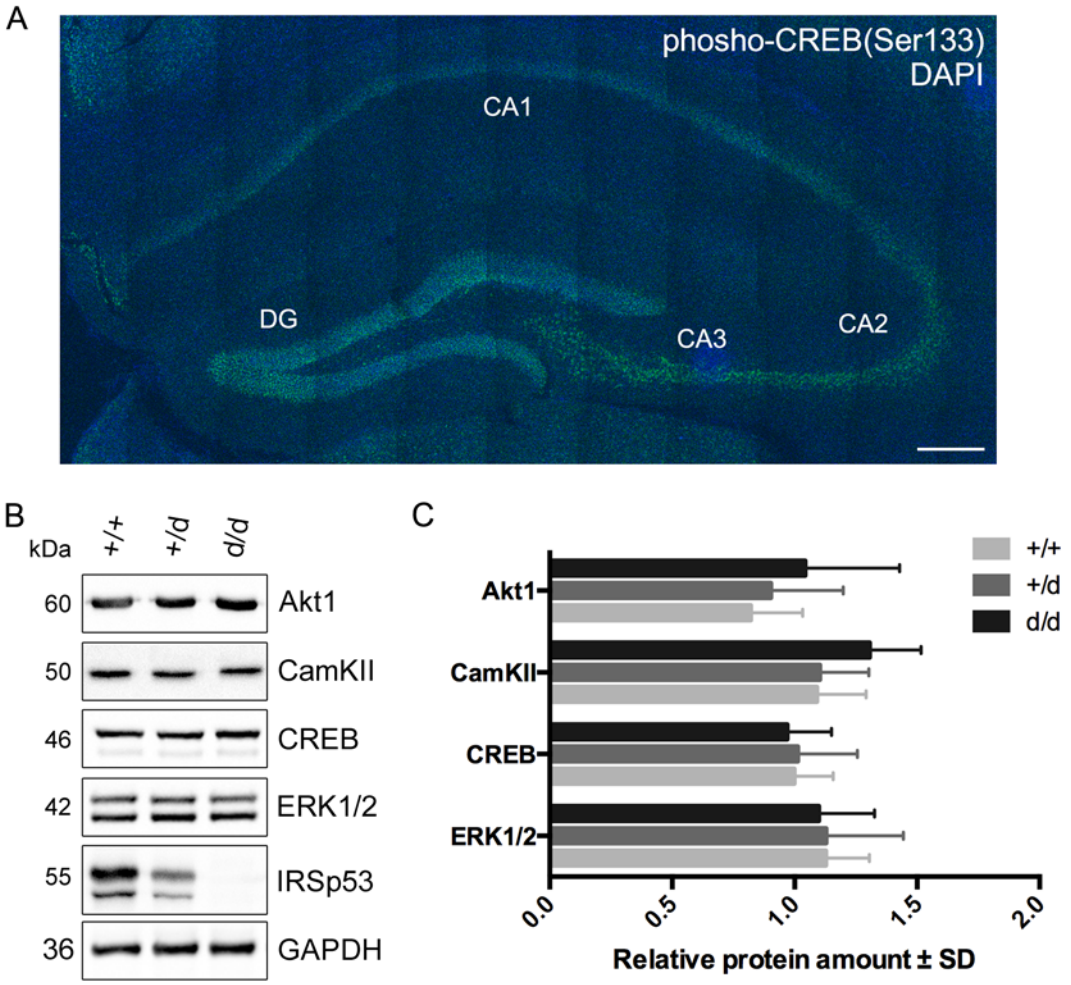


**Figure 31 Analysis of the basal expression levels of different signalling proteins in the hippocampus of wt, IRSp53 haploinsufficient and deficient animals.** [A] Phospho-CREB (Ser133) staining of the hippocampus of a coronal brain slice; the CA1, CA2 and CA3 region as well as the dentate gyrus (DG) are labelled. [B] Tissue lysates of the hippocampus from the different genotypes were analysed by western blot using the antibodies indicated. [C] Quantification demonstrates no differences in the basal protein levels in the hippocampus of IRSp53 +/d and d/d mice compared to wt littermates (n = 6). Scale bar: 50 µm.

One key player activated following LTP induction is CREB, which controls the synthesis of various proteins (Ahn *et al.* 2000). CREB is phosphorylated at serin 133 (S133) and a histological staining of phosphorylated CREB in coronal sections of the hippocampus of naïve wt mice represents a faint uniform signal throughout the granular layer (Figure 31 A). Besides CREB, three additional protein kinases: Akt1, CamKII and ERK1/2, which functions upstream of CREB were evaluated in their basic expression levels in the hippocampus (Figure 31 B, C). Tissue lysates of the hippocampus were prepared and analysed by western blot. Quantification of the protein bands were then normalised to the housekeeping protein GAPDH and further standardised to wt levels. All genotypes display equal levels of the four analysed signalling proteins.

To study signalling pathways after synaptic activation, stimulation of acute hippocampal slices was established guided by Osterweil *et al.* (2010) and De Simoni & Yu (2006). First, juvenile animals (P21 – P28) were sacrificed to remove the brain, followed by preparation of hippocampal slices. Slices were left to recover for at least 4 h in oxygenated ACSF, as described above. After stimulation, tissue lysates were prepared of control and stimulated slices and analysed by western blot. Band intensities were then normalised through the housekeeping protein GAPDH and further standardised to control levels. Relative phosphorylation states were calculated as the proportions between phosphorylated to total protein amount.

To investigate the activation pattern of signalling molecules after LTP induction, chemical stimulation with rolipram and forskolin was chosen, which mimics NDMA receptor dependent LTP (Otmakhov *et al.*, 2004) (Figure 32). Comparison of the phosphorylation state of CamKII within each group reveals no changed activation. This was expected, because LTP induction by forskolin and rolipram increases the cAMP level through the induction of PKA (Otmakhov *et al.*, 2004) and does not activate CamKII. Analysis of the phosphorylation of ERK1/2 demonstrates a significant increase within each group (+/+ $p < 0.0001$, +/d $p = 0.0043$, d/d $p = 0.001$). The within group comparison of IRSp53 +/d and d/d mice reveals a markedly increased CREB phosphorylation (+/d $p = 0.0022$, d/d $p = 0.0067$). Statistics of wt littermates did not show a significant rise despite an increased phosphorylation of about 70%. However, when comparing only control and treatment of wt slices in a paired t-test, the activation is substantial. Surprisingly, the Akt1 signalling is deactivated through de-phosphorylation following chemical LTP stimulation in all three groups (+/+ $p = 0.0027$, +/d $p < 0.0001$, d/d $p < 0.0001$).

The loss of IRSp53 or even the reduction leads to far-reaching consequences in regard to the phosphorylation pattern of the investigated kinases following chemical LTP induction. The activation of CREB is prominently enhanced up to about 170% in stimulated IRSp53 +/d and d/d slices compared to slices of wt littermates. In contrast, activation of ERK1/2 declines to roughly 50% in hippocampal slices of IRSp53 haploinsufficient and deficient mice. Moreover, the de-phosphorylation of Akt1 is much greater (≈ 20%) in IRSp53 +/d and d/d slices than in wt slices.

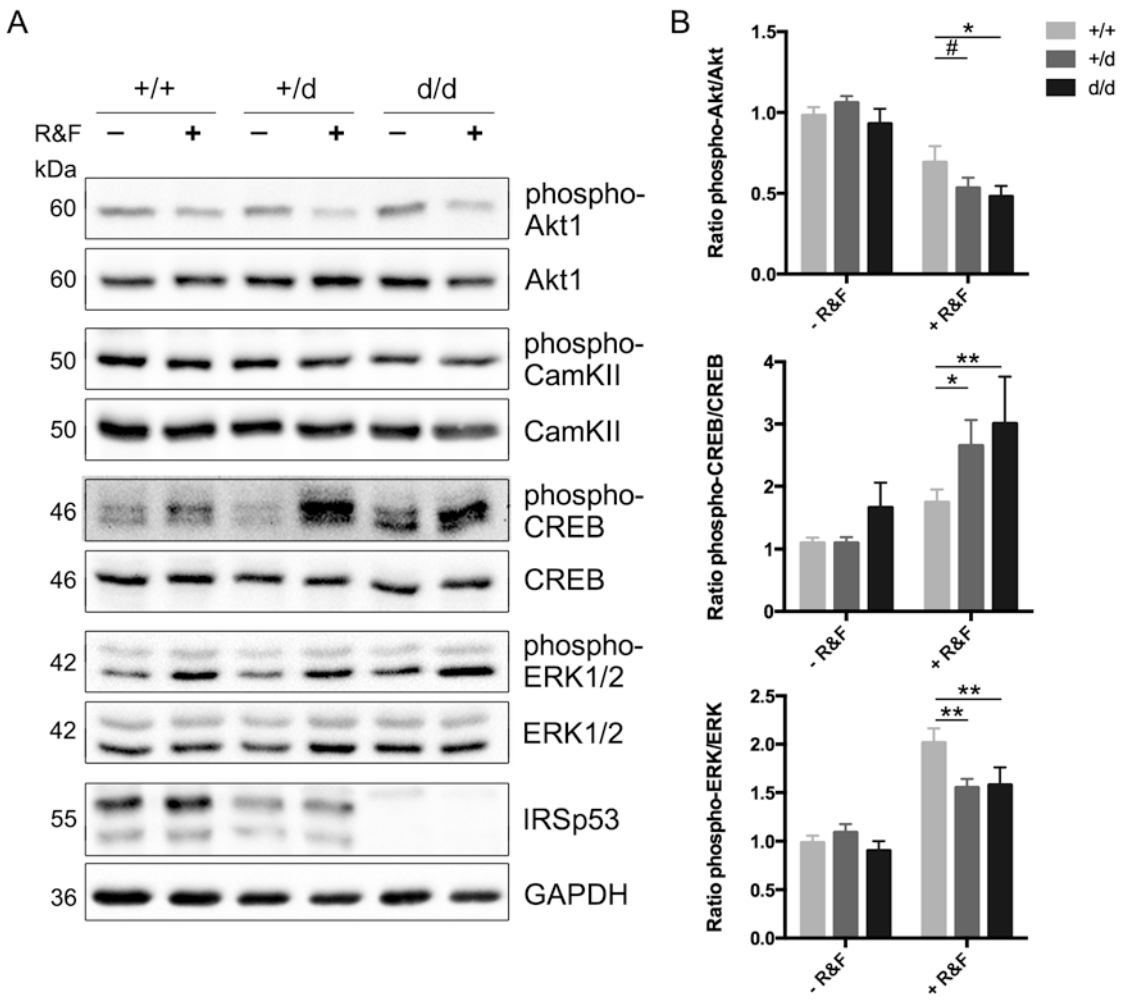


**Figure 32 Rolipram and forskolin stimulation of acute hippocampal slices of wt, IRSp53 haploinsufficient and deficient mice.** [A] Acute hippocampal slices of P21 to P30 old mice were prepared and incubated in oxygenated ACSF for at least 4 hour. Then, slices were stimulated with 0.1 µM Rolipram and 50 µM Forskolin for 30 min in magnesium free oxygenated ACSF. After tissue lysis, control and stimulation samples were analysed by western blot using the antibodies indicated. [B] Relative phosphorylation states were calculated as the proportions between phosphorylated to total protein amount. Quantification of the phospho-Akt1/Akt1 ratio demonstrates a stronger decrease in stimulated +/d slices as well as a significant stronger decline in stimulated d/d slices (n = 4, Two-way Repeated-measurement ANOVA: +/d p = 0.0700, d/d p = 0.0168). The phosphorylation of CREB is in both genotypes significantly increased after stimulation compared to wt ones (n = 4, Two-way Repeated-measurement ANOVA: +/d p = 0.0452, d/d p = 0.0067). Otherwise, phosphorylation of ERK1/2 is significantly demeaned in IRSp53 +/d and d/d stimulated slices (n = 4, Two-way Repeated-measurement ANOVA: +/d p = 0.0026, d/d p = 0.0042).

In a second approach stimulation of excitatory synaptic signal transmission was achieved by repressing inhibitory GABAergic synapses by bicuculline (Dieterich *et al.*, 2010). This leads to a summation of spontaneous activation of glutamatergic synapses and thereby triggering of action potentials. This effect was further intensified through addition of the potassium channel blocker 4-AP by maintaining the depolarisation of the dendrites (Colbert & Pan, 1999). This leads to activation of ERK1/2 (+/+ p = 0.0494, +/d p = 0.0219, d/d p = 0.0085) and CREB in all three genotypes, although CREB activation was not statistically significant. The kinases Akt1 and CamKII are not

activated. CamKII is activated following $Ca^{2+}$ influx through the NMDA receptors. In this respect, a stimulation of hippocampal slices by bicuculline and 4-AP was not sufficient for the initiation of a NMDA receptor dependent LTP. Comparisons of the phosphorylation pattern of the kinases investigated display no differences between wt slices and IRSp53 +/d as well as d/d slices. Neither activation nor deactivation of the signalling molecules CamKII and Akt1 can be detected after bicuculline and 4-AP stimulation (Figure 33).

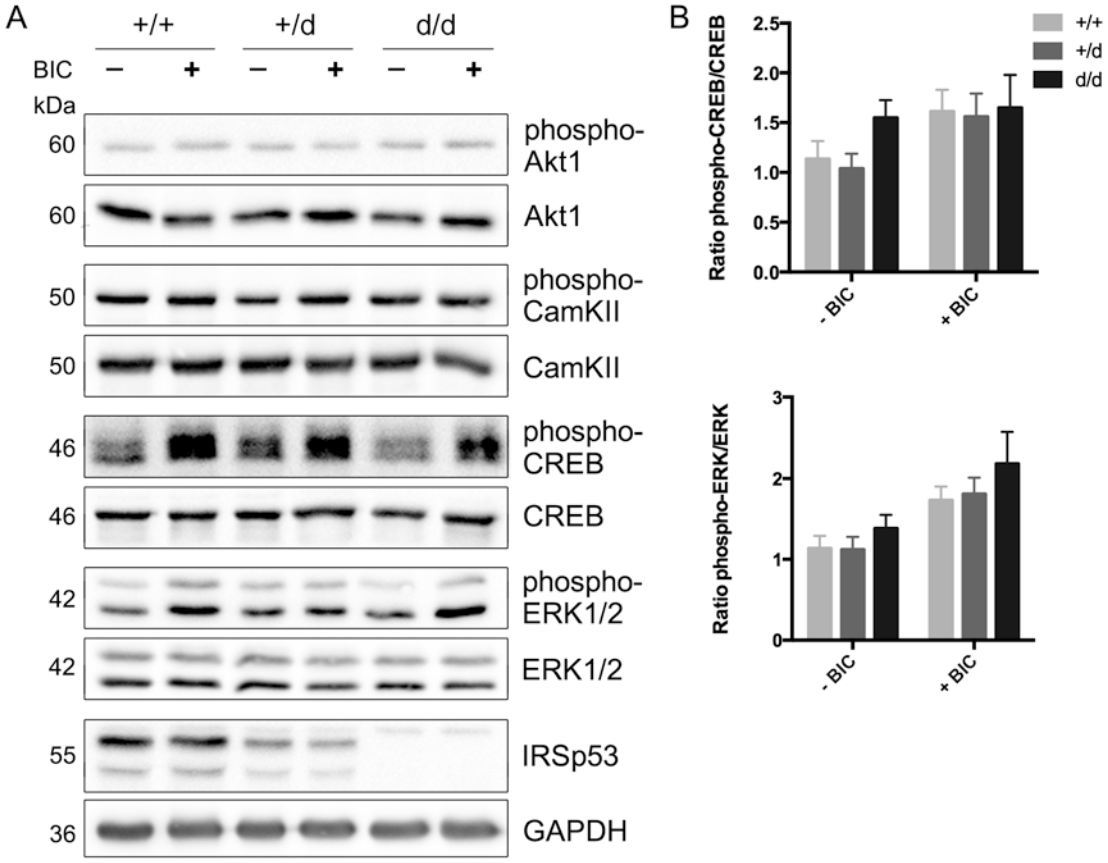


**Figure 33 Bicuculline and 4-AP stimulation of acute hippocampal slices of wt, IRSp53 haploinsufficient and deficient mice.** [A] Acute hippocampal slices of P21 to P30 old mice were prepared and incubated in oxygenated ACSF for at least 4 hour. Then, slices were stimulated with 50 µM bicuculline and 2.5 mM 4-AP for 30 min in oxygenated ACSF. After tissue lysis, samples were analysed by western blot using the antibodies indicated. [B]. Relative phosphorylation states were calculated as the proportions between phosphorylated to total protein amount. Quantification of the kinases activated demonstrates no altered signalling comparing IRSp53 +/d and d/d hippocampal slices with wt ones (n = 4).

The opposite of LTP is LTD. One prominent pathway for LTD induction proceeds via mGluR1/5 receptors and can be simulated by the mGluR1/5 selective agonist DHPG (Osterweil *et al.*, 2010) (Figure 34). After treating the slices with 100 µM DHPG, signalling via Akt1 (+/+ p = 0.0207, +/d p = 0.0047, d/d p = 0.0255), ERK1/2 (+/+ p = 0.0003, +/d p = 0.0011, d/d p = 0.0037) and CREB (+/+ p = 0.0002, +/d p = 0.0013, d/d p = 0.0306) is activated in all groups. However, no differences between treated slices of IRSp53 +/d and d/d mice compared to wt littermates were detected. An unexpected activation of CamKII following DHPG treatment was examined

here; again no differences were detectable between all genotypes. Hence, the mGluR1/5 signalling pathways involved in LTD seems to be independent on IRSp53.

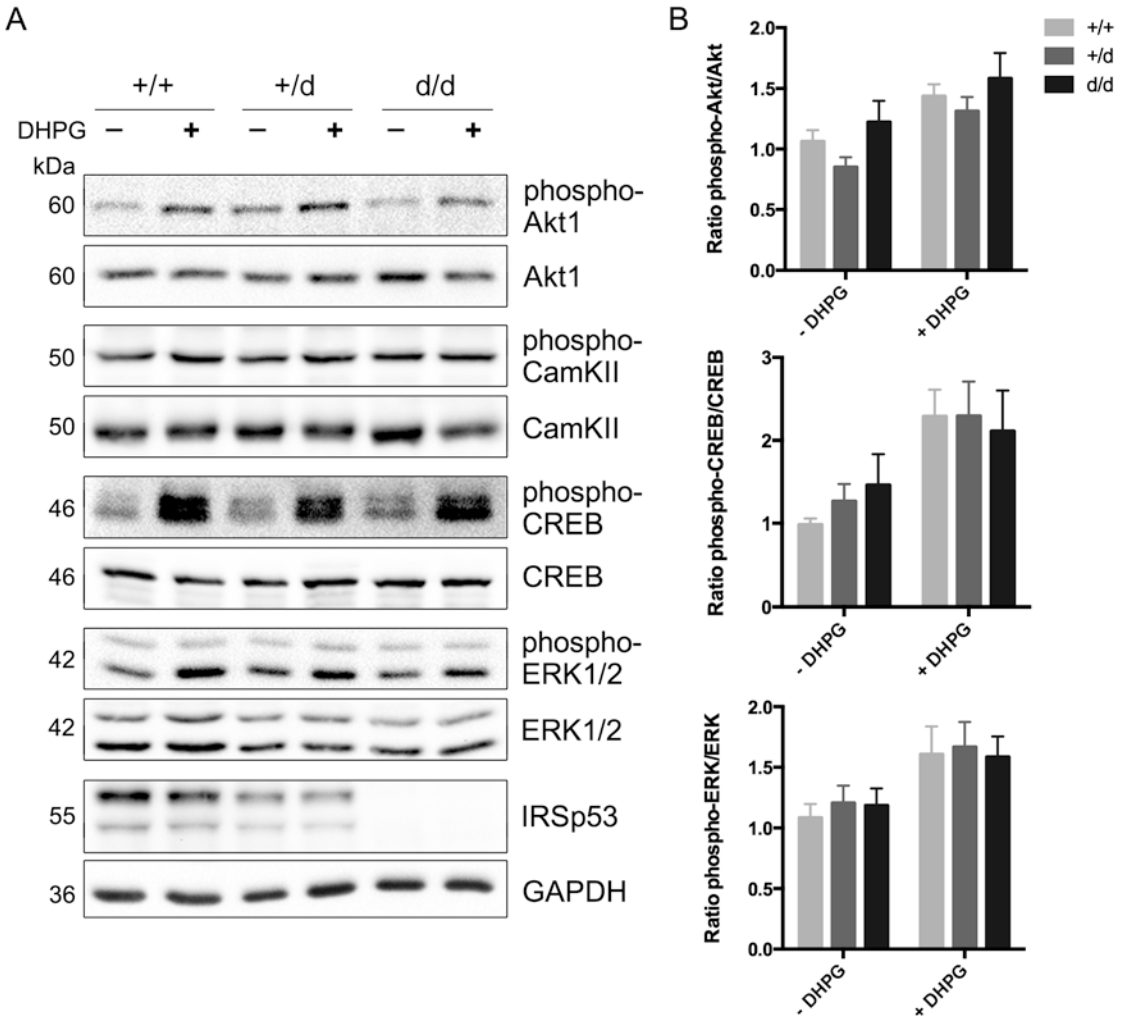


**Figure 34 DHPG stimulation of acute hippocampal slices of wt, IRSp53 haploinsufficient and deficient mice.** [A] Acute hippocampal slices of P21 to P25 old mice were prepared and incubated in oxygenated ACSF for at least 4 hour. Then, slices were stimulated with 100 µM DHPG for 5 min in oxygenated ACSF. After tissue lysis, samples were analysed by western blot using the antibodies indicated. [B] Relative phosphorylation states were calculated as the proportions between phosphorylated to total protein amount. Quantification of the kinases activated demonstrates no altered signalling comparing IRSp53 +/d and d/d slices with wt ones (n = 4).

In conclusion, signal transduction activated following bicuculline and 4-AP as well as DHPG treatment is not changed. However, reduction or loss of IRSp53 leads to severe changes in the signaling pattern following chemical LTP induction by rolipram and forskolin in acute hippocampal slices. On the one hand ERK1/2 signalling declines significantly and on the other hand deactivation of Akt1 is significantly enhanced. Furthermore, the phosphorylation of the transcription initiation factor CREB is significantly increased in slices of IRSp53 +/d and d/d mice compared to wt littermates. Based on these results, the signaling pathways induced following NMDA receptor activation are altered in IRSp53 haploinsufficient and deficient animals, which could contribute to the cognitive deficits of both genotypes in the fear-conditioning paradigm.

# 4 Discussion

More than a decade ago, the postsynaptic protein IRSp53 was discovered and quite a few studies outlined IRSp53 as a powerful regulator of the actin cytoskeleton. Moreover, genetic screens of patients suffering e.g. from ASD unveiled in rare cases a deletions of the *Baiap2* gene, which encodes IRSp53. Studies on IRSp53 ko mice which became available in 2009 an impaired cognition could be proven due to the loss of IRSp53. The evidence from these studies suggests that IRSp53 plays an important role in synaptic function underlying learning and memory formation. However, studies that address molecular and cellular mechanisms how IRSp53 could influences synaptic functions are missing. The purpose of this thesis was to gain insight into the role of IRSp53 in the CNS of *Mus musculus*.

## 4.1 An IRSp53 haploinsufficiency in mice results in a severe impairment in a fear-based hippocampal learning task

Based on studies in neuronal culture systems (Choi et al., 2005; Sawallisch et al., 209) the hypothesis arises that a critical amount of IRSp53 is required for the protein to fulfil its function. Therefore, investigation of mice haploinsufficient in IRSp53 was chosen as a suitable approach to test this hypothesis in a physiological context. Analysis of IRSp53 expression in IRSp53 +/d mice showed a 50 % reduction of IRSp53 suggesting no compensatory response due to the loss of one allele coding for IRSp53. The expression profile showed that IRSp53 is mainly expressed in the forebrain structures cortex, hippocampus and striatum as published by several groups (Bockmann *et al.*, 2001; Thomas *et al.*, 2001; Kim *et al.*, 2009; Sawallisch *et al.*, 2009). Furthermore, IRSp53 expression was found in the subthalamic nucleus, pons, amygdala and hypothalamus (Bockmann *et al.*, 2001; Thomas *et al.*, 2001), which correspond to the results obtained here. Thus, IRSp53 is expressed in brain regions important in higher-cognitive functions.

The available knockout mice offer the possibility to test behavioural consequences due to the loss of one particular protein. Kim *et al.* (2009) and Sawallisch *et al.* (2009) observed that the

cognition of IRSp53 deficient mice is impaired in simple learning tasks. Paradigms to test learning behaviour in mice often use cues related to anxiety. Mice are nocturnal and a brightly lit field reflects a threatening situation regarding the appearance of predators. However, mice are also interested to explore a novel environment (Cowen *et al.*, 2013) to find e.g. new sources of food. Tasks to test this innate anxiety are for example the open field, EPM and novel object recognition tests (van Gaalen & Steckler, 2000). The IRSp53 ko mice demonstrate no increased innate anxiety in an open field (Sawallisch *et al.*, 2009). However, Kim *et al.* (2009) observed a reduced exploration of a novel object of IRSp53 ko mice in the novel object recognition test. Therefore, the IRSp53 +/d mice were first observed in an EPM where they demonstrated no increased anxiety-related behaviour compared to their wt and ko littermates.

Behavioural tests analysing learning and memory are the Morris water maze test and the contextual fear-conditioning paradigm. These two tests are dependent on the hippocampus and uses fear-evoking conflict situations. In the Morris water maze paradigm the animals must navigate in a swimming pool to find a platform to escape from the water (D'Hooge & De Deyn, 2001). The contextual fear conditioning represents another approach. This test is based on the Pavlovian conditioning and connects a painful stimulus to the context where the animals were trained (Rudy & O'Reilly, 2001; Rudy *et al.*, 2004). Analysis of IRSp53 null-mice showed a severe impairment in both learning paradigms compared to their wt littermates (Kim *et al.*, 2009; Sawallisch *et al.*, 2009). It is a general observation that stress influences the learning aptitude. For that reason, a further behavioural test was chosen to investigate the learning behaviour of IRSp53 +/d and ko mice. This test is called puzzle box and allows a quick investigation of higher-order cognitive function. In this test the animal has to escape from a brightly lit compartment into a dark 'home cage' zone, which requires the solving of different tasks with increasing difficulty (Ben Abdallah *et al.*, 2010). The IRSp53 +/d and d/d mice show no learning deficits in this test compared to wt littermates. Surprisingly, the ko animals escape faster into the goal compartment in the second trial of the habituation phase as the wt and +/d mice. A closer observation of this trial then unveiled that the IRSp53 deficient mice do not explore the environment although the surrounding is familiar. This behaviour corresponds to the results obtained for the novel object recognition test (Kim *et al.*, 2009) in which also the exploration of novelty within a familiar environment is analysed (van Gaalen & Steckler, 2000). Thus, IRSp53 deficient mice seem to avoid novel situations.

Next, the learning ability of IRSp53 +/d mice was investigated in the contextual fear-conditioning paradigm where IRSp53 deficient mice displayed a learning impairment (Sawallisch *et al.*, 2009). Indeed, a reduced expression of IRSp53 in mice is associated with a similar severe cognitive deficit as observed for the ko littermates. IRSp53 haploinsufficient mice show only a slightly improved learning effect compared to their ko littermates. Interestingly, IRSp53 haploin-

sufficient and deficient mice display a conspicuous rearing behaviour, which appears to be more a prominent flight instinct instead of freezing. This could mean that the mice try to escape from the chamber.

The contextual fear conditioning is strongly dependent on the hippocampus (Bourtchuladze *et al.*, 1994; Rudy *et al.*, 2004; Frankland *et al.*, 2006; Krasne *et al.*, 2011). However, the brain region responsible for the initial storage of a memory differs from the permanent one. The newly learned associations are stored in the hippocampus but are shifted later into the cortex (Abraham, 2003; Frankland *et al.*, 2006; Biedenkapp & Rudy, 2007). Moreover, a massive glutamatergic input to the striatum from cortical and thalamic brain regions determines the GABAergic output of the striatum important for goal directed and habitual learning as well as avoidance learning (Gardoni 2008; Do *et al.*, 2012). Thence, different brain regions participate in different learning tasks. IRSp53 is mainly expressed in the cortex, hippocampus and striatum. Consequently, the accumulation of IRSp53 in the PSD of wt and IRSp53 +/d animals was analysed in these particular brain regions. Surprisingly, the synaptic IRSp53 levels differ in the three brain regions analysed, despite a halving of the total amount in the post-nuclear lysates. In the striatum and the cortex of +/d mice, the amount of IRSp53 in the PSD is significantly reduced compared to wt PSDs. However in cortical PSDs of +/d animals, the IRSp53 protein levels reaches about 70% of wt levels, and not only 50% as predicted. In the hippocampus, the IRSp53 protein level in the PSD of +/d mice reaches levels of up to 80% compared to wt animals. This indicates a depletion of the extrasynaptic IRSp53 especially in the hippocampus. A quantification of the PSD proteome from the rat forebrain by Cheng *et al.* (2006) demonstrates a large number of molecules of IRSp53 per individual PSD, greater than that measured for the different Shank family members, AMPA receptor subunit GluA1, NMDA receptor subunit GluN1 or Homer1. Therefore, a 20% reduction of the IRSp53 molecules in the PSD and the depletion of the dendritic pool seem to be sufficient to impede IRSp53 to fulfil its function.

The observation that IRSp53 haploinsufficient animals perform as bad as their ko littermates in the contextual fear conditioning paradigm could have two possible causes: First, the amount of IRSp53 in +/d animals is not sufficient to maintain contextual fear learning. Second, the tr.IMD/Neo/β-Gal fusion expressed from the mutant allele acts in a dominant-negative manner caused by IM domain dimerisation (Millard *et al.*, 2005). However, the tr.IMD/Neo/β-Gal fusion protein is restricted to neuronal cell bodies and not present in dendrites or at synapses. Moreover, co-immunoprecipitation experiments with the truncated IMD and full-length IRSp53 did not demonstrate any interaction. Thus, the tr.IMD/Neo/β-Gal fusion protein is not likely to interfere with the IRSp53 expressed from the wt allele and therefore a dominant-negative affect can be excluded.

## 4.2 Three functional domains of IRSp53 are important for its synaptic targeting

Immunocytochemical studies in primary hippocampal neurons unveiled a predominant postsynaptic localisation of IRSp53 (Abbott *et al.*, 1999; Bockmann *et al.*, 2002; Soltau *et al.*, 2002) in line with my observations. Furthermore, IRSp53 accumulation in the PSD fraction of IRSp53 haploinsufficient mice differs in the cortex, hippocampus and striatum. Those findings raised two questions: (1) How is IRSp53 targeted to the synapse and (2) which domains are important? First studies to investigate the synaptic targeting of IRSp53 in neurons were done by Hori *et al.* (2005) and Choi *et al.* (2005) demonstrating partially contradictory results. Hori and coworkers (2005) showed that the IM and CRIB domain as well as the PDZ ligand motif are necessary for IRSp53 accumulation at the PSD using deletion constructs. However, the study by Choi *et al.* (2005), which analysed the contribution of the SH3 domain and the PDZL by using missense mutations, revealed that both domains are important for the postsynaptic localisation of IRSp53. To further verify the impact of the four functional IRSp53 domains and to clarify the contradictory results obtained for the SH3 domain, mature primary hippocampal neurons expressing GFP-tagged wt and mutant IRSp53 were analysed regarding a co-localisation with endogenous Shank1 clusters. Approximately 55% of the Shank1 clusters were positive for IRSp53. The IRSp53 targeting to the PSD was significantly reduced if the binding to phospholipids, activated Cdc42 and PSD95 was inhibited. However, the loss of the interaction to the Shank proteins does not impede the synaptic targeting of IRSp53, in contrast to data by Choi *et al.* (2005).

The mutation of the IRSp53 IM domain results in a dramatic loss of synaptic IRSp53. $PI(4,5)P_2$ clusters are the preferential targets of the IRSp53 IMD (Mattila *et al.*, 2007; Futo *et al.*, 2013). These clusters provide a local environment for signalling components affecting the actin-cytoskeleton and vesicle trafficking (Caroni, 2001) important for synaptic function. Moreover, $PI(4,5)P_2$ is the substrate of the phospholipase C (PLC) involved in mGluR1/5 dependent signalling (Nelson *et al.*, 2008) and the postsynaptically enriched PI3K (Kennedy & Ehlers, 2006). Based on those findings, the postsynapse needs to be enriched in $PI(4,5)P_2$. Thus it is conceivable that postsynaptic $PI(4,5)P_2$ contributes to postsynaptic targeting of IRSp53. Interestingly, analysis of the IRSp53 membrane association in HEK293 cells unveiled an increased membrane localisation of IRSp53 if the SH3 domain is mutated. Possibly, this increased membrane association may be attributed to a more efficient binding of the IM domain to phospholipids. Rao *et al.* (2010) found an autoinhibitory interaction of the SH3 domain of syndapin1 with its BAR domain, which restricts syndapin1 binding to the plasma-membrane. As the IRSp53 IM domain is in fact an inverse BAR domain (Matilla *et al.*, 2007; Scita *et al.*, 2008; Zhao *et al.*, 2011; Veltman *et al.*, 2010) the IMD based binding of IRSp53 to phospholipids could be limited through an intramolec-

ular interaction with its SH3 domain. Indeed, interaction studies demonstrated the appearance of such an intramolecular interaction for IRSp53, which is sensitive to high salt concentrations (MD thesis by Y. Gerhard, in preparation). Thus, IRSp53 may exist in an open or closed conformation (Figure 35). Based on this, a mutation of the SH3 domain would favour an open conformation of IRSp53 and thereby facilitating the binding to the postsynaptic membrane, which could compensate for the missing interaction with the Shank protein family.


**Figure 35 Schematic model of two possible conformations of IRSp53.** IRSp53 may exist in two possible conformations, either an open, linear conformation or a closed conformation due to an intramolecular interaction of the IRSp53 IM and SH3 domain.

Soltau *et al.* (2002) demonstrated that binding of IRSp53 to activated Cdc42 enhances the association of IRSp53 to Shank1. In this respect, IRSp53 binding to Cdc42 might overcome the intramolecular interaction between the IM and SH3 domains. Accordingly, a mutation of the IRSp53 CRIB domain would impair either the IMD dependent interaction to phospholipids as well as SH3 dependent interaction with the Shank proteins. In agreement with this, the mutation of the IRSp53 CRIB domain strongly reduces the synaptic localisation of IRSp53.

Considering the importance of the PDZL for the targeting of IRSp53 to the synapse the postsynaptic amount of IRSp53 was analysed in PSD fractions of PSD95 null-mice. PSD95 is the most abundant MAGUK in the PSD (Cheng *et al.*, 2006). Indeed, the postsynaptic accumulation of IRSp53 decreases significantly if PSD95 is lost. However, the effect was much smaller than expected, because of a compensatory up-regulation of SAP102 (Cuthbert *et al.*, 2007). Choi *et al.* (2005) showed that IRSp53 interacts with all four members of MAGUK protein family. I verified a strong interaction of IRSp53 with SAP102 but only a slight for SAP97 by co-immunoprecipitation. A study by Cuthbert and co-workers (2007) demonstrates that PSD95 and SAP102 have overlapping functions in the CNS and that the knock out of both proteins in mice results in the death shortly after birth. Thus, SAP102 can in part rescue the loss of postsynaptic IRSp53 caused by PSD95 depletion. It is unknown, why SAP97 binds IRSp53 only weakly in contrast to PSD95 and SAP102 as their structural build-ups are very similar (Kim & Sheng, 2004; Feng & Zhang; 2009). However, an interaction study of PSD95 and SAP97 with kainate receptors demonstrated a similar effect. While PSD95 strongly interacts with kainate receptors, the association to SAP97 is very poor due to a SAP97 specific intramolecular interaction (Mehta *et al.*, 2001). Interestingly, the silencing of Lin-7, a further binding partner of the IRSp53 PDZL, prevents the recruitment of IRSp53 into the PSD (Ferrari *et al.*, 2012), which further demonstrates the importance of the PDZ ligand.

Besides determining the IRSp53 domains that are needed for the synaptic localisation Hori *et al.* (2005) investigated a possible translocation of IRSp53 to synapses following synaptic activity. They described a translocation of IRSp53 to the synapse dependent on NMDA receptor activation and the presence of F-actin. To gain insight into the mobility and translocation of IRSp53 upon NMDA receptor stimulation, live-cell imaging experiments were performed. By using *Kaede-* or *GFP- IRSp53* fusion constructs the mobility of IRSp53 was traced in highly branched dendrites of mature primary hippocampal neurons. The observation in non-stimulated neurons demonstrated a strong accumulation of IRSp53 at synapses and a diffuse dendritic pool of IRSp53 exhibiting a high mobility. Studies on the axonal transport reveals that cargo-vesicle based transport driven by motor-proteins is fast with a velocity of 200 – 400 mm/day. However, a lot of cytosolic molecules like actin or tubulin move slowly (0.1 to 6 mm/day) (Oztas, 2003). Based on this, I suppose that IRSp53 diffuses throughout the cell and is tethered at the synapse by its postsynaptic interaction partners.

The next step was to analyse whether the diffuse dendritic IRSp53 translocates to the synapse following NMDA receptor stimulation with the agonist NMDA in a $Mg^{2+}$-free environment. Here, the cytosolic IRSp53 showed no altered mobility and accumulation at dendritic sites after addition of the stimulant. Instead, the dendrites start to swell approximately 3 minutes after addition of NMDA, which indicates the beginning of neuronal cell death. Hence, a NMDA receptor dependent translocation of IRSp53 to the synapse described by Hori *et al.* (2005) cannot be ascertained. An explanation for this could be the different culture conditions used. Hori *et al.* (2005) reports a change from plating medium to Neurobasal after one week, whereas usually the medium is exchanged 4h after plating as published by several other protocols (Kaech & Banker, 2006; Beaudoin *et al.*, 2012). According to my experience, a prolonged cultivation time in the plating medium leads to a delayed maturation of the neurons seen by a reduced expression of postsynaptic proteins such as Shank1 and Shank3. This could explain, why Hori and co-workers (2005) also found that only 5% of the synapses contain IRSp53 contrary to the results obtained here as well as those published by other groups (Abbott *et al.*, 1999; Bockmann *et al.*, 2002; Soltau *et al.*, 2002; Choi *et al.*, 2005).

Thus, several conclusions can be drawn: (1) IRSp53 is enriched in more than 50% of the synapses. (2) The PSD accumulation of IRSp53 is dependent on three functional domains: the IM- and CRIB domain as well as the PDZ ligand. (3) The anchoring of IRSp53 to the postsynapse is influenced by an autoinhibitory interaction of its IMD and SH3 domain probably controlled by activated Cdc42. (4) IRSp53 diffuses throughout the cell and is anchored at the synapse by its interaction partners. (5) The translocation of IRSp53 to the synapse is independent on the NMDA receptor.

## 4.3 The PSD compositions of different forebrain regions of IRSp53 haploinsufficient and deficient mice are altered

Sawallisch *et al.* (2009) observed an altered composition of the PSD of IRSp53 deficient mice derived from whole brains. In particular, the amount of the NMDA receptor subunits GluN1, GluN2A and GluN2B was increased, whereas the total amount remained constant (Kim *et al.*, 2009, Sawallisch *et al.*, 2009). As described above, different brain regions participate in different learning tasks. Thus, a more detailed analysis was performed with respect to those brain regions where IRSp53 is expressed, i.e. cortex, hippocampus and striatum. The analysis of the cortical PSDs shows no changed protein levels in the pnl and PSD. However, components of glutamatergic signalling are changed in the hippocampus and striatum. Hippocampal PSDs of IRSp53 +/d and d/d mice demonstrate an increased amount of the NMDA receptor subunit GluN1, which is the obligatory NMDA receptor subunit (Lee & Silva, 2009; Sanz-Clemente *et al.*, 2013; Collingridge *et al.*, 2013), whereas the total protein amount remains constant. In contrast, in the striatum the amount of the GluA1 containing AMPA receptors is increased in the pnl as well as in the PSD of IRSp53 +/d and d/d mice compared to wt littermates.

The up-regulation of NMDA receptor related signalling is often associated with enhanced learning and memory (Lee & Silva, 2009; Collingridge *et al.*, 2013). One example is the increased expression of the GluN2B subunit in the forebrain of mice. These so called ‘doggy mice’ display an improved learning ability in simple learning tasks such as the contextual fear conditioning (Tang *et al.*, 1999; Tang *et al.*, 2001). Despite the increase in NMDA receptor subunits in the hippocampus of IRSp53 haploinsufficient and deficient mice shown here and despite an enhanced hippocampal LTP observed for IRSp53 null-mice (Kim *et al.*, 2009; Sawallisch *et al.*, 2009), behavioural tests reveal an impaired cognition. Investigation of several knock out mouse lines unveiled that enhanced or decreased LTP does not always correspond to improved or impaired cognition (Lynch, 2004; Lee & Silva, 2009; Collingridge *et al.*, 2013). PSD95 null-mice also display an impaired spatial learning that is attended with an increased LTP (Migaud *et al.*, 1998). Moreover, the analysis of the PSD fraction of these mice demonstrated a reduced synaptic targeting of IRSp53. Thence, the loss of IRSp53 or its interaction partner PSD95 allows the induction of LTP. However, the signalling events important to consolidate and maintain LTP seem to be impaired.

The amount of the GluA1 containing AMPA receptors increases in the striatum. It is a well-known fact that following LTP induction GluA1 containing AMPA receptors are inserted into the PSD to improve synaptic function (Lisman *et al.*, 2002; Abraham & Williams, 2003; Lynch, 2004; Murakoshi & Yasuda, 2012). The striatum consist to 95% of GABAergic neurons (Havekes *et al.*,

2012), thus the excitatory innervation of the striatum determines the inhibitory output to various brain regions. Additionally, mice in which the striatum was ablated displayed impaired avoidance learning (Havekes *et al.*, 2012). The evidence from these studies suggests that a strong glutamatergic input to the striatum increases the avoidance of novelty in mice as observed for IRSp53 deficient mice.

Besides the change of the postsynaptic NMDA and AMPA receptors in the hippocampus and striatum a slight increase in the total SynGAP levels could be detected. However, the amount of SynGAP is not increased in the PSD. SynGAP is an abundant protein of the PSD (Cheng *et al.*, 2006) and mainly expressed in the cortex, hippocampus and striatum (Komiyama *et al.*, 2002). As a GTPase activating protein for Ras, SynGAP regulates the Ras-ERK signalling pathway (Komiyama *et al.*, 2002; Krapivinsky *et al.*, 2004). In primary cell culture an overexpression of SynGAP reduces synaptic function including a decrease of the AMPA receptor surface expression and ERK signalling (Rumbaugh *et al.*, 2006). IRSp53 deficient mice demonstrate an increased hippocampal LTP (Kim *et al.*, 2009; Sawallisch *et al.*, 2009) and a rise in the GluA1 containing AMPA receptors within the striatum. Therefore, an increase of the basal SynGAP levels could be a compensatory effect due to the reduction or loss of IRSp53.

In recent decades a lot of efforts have been undertaken to study NMDA receptors and their central role in synaptic plasticity. In IRSp53 deficient mice the NMDA receptor dependent transmission is remarkably enhanced in the hippocampus (Kim *et al.*, 2009). As a tetramer the NMDA receptor is assembled of two obligatory GluN1 subunits and two GluN2A-D or GluN3A/B subunits (Collingridge *et al.*, 2013; Sanz-Clemente *et al.*, 2013). In PSD fractions derived from the whole brain of IRSp53 null-mice the NMDA receptor subunits GluN2A and GluN2B were increased (Sawallisch *et al.*, 2009) while total levels remain constant (Kim *et al.*, 2009). It is well established that the GluN2 subunits determine the kinetics of the NMDA receptor. The currents of GluN2A containing NMDA receptors are much larger and decays much faster as those of receptors comprising GluN2B subunits (Punnakkal *et al.*, 2012; Sanz-Clemente *et al.*, 2013). So the NMDA receptor composition was analysed in the cortex, hippocampus and striatum of IRSp53 +/d and d/d mice regarding the PSD levels of the GluN2A and GluN2B subunits. The results show a changed pattern of the NMDA receptor subunit GluN2A and GluN2B in the PSD of the cortex and hippocampus whereas no genotype differences were found in striatal PSDs.

In the cortex the PSD levels of the GluN2B subunits are increased but the amount of the GluN2A subunit slightly decreases. In contrast, the GluN1 subunits remain constant indicating that the total number of NMDA receptors is unchanged. In the early development the majority of the NMDA receptors comprises the GluN2B subunit. However, in the mature brain predominantly GluN2A containing NMDA receptors are located at synaptic sites (Feng & Zhang, 2009; Philpot & Zukin, 2010; Sanz-Clemente *et al.*, 2013). This shift from the GluN2B to GluN2A containing

NMDA receptors is developmentally regulated and based on experiences (Sanz-Clemente *et al.*, 2013). Matta *et al.* (2011) demonstrated that the developmental switch requires the synergistic activation of NMDA receptors and mGluR5. Mice lacking the mGluR5 unveiled a defective GluN2B to GluN2A switch especially in the cortex and hippocampus. Thence, the experience-based maturation of cortical synapses seems to be retarded in IRSp53 haploinsufficient and deficient mice.

A different pattern emerges when I analysed the NMDA receptor subunit levels in the PSD of the hippocampus. There, the amount of the GluN2B and GluN2A as well as the obligatory GluN1 subunits increases due to the loss or even the reduction of IRSp53. Thus, the number of NMDA receptors is increased in the PSD, which could be responsible for the enhanced LTP in IRSp53 null-mice (Kim *et al.*, 2009; Sawallisch *et al.*, 2009). Considering that the total NMDA receptor amount is unchanged in post-nuclear lysates the targeting of NMDA receptors to the PSD is affected. Two aspects may contribute to the increased NMDA receptor amount in the PSD in IRSp53 +/d and d/d mice: (1) IRSp53 may interfere with the surface localisation of NMDA receptors. (2) The extrasynaptic NMDA receptors are targeted to the postsynaptic site. According to this, I investigated the surface localisation of NMDA receptors by measuring the relative surface amount of NMDA receptors in neurons overexpressing IRSp53. For this purpose a rAAV based gene delivery system was used that allows a uniform transduction of the primary culture. To exclude adverse effect through the expression of a GFP-IRSp53 fusion the 2A peptide tool (Tang *et al.*, 2009) was used, which enables the expression of GFP as a fluorescent marker and an almost native IRSp53. The results demonstrate a rise in the total NMDA receptor amount in immature neurons in contrast to mature neurons, whereas AMPA receptor levels remain constant. In developing neurons the NMDA receptor surface amount is reduced. However, in mature neurons the surface localisation of both the AMPA and NMDA receptor decreases. Consequently, the influence of the individual IRSp53 domains was investigated. However, the effects observed cannot be ascribed to a specific functional domain of IRSp53. Nevertheless, an overexpression of IRSp53 in primary neurons results in morphological changes of the dendrites and spines (Choi *et al.*, 2005; Sawallisch *et al.*, 2009) not observed in the brain of IRSp53 ko mice (Kim *et al.*, 2009; Sawallisch *et al.*, 2009). Hence, the NMDA receptor surface localisation were analysed in hippocampal brain slices of IRSp53 +/d and d/d mice. There, no alterations in the surface expression of NMDA receptors and GluA1 containing AMAA receptors are detectable. Thus, a shift of the extrasynaptic NMDA receptors usually containing the GluN2B subunits (Stocca & Vicini, 1998; Rumbaugh & Vicini, 1999; Tovar & Westbrook, 1999) towards the synapse can be assumed.

Taken together, though the total number of NMDA receptors and their surface localisation are normal but their amounts in the PSD increase significantly in the hippocampus. A remarkable

aspect is that IRSp53 and the NMDA receptor bind to the same PDZ domain of PSD95 (Konrau *et al.*, 1995; Soltau *et al.*, 2004). In this respect, IRSp53 could compete with the NMDA receptor for anchoring to PSD95 to regulate the subcellular location of the NMDA receptor. Several studies demonstrated that PSD95 preferentially interacts with the C-termini of the GluN2A subunits, whereas SAP102 is usually associated with the GluN2B subunit (Sans *et al.*, 2000; Kim & Sheng, 2004; Zheng *et al.*, 2011). In contrast to the highly mobile SAP102, PSD95 is linked to the postsynaptic membrane through a N-terminal palmitoylation, thereby stabilising the NMDA receptors at the postsynapse (Kim & Sheng, 2004; Zheng *et al.*, 2011). At early stages predominantly SAP102 is expressed while the PSD95 expression gradually increases (Zheng *et al.*, 2011) similarly to the developmental GluN2B-GluN2A switch (Matta *et al.*, 2011). A study by Roche *et al.* (2001) showed that the NMDA receptors are internalised by clathrin-mediated endocytosis in immature neurons dependent on the GluN2B C-terminal PDZ domain. With increasing PSD95 levels this internalisation is inhibited. Interestingly, Veltman and co-workers (2011) demonstrated that I-BAR domains are involved in clathrin-mediated endocytosis. As IRSp53 belongs to the family of I-BAR domain containing proteins (Millard *et al.*, 2005; Cory & Cullen, 2007; Mattila *et al.*, 2007; Scita *et al.*, 2007; Zhao *et al.*, 2011) a diminished endocytosis of the NMDA receptors appears possible.

## 4.4 Altered postsynaptic signal transduction in the hippocampus of IRSp53 haploinsufficient and deficient mice

It is generally agreed today, that the hippocampus is an important brain region in respect to the formation of new memories. One behavioural test dependent on hippocampal function is the contextual fear conditioning (Bourtchuladze *et al.*, 1994; Rudy *et al.*, 2004; Frankland *et al.*, 2006; Krasne *et al.*, 2011). IRSp53 deficient as well as haploinsufficient animals demonstrate a severe impairment in the contextual fear-conditioning paradigm. In correspondence to that, Sawallisch *et al.* (2009) and Kim *et al.* (2009) demonstrate an increased LTP in IRSp53 null-mice dependent on an enhanced NMDA receptor transmission. These discoveries lead to the assumption that signalling pathways activated following NMDA receptor stimulation are altered in mice due to the loss or even a reduction of IRSp53. A high throughput screening exhibited that the phosphorylation status of 127 proteins changes after NMDA receptor activation (Coba *et al.*, 2009). To gain insight into NMDA receptor-mediated signalling pathways the phosphorylation pattern of three kinases and the transcription factor CREB were analysed following acute hippocampal slice stimulation. First, a forskolin and rolipram stimulation protocol from Otmakhov *et al.*

(2004) was chosen to activate the increase in the cAMP levels usually triggered by the NMDA receptor-dependent $Ca^{2+}$ influx. The results reveal a drastic change in the phosphorylation pattern of Akt1, ERK1/2 and CREB following stimulation of IRSp53 +/d and d/d slices compared to their wt ones (Figure 36). As predicted, the phosphorylation of CamKII did not change following stimulation considering that CamKII is activated on the basis of a $Ca^{2+}$ influx through the NMDA receptors (Lisman et al., 2002; Lynch, 2004; Murakoshi & Yasuda, 2012).

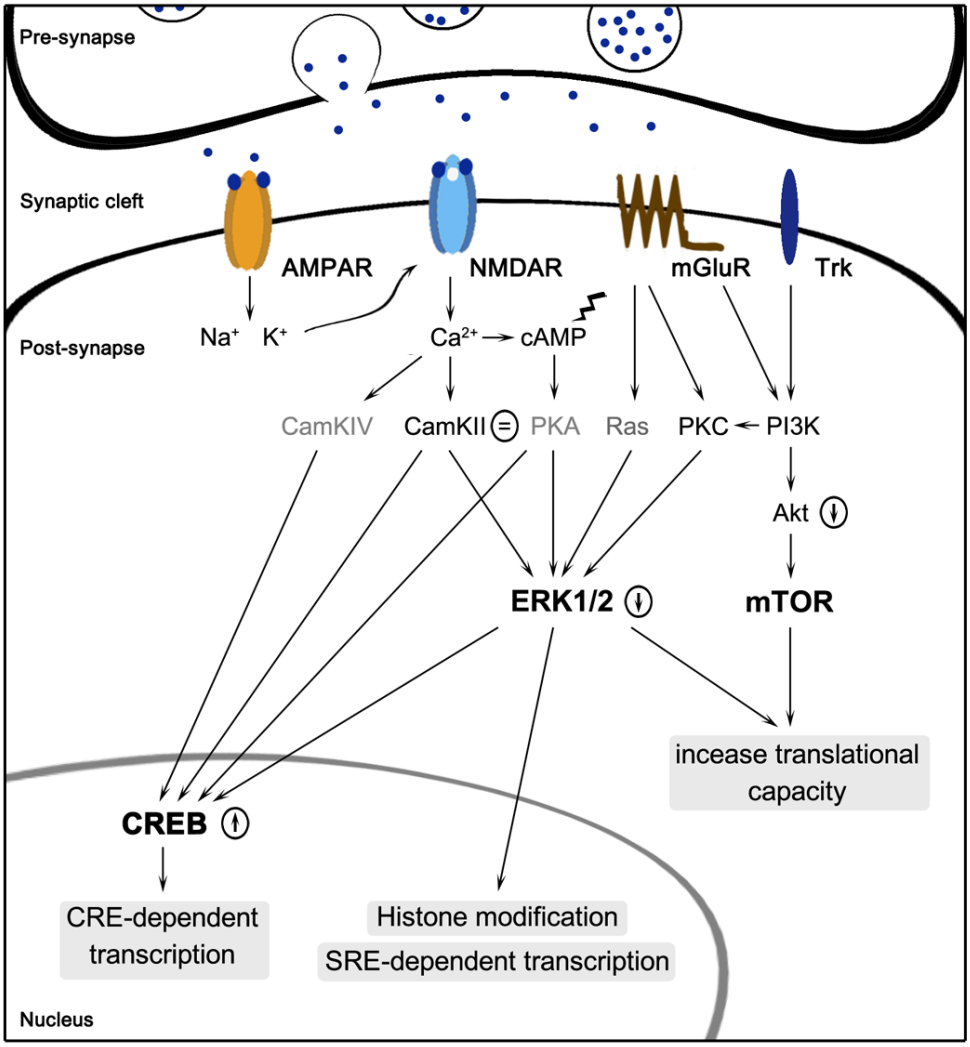


**Figure 36 Severe alteration of different signalling pathways in the hippocampus of IRSp53 haploinsufficient and deficient mice following NMDA receptor dependent LTP induction.** The forskolin and rolipram stimulation of acute hippocampal slices of IRSp53 +/d and d/d mice exhibit severe alterations in the phosphorylation pattern of the kinases Akt1 and ERK1/2 as well as the transcription initiation factor CREB compared to slices from wt mice. The phosphorylation state of the kinases Akt1 and ERK1/2 is decreased in IRSp53 +/d and d/d mice compared to wt littermates. In contrast, the phosphorylation of the transcription factor CREB at S133 is remarkably increased due to the reduction or loss of IRSp53.

Akt1 gets dephosphorylated following LTP induction in wt hippocampal slices and this effect is increased due to the loss as well as the reduction of IRSp53. The decrease in the phosphorylation in wt slices after LTP induction was surprising. It is known that Akt1 signalling promotes neuronal survival regulated by the action of growth factors (Downward, 1998). However, its role

in the modulation of synaptic plasticity is largely unknown. A study by Wang and co-workers (2003) showed that Akt1 phosphorylates $GABA_A$ receptors, which are responsible for a fast inhibitory synaptic transmission. This phosphorylation induces an insertion of $GABA_A$ receptors into the PM, thereby increasing inhibitory synaptic currents within a neuronal network. In respect to this, the strong activation of the excitatory synapses by forskolin and rolipram could influences the action of inhibitory neurons by the suppression of the Akt1 signalling.

Conspicuously, the deactivation of Akt1 is further increased in stimulated slices of IRSp53 +/d and d/d mice. Akt1 is a target of PI3K suggesting that the induction of the PI3K signalling pathway is impaired. Main consequences of PI3K signalling are the initiation of the opening of intracellular $Ca^{2+}$ stores (Bliss & Collingridg, 1993; Raymond, 2007) and the activation of the mTOR pathway via Akt1 (Lynch, 2004; Kelleher et al., 2004; Raymond, 2007). An interference with the opening of intracellular $Ca^{2+}$ stores seems unlikely based on the strong increase of the CREB phosphorylation, which is in part dependent on an elevated cytosolic $Ca^{2+}$ concentration to activate further CREB kinases (Ahn *et al.*, 2000; Bading, 2000; Raymond, 2007). More likely is a reduced activation of the mTOR pathway, a signalling pathway involved in the initiation of activity dependent translation (Lynch, 2004; Kelleher *et al.*, 2004; Raymond, 2007).

Besides the activation of the mTOR pathway the Erk1/2 pathway needs to be activated to achieve a sufficient activity-dependent translation (Kelleher *et al*., 2004). Notably, the phosphorylation of ERK1/2 is significantly reduced in slices of IRSp53 haploinsufficient and deficient mice compared to wt ones following forskolin and rolipram treatment. Interestingly, the ERK1/2 phosphorylation in the hippocampus strongly increases after contextual fear conditioning (Lynch, 2004; Sindreu *et al.*, 2007). An elegant study by Kelleher *et al.* (2004b) demonstrates that mice expressing selectively a dominant-negative form of the ERK1/2 kinase MEK1 in the forebrain have a severe learning impairment in the contextual fear conditioning. However, this cognitive deficit emerges after 24 h and not after 1 h. Electrophysiological measurements then exhibited that in particular the protein translation-depended phase of LTP is blocked in these mutants (Kelleher *et al*.; 2004b). A further important function of ERK1/2 is the facilitation of the nuclear transcription. On the one hand ERK1/2 by itself initiates SRE-dependent transcription (Raymond, 2007) and supports the transcription through simplifying the access to the DNA by remodelling of the chromatin structure (Ahn *et al.*, 2000; Levenson *et al.*, 2004; Chwang *et al.*, 2006). Following contextual fear conditioning in particular an enhanced histone 3 acetylation in the hippocampus was found, which promotes transcription initiation (Levenson *et al.,* 2004; Chwang *et al.*, 2006). On the other hand ERK1/2 translocates into the nucleus induced by $Ca^{2+}$ to activate further CREB kinases such as Rsk2 (Impey *et al.*, 1998) and Msk1 (Sindreu *et al.*, 2007).

However, CREB phosphorylation is significantly increased in stimulated IRSp53 +/d and d/d slices. CREB induces plasticity-related gene transcription (Ahn *et al*., 2000; Abraham & Williams,

2003; Johannessen *et al.*, 2004) and hippocampus-based learning tasks require CREB activation to consolidate memories (Bourtchuladze *et al.*, 1994; Guzowski & McGaugh, 1997; Kida *et al.*, 2002; Peters *et al.*, 2009). Interestingly, a chronic increase in CREB function results in an impaired learning of mice in the Morris water maze paradigm (Viosca *et al.*, 2009). The IRSp53 +/d and d/d mice demonstrate an increased CREB activity following chemical LTP stimulation and not a chronic increase, what would had become apparent in non-stimulated controls or by investigating the CREB phosphorylation in brain slices of naïve animals. So, the activation of CREB alone is not sufficient to induce late LTP. Indeed, Trifilieff *et al.* (2006) discovered that a co-incidence activation of CREB as well as ERK1/2 is needed. Moreover, they describe a biphasic activation of CREB due to two activation waves by ERK1/2. This biphasic activation is also thought to be caused by a fast phosphorylation of CREB e.g. by PKA and CamKIV and a later induction by the ERK1/2 pathway (Ahn *et al.*, 2000; Johannessen *et al.*, 2004; Lynch, 2004). Thus it is possible that in IRSp53 haploinsufficient and deficient mice, the reduced activation of ERK1/2, i.e. a lack of co-incidence between Erk1/2 and CREB activation, interferes with gene transcription events despite high levels of phosphorylated CREB.

A further protocol thought to induce NMDA receptor dependent LTP uses the $GABA_A$ receptor inhibitor bicuculline and the potassium channel blocker 4-AP. The main idea is that by inhibition of inhibitory synapses the spontaneous activity of excitatory synapses potentiates itself, which leads to a burst of action potentials (Hardingham *et al.*, 2002; Dieterich *et al.*, 2008). This would open up the opportunity to investigate the signalling pathways following NMDA receptor activation. A study by Segal & Murphy (1998) demonstrated an efficient CREB phosphorylation in primary neurons after 30 min stimulation with bicuculline. However, the experiments performed in this study did not show a sufficient increase in CREB phosphorylation. Moreover, no phosphorylation of CamKII could be detected as expected. This probably means that no NMDA receptors were activated following bicuculline and 4-AP treatment. Nevertheless, the phosphorylation of ERK1/2 is increased, possibly caused by the activation of mGluRs. In this experiment, no genotype differences were detected. Thus, the reduced activation of the ERK1/2 pathway in IRSp53 +/d and d/d slices treated with rolipram and forskolin seems to be dependent on a faulty cooperation of the signalling pathways activated through a NMDA receptor dependent $Ca^{2+}$ influx.

LTP describes an activity dependent increase in the synaptic strength. Opposite to this is the model of LTD that explains the weakening of synapses (Bliss & Collingridge 1993; Yang *et al.*, 1999; Bading, 2000; Kim & Sheng, 2004). Analysis of hippocampal FMR1 ko slices stimulated with the mGluR agonist DHPG demonstrates an hypersensitivity to the mGluR5-ERK1/2 pathway (Osterweil *et al.*, 2010). Activation of the ERK1/2 and mTOR pathways is reduced due to an IRSp53 haploinsufficiency and deficiency following LTP stimulation. According to this, a possible influence of IRSp53 on the mGluR5-ERK1/2 and mTOR pathway following DHPG stimulation

was analysed. Electrophysiological recordings by Kim *et al.* (2009) showed no alterations in LTD formation of hippocampal IRSp53 ko slices. In agreement with this, no changes in phosphorylation patterns were observed in IRSp53 +/d and d/d slices compared to wt slices.

In conclusion, both the loss and the reduction of IRSp53 results in an increased phosphorylation of the transcription initiation factor CREB. However, the activation of the kinases ERK1/2 and Akt1 decreases, which are responsible for boosting the translational capacity of the cell necessary to consolidate and maintain LTP. Consequently, the NMDA receptor dependent LTP in the hippocampus requires the presence of IRSp53 in an adequate amount for a proper synaptic signalling. The question then is: How is IRSp53 involved in the formation of an NMDA receptor dependent LTP in the hippocampus?

Following synaptic stimulation a reorganisation of the postsynapse is postulated (Abraham & Williams, 2003; Murakoshi & Yasuda, 2012). This includes the degradation of postsynaptic proteins such as the Shank proteins and PSD95 through the ubiquitin-proteasome system (Colledge *et al.*, 2003; Ehlers *et al.*, 2003; Pak & Sheng, 2003). Of particular interest is the degradation of the Shank proteins considering that the actin-regulatory function of IRSp53 is blocked by the interaction of Shank with the IRSp53 SH3 domain (Soltau *et al.*, 2002; Sawallisch *et al.*, 2009). Following synapse specific stimulation a transient synapse specific growth was shown to persist for about 72 h (Casadio *et al.*, 1999). Here, IRSp53 could serve as a powerful effector to regulate the reorganization of the actin-cytoskeleton after LTP induction, thereby stabilising plasticity induced changes at synapses. Several findings support this hypothesis. (1) The size of the PSD decreases due to the loss of IRSp53 (Sawallisch *et al.*, 2009). (2) The inactivation of the IRSp53 SH3 domain as well as the inhibition of the IRSp53 binding partner WAVE2 leads to the reduction of the spine density in primary culture (Choi *et al.*, 2005). From studies in non-neuronal cells it is well known that IRSp53 affects the actin dynamics by connecting Cdc42 to various effector proteins like N-WASP, Mena and Eps8 (Krugmann *et al.*, 2001; Disanza *et al.*, 2006; Lim *et al.*, 2008). Interestingly, the activation of the small GTPase Cdc42 increases rapidly following LTP induction, which is dependent on CamKII activation (Murakoshi & Yasuda, 2012). Moreover, the binding of activated Cdc42 and WAVE2 to IRSp53 can be blocked by the interaction of the protein 14-3-3 to IRSp53 (Robens *et al.*, 2010). Following contextual fear conditioning an increase in the expression of the protein 14-3-3 could be observed in the hippocampus (Kida *et al.*, 2002). Thus, the increase of the 14-3-3 protein amount could limit the actin-regulatory function of IRSp53 in time.

However, this does not explain the reduction of the ERK1/2 and mTOR signalling. The selective repression of the mGluR1/5 signalling following LTP induction diminishes the translation-dependent phase of LTP (intermediate LTP) (Raymond, 2007). One theory implies that this phase could be positively regulated by extrasynaptic NMDA receptors, activated through a spill-

over of the neurotransmitter glutamate (Raymond, 2007). In the hippocampus of IRSp53 haploinsufficient and deficient mice the extrasynaptic NMDA receptors are depleted. Hence, the positive impact on mGluR1/5 signalling pathways after LTP induction through the extrasynaptic NMDA receptors is lost.

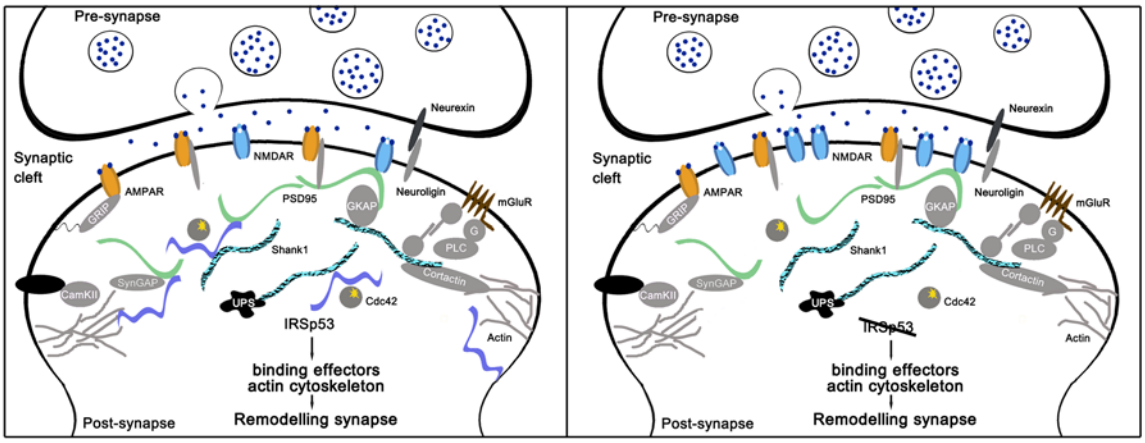


**Figure 37 A model describing an impaired activity-dependent remodelling of the actin cytoskeleton due to the loss of IRSp53.** The postsynapse is remodelled following NMDA receptor activation. Therefore, the actin cytoskeleton is reorganised and new proteins are incorporated to improve synaptic function. This includes the degradation of the Shank proteins through the ubiquitin-proteasome system and a spine-specific activation of the small GTPase Cdc42. In the presence of the Shank proteins the IRSp53 SH3 domain is blocked, which interacts with various actin-regulatory proteins. Hence, following synaptic activity IRSp53 can link Cdc42 activity to effectors of the actin cytoskeleton due to degradation of the Shank proteins. This would support the reorganisation of the actin cytoskeleton necessary to stabilise plasticity-induced changes at synapses.

## 4.5 The potential role of IRSp53 in synaptic plasticity and future perspectives

Genetic screens of patients suffering from ASD and ADHS as well as biochemical analysis of the brain of definite AD cases imply that IRSp53 plays an important role in synaptic function. As an abundant postsynaptic multidomain protein IRSp53 influences synaptic plasticity. This study carried out here verified relevant factors important for the synaptic targeting of IRSp53 and provides an insight into the central question of how could IRSp53 affect synaptic function. Nevertheless, a lot of new questions emerge.

IRSp53 is predominantly located at the postsynapse and PSD preparations of the hippocampus and cortex unveiled an improved IRSp53 accumulation if the amount of IRSp53 is halved. IRSp53 is targeted to the synapse dependent on the IM and CRIB domain as well as PDZ ligand motif. Through the binding to $PI(4,5)P_2$ rich membranes and PSD95 IRSp53 is tethered to the postsynapse, whereas its binding to the PM is limited through an intramolecular interaction be-

tween the IM and SH3 domain. The binding of activated Cdc42 to the CRIB domain probably resolve this intramolecular interactions, thereby facilitating the binding to the PM. Considering the fact that the intramolecular interaction of IRSp53 is salt-sensitive raises the question: Does a $Ca^{2+}$ influx through the NMDA receptors after LTP induction supports maintaining IRSp53 in an open conformation? The observation of the IRSp53 mobility presumes that IRSp53 diffuses to the postsynapse independent on NMDA receptor activation. However, further experiments are needed to test whether other stimulation protocols known to induce LTP may lead to a changed IRSp53 dynamic.

Behavioural and electrophysiological analysis of IRSp53 null-mice demonstrates that IRSp53 is an important regulator of synaptic plasticity. IRSp53 haploinsufficient and deficient animals demonstrate severe cognitive impairments in fear-evoking learning tasks. Moreover biochemical quantifications indicate that the experience-based maturation of the cortical and hippocampal synapses is retarded due to the reduction or loss of IRSp53. Does the learning ability improve by a more intense training prior to the conditioning? The contextual fear conditioning is strongly dependent on the hippocampus in contrast to the cued version of this test (Rudy *et al.*, 2004; Krasne *et al.*, 2011). Therefore, it would be interesting to examine IRSp53 haploinsufficent and deficient mice in the cued fear conditioning. Nevertheless, observation of higher cognitive function in a puzzle box revealed no learning impairments, but rather an increased avoidance of novelty specifically for IRSp53 ko mice. Do mice haploinsufficient in IRSp53 perform as bad as their ko littermates in the novel object recognition? In addition, further behavioural test are required to analyse whether the loss or reduction of IRSp53 in mice leads to an impaired cognition in paradigms related to positive cues such as food reward as seen for fear-evoking approaches.

Biochemical studies on the PSD composition of the cortex, hippocampus and striatum as well as analysis of the surface receptor expression in the hippocampus then showed a change in the ionotropic glutamate receptor signalling. The developmental GluN2B to GluN2A switch seems to be retarded in the cortex and also presumably in the hippocampus. Moreover, in the hippocampus the postsynaptic NMDA receptors levels increases due to the loss or even reduction of IRSp53, while the total number and the surface localisation are normal. Thus, a depletion of the extrasynaptic NMDA receptors can be assumed and should be further verified by analysis of signalling pathways depending on extrasynaptic NMDA receptors often related to CREB shut off pathways (Hardingham *et al.*, 2002; Hardingham & Bading, 2002; Fainzilber *et al.*, 2011). Furthermore, experiments are required to clarify, which IRSp53 domains are responsible for the changed distribution of the NMDA receptors.

In addition, an altered phosphorylation pattern of different signalling molecules can be proven following LTP induction in the hippocampus of IRSp53 +/d and d/d mice. The induction of the transcription factor CREB is remarkably increased. In contrast, the phosphorylation of Akt1 and

ERK1/2 is decreased suggesting that important steps required to consolidate memories are affected. The results open a lot of issues in respect to the role of IRSp53 following NMDA receptor dependent-mediated signaling. Is the activity-dependent transcription enhanced following LTP induction or only the induction of CREB? Does the CREB phosphorylation decay faster due to a reduction or loss of IRSp53? Which factors are responsible for the decreased induction of Akt1 and ERK1/2? Which functional domains of IRSp53 are relevant for the altered signalling observed?

Three approaches briefly introduced here could give further insights. (1) The stimulation of acute hippocampal slices offers a lot of possibilities to analyse the NMDA receptor dependent signalling in more detail by e.g. selectively inhibiting the activation of the different types of glutamate receptors or kinases stimulated. (2) The culturing of hippocampal slices (De Simoni & Yu, 2006; Gogolla *et al*., 2006) from IRSp53 ko mice would allow the re-expression of wt and mutant IRSp53 variants. Thus, the contribution of the individual IRSp53 domains can be analysed regarding the altered phosphorylation pattern observed following LTP induction. (3) Several groups observed the phosphorylation pattern of CREB (Josselyn *et al.*, 2001; Josselyn, 2010) and changes in the expression of the immediate early genes such as *c-fos* and *BDNF* (Frankland *et al.*, 2006; Viosca *et al.*, 2009) in brain slices of conditioned mice. This method offers the opportunity to analyse the activation pattern of signalling molecules and activity-dependent transcription in various brain regions. Moreover, the CREB phosphorylation could be observed over time by choosing different time points reflecting the different stages of LTP.

Almost no studies have been done to investigate a possible link between the action of insulin and IRSp53. It is known that the insulin receptor is expressed in several forebrain structures such as the cortex and hippocampus. The performances of mice in passive-avoidance tasks improve after acute insulin administration. Additionally, the insulin receptor mRNA levels in the hippocampus rise following training in spatial-learning tasks (Zhao *et al.,* 2001; Craft & Watson, 2004). Experiments using hippocampal slices treated with insulin also unveiled an enhanced NMDA receptor activity caused by a tyrosin phosphorylation of the GluN2A/B subunit (Zhao *et al.*, 2001). Abbott and co-workers (1999) analysed the cellular distribution of IRSp53 and the insulin receptor in neurons and indeed they found a co-localisation. The action of insulin was shown to stimulate the phosphorylation of CREB dependent on the p42/44 MAPK pathway in non-neuronal cells (Klemm *et al.*, 1998; Kitamura *et al.*, 2002). This is interesting for this project since both pathways are altered due to the reduction or loss of IRSp53. Therefore, analysis of signalling pathways triggered after insulin administration of hippocampal slices could give a further insight into the functional role of IRSp53 in synaptic plasticity in the CNS.

# 5 Bibliography

Abbott MA, Wells DG, Fallon JR (1999) The insulin receptor tyrosine kinase substrate p58/53 and the insulin receptor are components of CNS synapses. J Neurosci 19:7300-7308.

Abraham WC (2003) How long will long-term potentiation last? Philos Trans R Soc Lond B Biol Sci 358:735-744.

Abraham WC, Williams JM (2003) Properties and mechanisms of LTP maintenance. Neuroscientist 9:463-474.

Ahn S, Riccio A, Ginty DD (2000) Spatial considerations for stimulus-dependent transcription in neurons. Annu Rev Physiol 62:803-823.

Alvarez CE, Sutcliffe JG, Thomas EA (2002) Novel isoform of insulin receptor substrate p53/p58 is generated by alternative splicing in the CRIB/SH3-binding region. J Biol Chem 277:24728-24734.

Andersen P (2003) A prelude to long-term potentiation. Philos Trans R Soc Lond B Biol Sci 358:613-615.

Ando R, Hama H, Yamamoto-Hino M, Mizuno H, Miyawaki A (2002) An optical marker based on the UV-induced green-to-red photoconversion of a fluorescent protein. Proc Natl Acad Sci U S A 99:12651-12656.

Bading H (2000) Transcription-dependent neuronal plasticity the nuclear calcium hypothesis. Eur J Biochem 267:5280-5283.

Banker G, Goslin K (2002) Culturing Nerve cells. Cambridge: The MIT Press.

Bard L, Sainlos M, Bouchet D, Cousins S, Mikasova L, Breillat C, Stephenson FA, Imperiali B, Choquet D, Groc L (2010) Dynamic and specific interaction between synaptic NR2-NMDA receptor and PDZ proteins. Proc Natl Acad Sci U S A 107:19561-19566.

Barilari M, Dente L (2010) The neuronal proteins CIPP, Cypin and IRSp53 form a tripartite complex mediated by PDZ and SH3 domains. Biol Chem 391:1169-1174.

Beaudoin GM, 3rd, Lee SH, Singh D, Yuan Y, Ng YG, Reichardt LF, Arikkath J (2012) Culturing pyramidal neurons from the early postnatal mouse hippocampus and cortex. Nat Protoc 7:1741-1754.

Ben Abdallah NM, Fuss J, Trusel M, Galsworthy MJ, Bobsin K, Colacicco G, Deacon RM, Riva MA, Kellendonk C, Sprengel R, Lipp HP, Gass P (2011) The puzzle box as a simple and efficient behavioral test for exploring impairments of general cognition and executive functions in mouse models of schizophrenia. Exp Neurol 227:42-52.

Biedenkapp JC, Rudy JW (2007) Context preexposure prevents forgetting of a contextual fear memory: implication for regional changes in brain activation patterns associated with recent and remote memory tests. Learn Mem 14:200-203.

Bliss TV, Collingridge GL (1993) A synaptic model of memory: long-term potentiation in the hippocampus. Nature 361:31-39.

Bockmann J, Kreutz MR, Gundelfinger ED, Bockers TM (2002) ProSAP/Shank postsynaptic density proteins interact with insulin receptor tyrosine kinase substrate IRSp53. J Neurochem 83:1013-1017.

Bourtchuladze R, Frenguelli B, Blendy J, Cioffi D, Schutz G, Silva AJ (1994) Deficient long-term memory in mice with a targeted mutation of the cAMP-responsive element-binding protein. Cell 79:59-68.

Burger C, Gorbatyuk OS, Velardo MJ, Peden CS, Williams P, Zolotukhin S, Reier PJ, Mandel RJ, Muzyczka N (2004) Recombinant AAV viral vectors pseudotyped with viral capsids from serotypes 1, 2, and 5 display differential efficiency and cell tropism after delivery to different regions of the central nervous system. Mol Ther 10:302-317.

Burnette WN (1981) "Western blotting": electrophoretic transfer of proteins from sodium dodecyl sulfate--polyacrylamide gels to unmodified nitrocellulose and radiographic detection with antibody and radioiodinated protein A. Anal Biochem 112:195-203.

Burova E, Ioffe E (2005) Chromatographic purification of recombinant adenoviral and adeno-associated viral vectors: methods and implications. Gene Ther 12 Suppl 1:S5-17.

Caroni P (2001) New EMBO members' review: actin cytoskeleton regulation through modulation of PI(4,5)P(2) rafts. EMBO J 20:4332-4336.

Casadio A, Martin KC, Giustetto M, Zhu H, Chen M, Bartsch D, Bailey CH, Kandel ER (1999) A transient, neuron-wide form of CREB-mediated long-term facilitation can be stabilized at specific synapses by local protein synthesis. Cell 99:221-237.

Celestino-Soper PB, Shaw CA, Sanders SJ, Li J, Murtha MT, Ercan-Sencicek AG, Davis L, Thomson S, Gambin T, Chinault AC, Ou Z, German JR, Milosavljevic A, Sutcliffe JS, Cook EH, Jr., Stankiewicz P, State MW, Beaudet AL (2011) Use of array CGH to detect exonic copy number variants throughout the genome in autism families detects a novel deletion in TMLHE. Hum Mol Genet 20:4360-4370.

Cheng D, Hoogenraad CC, Rush J, Ramm E, Schlager MA, Duong DM, Xu P, Wijayawardana SR, Hanfelt J, Nakagawa T, Sheng M, Peng J (2006) Relative and absolute quantification of postsynaptic density proteome isolated from rat forebrain and cerebellum. Mol Cell Proteomics 5:1158-1170.

Choi J, Ko J, Racz B, Burette A, Lee JR, Kim S, Na M, Lee HW, Kim K, Weinberg RJ, Kim E (2005) Regulation of dendritic spine morphogenesis by insulin receptor substrate 53, a downstream effector of Rac1 and Cdc42 small GTPases. J Neurosci 25:869-879.

Chwang WB, O'Riordan KJ, Levenson JM, Sweatt JD (2006) ERK/MAPK regulates hippocampal histone phosphorylation following contextual fear conditioning. Learn Mem 13:322-328.

Coba MP, Pocklington AJ, Collins MO, Kopanitsa MV, Uren RT, Swamy S, Croning MD, Choudhary JS, Grant SG (2009) Neurotransmitters drive combinatorial multistate postsynaptic density networks. Sci Signal 2:ra19.

Cohen D, Fernandez D, Lazaro-Dieguez F, Musch A (2011) The serine/threonine kinase Par1b regulates epithelial lumen polarity via IRSp53-mediated cell-ECM signaling. J Cell Biol 192:525-540.

Colbert CM, Pan E (1999) Arachidonic acid reciprocally alters the availability of transient and sustained dendritic K(+) channels in hippocampal CA1 pyramidal neurons. J Neurosci 19:8163-8171.

Colledge M, Snyder EM, Crozier RA, Soderling JA, Jin Y, Langeberg LK, Lu H, Bear MF, Scott JD (2003) Ubiquitination regulates PSD-95 degradation and AMPA receptor surface expression. Neuron 40:595-607.

Collingridge GL, Volianskis A, Bannister N, France G, Hanna L, Mercier M, Tidball P, Fang G, Irvine MW, Costa BM, Monaghan DT, Bortolotto ZA, Molnar E, Lodge D, Jane DE (2013) The NMDA receptor as a target for cognitive enhancement. Neuropharmacology 64:13-26.

Cory GO, Cullen PJ (2007) Membrane curvature: the power of bananas, zeppelins and boomerangs. Curr Biol 17:R455-457.

Cowen PJ, Sharp T, Lau JYF (2013) Behavioral Neurobiology of Depression and Its Treatment. Heidelberg, New York, Dordrecht, London: Springer.

Craft S, Watson GS (2004) Insulin and neurodegenerative disease: shared and specific mechanisms. Lancet Neurol 3:169-178.

Cuthbert PC, Stanford LE, Coba MP, Ainge JA, Fink AE, Opazo P, Delgado JY, Komiyama NH, O'Dell TJ, Grant SG (2007) Synapse-associated protein 102/dlgh3 couples the NMDA receptor to specific plasticity pathways and learning strategies. J Neurosci 27:2673-2682.

D'Hooge R, De Deyn PP (2001) Applications of the Morris water maze in the study of learning and memory. Brain Res Brain Res Rev 36:60-90.

De Simoni A, Yu LM (2006) Preparation of organotypic hippocampal slice cultures: interface method. Nat Protoc 1:1439-1445.

Dieterich DC, Karpova A, Mikhaylova M, Zdobnova I, Konig I, Landwehr M, Kreutz M, Smalla KH, Richter K, Landgraf P, Reissner C, Boeckers TM, Zuschratter W, Spilker C, Seidenbecher CI, Garner CC, Gundelfinger ED, Kreutz MR (2008) Caldendrin-Jacob: a protein liaison that couples NMDA receptor signalling to the nucleus. PLoS Biol 6:e34.

Dingledine R, Borges K, Bowie D, Traynelis SF (1999) The glutamate receptor ion channels. Pharmacol Rev 51:7-61.

Disanza A, Mantoani S, Hertzog M, Gerboth S, Frittoli E, Steffen A, Berhoerster K, Kreienkamp HJ, Milanesi F, Di Fiore PP, Ciliberto A, Stradal TE, Scita G (2006) Regulation of cell shape by Cdc42 is mediated by the synergic actin-bundling activity of the Eps8-IRSp53 complex. Nat Cell Biol 8:1337-1347.

Do J, Kim JI, Bakes J, Lee K, Kaang BK (2012) Functional roles of neurotransmitters and neuromodulators in the dorsal striatum. Learn Mem 20:21-28.

Donnelly ML, Luke G, Mehrotra A, Li X, Hughes LE, Gani D, Ryan MD (2001) Analysis of the aphthovirus 2A/2B polyprotein 'cleavage' mechanism indicates not a proteolytic reaction, but a novel translational effect: a putative ribosomal 'skip'. J Gen Virol 82:1013-1025.

Downward J (1998) Mechanisms and consequences of activation of protein kinase B/Akt. Curr Opin Cell Biol 10:262-267.

Du Y, Weed SA, Xiong WC, Marshall TD, Parsons JT (1998) Identification of a novel cortactin SH3 domain-binding protein and its localization to growth cones of cultured neurons. Mol Cell Biol 18:5838-5851.

Ehlers MD (2003) Activity level controls postsynaptic composition and signaling via the ubiquitin-proteasome system. Nat Neurosci 6:231-242.

Fainzilber M, Budnik V, Segal RA, Kreutz MR (2011) From synapse to nucleus and back again--communication over distance within neurons. J Neurosci 31:16045-16048.

Feng W, Zhang M (2009) Organization and dynamics of PDZ-domain-related supramodules in the postsynaptic density. Nat Rev Neurosci 10:87-99.

Ferrari I, Crespi A, Scita G, Pietrini G (2012) LIN7-IRSp53: A novel pathway for filopodia and neurite formation? Commun Integr Biol 5:631-633.

Frankland PW, Ding HK, Takahashi E, Suzuki A, Kida S, Silva AJ (2006) Stability of recent and remote contextual fear memory. Learn Mem 13:451-457.

Fujiwara T, Mammoto A, Kim Y, Takai Y (2000) Rho small G-protein-dependent binding of mDia to an Src homology 3 domain-containing IRSp53/BAIAP2. Biochem Biophys Res Commun 271:626-629.

Funato Y, Terabayashi T, Suenaga N, Seiki M, Takenawa T, Miki H (2004) IRSp53/Eps8 complex is important for positive regulation of Rac and cancer cell motility/invasiveness. Cancer Res 64:5237-5244.

Futo K, Bodis E, Machesky LM, Nyitrai M, Visegrady B (2013) Membrane binding properties of IRSp53-missing in metastasis domain (IMD) protein. Biochim Biophys Acta.

Garber K (2007) Neuroscience. Autism's cause may reside in abnormalities at the synapse. Science 317:190-191.

Gardoni F (2008) MAGUK proteins: new targets for pharmacological intervention in the glutamatergic synapse. Eur J Pharmacol 585:147-152.

Gerhard Y (in preparation) Molekulare Interaktionen des Insulinrezeptorsubstratproteins von 53 kDa (IRSp53). MD thesis University of Hamburg.

Geschwind DH (2008) Autism: many genes, common pathways? Cell 135:391-395.

Gilman SR, Iossifov I, Levy D, Ronemus M, Wigler M, Vitkup D (2011) Rare de novo variants associated with autism implicate a large functional network of genes involved in formation and function of synapses. Neuron 70:898-907.

Gogolla N, Galimberti I, DePaola V, Caroni P (2006) Preparation of organotypic hippocampal slice cultures for long-term live imaging. Nat Protoc 1:1165-1171.

Goh WI, Sudhaharan T, Lim KB, Sem KP, Lau CL, Ahmed S (2011) Rif-mDia1 interaction is involved in filopodium formation independent of Cdc42 and Rac effectors. J Biol Chem 286:13681-13694.

Gorman JM, Kent JM, Sullivan GM, Coplan JD (2000) Neuroanatomical hypothesis of panic disorder, revised. Am J Psychiatry 157:493-505.

Govind S, Kozma R, Monfries C, Lim L, Ahmed S (2001) Cdc42Hs facilitates cytoskeletal reorganization and neurite outgrowth by localizing the 58-kD insulin receptor substrate to filamentous actin. J Cell Biol 152:579-594.

Grabrucker AM, Schmeisser MJ, Schoen M, Boeckers TM (2011) Postsynaptic ProSAP/Shank scaffolds in the cross-hair of synaptopathies. Trends Cell Biol 21:594-603.

Graham FL, Smiley J, Russell WC, Nairn R (1977) Characteristics of a human cell line transformed by DNA from human adenovirus type 5. J Gen Virol 36:59-74.

Graham FL, van der Eb AJ (1973) Transformation of rat cells by DNA of human adenovirus 5. Virology 54:536-539.

Guzowski JF, McGaugh JL (1997) Antisense oligodeoxynucleotide-mediated disruption of hippocampal cAMP response element binding protein levels impairs consolidation of memory for water maze training. Proc Natl Acad Sci U S A 94:2693-2698.

Hardingham GE, Bading H (2002) Coupling of extrasynaptic NMDA receptors to a CREB shut-off pathway is developmentally regulated. Biochim Biophys Acta 1600:148-153.

Hardingham GE, Fukunaga Y, Bading H (2002) Extrasynaptic NMDARs oppose synaptic NMDARs by triggering CREB shut-off and cell death pathways. Nat Neurosci 5:405-414.

Havekes R, Abel T, Van der Zee EA (2011) The cholinergic system and neostriatal memory functions. Behav Brain Res 221:412-423.

Hori K, Konno D, Maruoka H, Sobue K (2003) MALS is a binding partner of IRSp53 at cell-cell contacts. FEBS Lett 554:30-34.

Hori K, Yasuda H, Konno D, Maruoka H, Tsumoto T, Sobue K (2005) NMDA receptor-dependent synaptic translocation of insulin receptor substrate p53 via protein kinase C signaling. J Neurosci 25:2670-2681.

Impey S, Obrietan K, Wong ST, Poser S, Yano S, Wayman G, Deloulme JC, Chan G, Storm DR (1998) Cross talk between ERK and PKA is required for Ca2+ stimulation of CREB-dependent transcription and ERK nuclear translocation. Neuron 21:869-883.

Johannessen M, Delghandi MP, Moens U (2004) What turns CREB on? Cell Signal 16:1211-1227.

Josselyn SA (2010) Continuing the search for the engram: examining the mechanism of fear memories. J Psychiatry Neurosci 35:221-228.

Josselyn SA, Shi C, Carlezon WA, Jr., Neve RL, Nestler EJ, Davis M (2001) Long-term memory is facilitated by cAMP response element-binding protein overexpression in the amygdala. J Neurosci 21:2404-2412.

Kaech S, Banker G (2006) Culturing hippocampal neurons. Nat Protoc 1:2406-2415.

Kandel ERS, James H.; Jessel, Thomas M. (2000) Principles of Neural Science. New York: McGraw-Hill

Kauer JA, Malenka RC (2007) Synaptic plasticity and addiction. Nat Rev Neurosci 8:844-858.

Kelleher RJ, 3rd, Bear MF (2008) The autistic neuron: troubled translation? Cell 135:401-406.

Kelleher RJ, 3rd, Govindarajan A, Tonegawa S (2004) Translational regulatory mechanisms in persistent forms of synaptic plasticity. Neuron 44:59-73.

Kelleher RJ, 3rd, Govindarajan A, Jung HY, Kang H, Tonegawa S (2004b) Translational control by MAPK signaling in long-term synaptic plasticity and memory. Cell 116:467-479.

Kennedy MB (2000) Signal-processing machines at the postsynaptic density. Science 290:750-754.

Kennedy MJ, Ehlers MD (2006) Organelles and trafficking machinery for postsynaptic plasticity. Annu Rev Neurosci 29:325-362.

Kida S, Josselyn SA, Pena de Ortiz S, Kogan JH, Chevere I, Masushige S, Silva AJ (2002) CREB required for the stability of new and reactivated fear memories. Nat Neurosci 5:348-355.

Kim E, Sheng M (2004) PDZ domain proteins of synapses. Nat Rev Neurosci 5:771-781.

Kim MH, Choi J, Yang J, Chung W, Kim JH, Paik SK, Kim K, Han S, Won H, Bae YS, Cho SH, Seo J, Bae YC, Choi SY, Kim E (2009) Enhanced NMDA receptor-mediated synaptic transmission, enhanced long-term potentiation, and impaired learning and memory in mice lacking IRSp53. J Neurosci 29:1586-1595.

Kitamura T, Kimura K, Jung BD, Makondo K, Sakane N, Yoshida T, Saito M (2002) Proinsulin C-peptide activates cAMP response element-binding proteins through the p38 mitogen-activated protein kinase pathway in mouse lung capillary endothelial cells. Biochem J 366:737-744.

Klemm DJ, Roesler WJ, Boras T, Colton LA, Felder K, Reusch JE (1998) Insulin stimulates cAMP-response element binding protein activity in HepG2 and 3T3-L1 cell lines. J Biol Chem 273:917-923.

Komiyama NH, Watabe AM, Carlisle HJ, Porter K, Charlesworth P, Monti J, Strathdee DJ, O'Carroll CM, Martin SJ, Morris RG, O'Dell TJ, Grant SG (2002) SynGAP regulates ERK/MAPK signaling, synaptic plasticity, and learning in the complex with postsynaptic density 95 and NMDA receptor. J Neurosci 22:9721-9732.

Kornau HC, Schenker LT, Kennedy MB, Seeburg PH (1995) Domain interaction between NMDA receptor subunits and the postsynaptic density protein PSD-95. Science 269:1737-1740.

Krapivinsky G, Medina I, Krapivinsky L, Gapon S, Clapham DE (2004) SynGAP-MUPP1-CaMKII synaptic complexes regulate p38 MAP kinase activity and NMDA receptor-dependent synaptic AMPA receptor potentiation. Neuron 43:563-574.

Krasne FB, Fanselow MS, Zelikowsky M (2011) Design of a neurally plausible model of fear learning. Front Behav Neurosci 5:41.

Kreienkamp HJ (2008) Scaffolding proteins at the postsynaptic density: shank as the architectural framework. Handb Exp Pharmacol 365-380.

Krugmann S, Jordens I, Gevaert K, Driessens M, Vandekerckhove J, Hall A (2001) Cdc42 induces filopodia by promoting the formation of an IRSp53:Mena complex. Curr Biol 11:1645-1655.

Kutner RH, Zhang XY, Reiser J (2009) Production, concentration and titration of pseudotyped HIV-1-based lentiviral vectors. Nat Protoc 4:495-505.

Laumonnier F, Cuthbert PC, Grant SG (2007) The role of neuronal complexes in human X-linked brain diseases. Am J Hum Genet 80:205-220.

Lee HJ, Zheng JJ (2010) PDZ domains and their binding partners: structure, specificity, and modification. Cell Commun Signal 8:8.

Lee SH, Kerff F, Chereau D, Ferron F, Klug A, Dominguez R (2007) Structural basis for the actin-binding function of missing-in-metastasis. Structure 15:145-155.

Lee YS, Silva AJ (2009) The molecular and cellular biology of enhanced cognition. Nat Rev Neurosci 10:126-140.

Levenson JM, O'Riordan KJ, Brown KD, Trinh MA, Molfese DL, Sweatt JD (2004) Regulation of histone acetylation during memory formation in the hippocampus. J Biol Chem 279:40545-40559.

Levy D, Ronemus M, Yamrom B, Lee YH, Leotta A, Kendall J, Marks S, Lakshmi B, Pai D, Ye K, Buja A, Krieger A, Yoon S, Troge J, Rodgers L, Iossifov I, Wigler M (2011) Rare de novo and transmitted copy-number variation in autistic spectrum disorders. Neuron 70:886-897.

Lewis-Saravalli S, Campbell S, Claing A (2013) ARF1 controls Rac1 signaling to regulate migration of MDA-MB-231 invasive breast cancer cells. Cell Signal 25:1813-1819.

Lim KB, Bu W, Goh WI, Koh E, Ong SH, Pawson T, Sudhaharan T, Ahmed S (2008) The Cdc42 effector IRSp53 generates filopodia by coupling membrane protrusion with actin dynamics. J Biol Chem 283:20454-20472.

Lisman J, Schulman H, Cline H (2002) The molecular basis of CaMKII function in synaptic and behavioural memory. Nat Rev Neurosci 3:175-190.

Lomo T (2003) The discovery of long-term potentiation. Philos Trans R Soc Lond B Biol Sci 358:617-620.

Luo L (2002) Actin cytoskeleton regulation in neuronal morphogenesis and structural plasticity. Annu Rev Cell Dev Biol 18:601-635.

Lynch MA (2004) Long-term potentiation and memory. Physiol Rev 84:87-136.

Mameza MG, Dvoretskova E, Bamann M, Honck HH, Guler T, Boeckers TM, Schoen M, Verpelli C, Sala C, Barsukov I, Dityatev A, Kreienkamp HJ (2013) SHANK3 Gene Mutations Associated with Autism Facilitate Ligand Binding to the Shank3 Ankyrin Repeat Region. J Biol Chem 288:26697-26708.

Marshall CR, Noor A, Vincent JB, Lionel AC, Feuk L, Skaug J, Shago M, Moessner R, Pinto D, Ren Y, Thiruvahindrapduram B, Fiebig A, Schreiber S, Friedman J, Ketelaars CE, Vos YJ, Ficicioglu C, Kirkpatrick S, Nicolson R, Sloman L, Summers A, Gibbons CA, Teebi A, Chitayat D, Weksberg R, Thompson A, Vardy C, Crosbie V, Luscombe S, Baatjes R, Zwaigenbaum L, Roberts W, Fernandez B, Szatmari P, Scherer SW (2008) Structural variation of chromosomes in autism spectrum disorder. Am J Hum Genet 82:477-488.

Matta JA, Ashby MC, Sanz-Clemente A, Roche KW, Isaac JT (2011) mGluR5 and NMDA receptors drive the experience- and activity-dependent NMDA receptor NR2B to NR2A subunit switch. Neuron 70:339-351.

Mattila PK, Pykalainen A, Saarikangas J, Paavilainen VO, Vihinen H, Jokitalo E, Lappalainen P (2007) Missing-in-metastasis and IRSp53 deform PI(4,5)P2-rich membranes by an inverse BAR domain-like mechanism. J Cell Biol 176:953-964.

Mayer BJ (2001) SH3 domains: complexity in moderation. J Cell Sci 114:1253-1263.

Mehta S, Wu H, Garner CC, Marshall J (2001) Molecular mechanisms regulating the differential association of kainate receptor subunits with SAP90/PSD-95 and SAP97. J Biol Chem 276:16092-16099.

Migaud M, Charlesworth P, Dempster M, Webster LC, Watabe AM, Makhinson M, He Y, Ramsay MF, Morris RG, Morrison JH, O'Dell TJ, Grant SG (1998) Enhanced long-term potentiation and impaired learning in mice with mutant postsynaptic density-95 protein. Nature 396:433-439.

Miki H, Takenawa T (2002) WAVE2 serves a functional partner of IRSp53 by regulating its interaction with Rac. Biochem Biophys Res Commun 293:93-99.

Miki H, Yamaguchi H, Suetsugu S, Takenawa T (2000) IRSp53 is an essential intermediate between Rac and WAVE in the regulation of membrane ruffling. Nature 408:732-735.

Millard TH, Bompard G, Heung MY, Dafforn TR, Scott DJ, Machesky LM, Futterer K (2005) Structural basis of filopodia formation induced by the IRSp53/MIM homology domain of human IRSp53. EMBO J 24:240-250.

Misra A, Rajmohan R, Lim RP, Bhattacharyya S, Thanabalu T (2010) The mammalian verprolin, WIRE induces filopodia independent of N-WASP through IRSp53. Exp Cell Res 316:2810-2824.

Miyahara A, Okamura-Oho Y, Miyashita T, Hoshika A, Yamada M (2003) Genomic structure and alternative splicing of the insulin receptor tyrosine kinase substrate of 53-kDa protein. J Hum Genet 48:410-414.

Morimura S, Suzuki K, Takahashi K (2011) Nonmuscle myosin IIA is required for lamellipodia formation through binding to WAVE2 and phosphatidylinositol 3,4,5-triphosphate. Biochem Biophys Res Commun 404:834-840.

Murakoshi H, Yasuda R (2012) Postsynaptic signaling during plasticity of dendritic spines. Trends Neurosci 35:135-143.

Nelson TJ, Sun MK, Hongpaisan J, Alkon DL (2008) Insulin, PKC signaling pathways and synaptic remodeling during memory storage and neuronal repair. Eur J Pharmacol 585:76-87.

Oda K, Shiratsuchi T, Nishimori H, Inazawa J, Yoshikawa H, Taketani Y, Nakamura Y, Tokino T (1999) Identification of BAIAP2 (BAI-associated protein 2), a novel human homologue of hamster IRSp53, whose SH3 domain interacts with the cytoplasmic domain of BAI1. Cytogenet Cell Genet 84:75-82.

Oh SY, Knelson EH, Blobe GC, Mythreye K (2013) The type III TGFbeta receptor regulates filopodia formation via a Cdc42-mediated IRSp53-N-WASP interaction in epithelial cells. Biochem J 454:79-89.

Osten P, Grinevich V, Cetin A (2007) Viral vectors: a wide range of choices and high levels of service. Handb Exp Pharmacol 177-202.

Osterweil EK, Krueger DD, Reinhold K, Bear MF (2010) Hypersensitivity to mGluR5 and ERK1/2 leads to excessive protein synthesis in the hippocampus of a mouse model of fragile X syndrome. J Neurosci 30:15616-15627.

Otmakhov N, Tao-Cheng JH, Carpenter S, Asrican B, Dosemeci A, Reese TS, Lisman J (2004) Persistent accumulation of calcium/calmodulin-dependent protein kinase II in dendritic spines after induction of NMDA receptor-dependent chemical long-term potentiation. J Neurosci 24:9324-9331.

Oztas E (2003) Neuronal tracing. Neuroanatomy 2:2-5.

Pak DT, Sheng M (2003) Targeted protein degradation and synapse remodeling by an inducible protein kinase. Science 302:1368-1373.

Peters M, Bletsch M, Catapano R, Zhang X, Tully T, Bourtchouladze R (2009) RNA interference in hippocampus demonstrates opposing roles for CREB and PP1alpha in contextual and temporal long-term memory. Genes Brain Behav 8:320-329.

Philpot BD, Zukin RS (2010) Synapse-specific metaplasticity: to be silenced is not to silence 2B. Neuron 66:814-816.

Pringle FM, Gordon KH, Hanzlik TN, Kalmakoff J, Scotti PD, Ward VK (1999) A novel capsid expression strategy for Thosea asigna virus (Tetraviridae). J Gen Virol 80 ( Pt 7):1855-1863.

Punnakkal P, Jendritza P, Kohr G (2012) Influence of the intracellular GluN2 C-terminal domain on NMDA receptor function. Neuropharmacology 62:1985-1992.

Rajagopal S, Ji Y, Xu K, Li Y, Wicks K, Liu J, Wong KW, Herman IM, Isberg RR, Buchsbaum RJ (2010) Scaffold proteins IRSp53 and spinophilin regulate localized Rac activation by T-lymphocyte invasion and metastasis protein 1 (TIAM1). J Biol Chem 285:18060-18071.

Ranganathan R, Ross EM (1997) PDZ domain proteins: scaffolds for signaling complexes. Curr Biol 7:R770-773.

Rao Y, Ma Q, Vahedi-Faridi A, Sundborger A, Pechstein A, Puchkov D, Luo L, Shupliakov O, Saenger W, Haucke V (2010) Molecular basis for SH3 domain regulation of F-BAR-mediated membrane deformation. Proc Natl Acad Sci U S A 107:8213-8218.

Raymond CR (2007) LTP forms 1, 2 and 3: different mechanisms for the "long" in long-term potentiation. Trends Neurosci 30:167-175.

Ribases M, Bosch R, Hervas A, Ramos-Quiroga JA, Sanchez-Mora C, Bielsa A, Gastaminza X, Guijarro-Domingo S, Nogueira M, Gomez-Barros N, Kreiker S, Gross-Lesch S, Jacob CP, Lesch KP, Reif A, Johansson S, Plessen KJ, Knappskog PM, Haavik J, Estivill X, Casas M, Bayes M, Cormand B (2009) Case-control study of six genes asymmetrically expressed in the two cerebral hemispheres: association of BAIAP2 with attention-deficit/hyperactivity disorder. Biol Psychiatry 66:926-934.

Robens JM, Yeow-Fong L, Ng E, Hall C, Manser E (2010) Regulation of IRSp53-dependent filopodial dynamics by antagonism between 14-3-3 binding and SH3-mediated localization. Mol Cell Biol 30:829-844.

Roche KW, Standley S, McCallum J, Dune Ly C, Ehlers MD, Wenthold RJ (2001) Molecular determinants of NMDA receptor internalization. Nat Neurosci 4:794-802.

Rudy JW, Huff NC, Matus-Amat P (2004) Understanding contextual fear conditioning: insights from a two-process model. Neurosci Biobehav Rev 28:675-685.

Rudy JW, O'Reilly RC (2001) Conjunctive representations, the hippocampus, and contextual fear conditioning. Cogn Affect Behav Neurosci 1:66-82.

Rumbaugh G, Adams JP, Kim JH, Huganir RL (2006) SynGAP regulates synaptic strength and mitogen-activated protein kinases in cultured neurons. Proc Natl Acad Sci U S A 103:4344-4351.

Rumbaugh G, Vicini S (1999) Distinct synaptic and extrasynaptic NMDA receptors in developing cerebellar granule neurons. J Neurosci 19:10603-10610.

Saarikangas J, Zhao H, Pykalainen A, Laurinmaki P, Mattila PK, Kinnunen PK, Butcher SJ, Lappalainen P (2009) Molecular mechanisms of membrane deformation by I-BAR domain proteins. Curr Biol 19:95-107.

Sahun I, Gallego X, Gratacos M, Murtra P, Trullas R, Maldonado R, Estivill X, Dierssen M (2007) Differential responses to anxiogenic drugs in a mouse model of panic disorder as revealed by Fos immunocytochemistry in specific areas of the fear circuitry. Amino Acids 33:677-688.

Sambrook J, Russell DW (2001) Molecular Cloning: A Laboratory Manual. New York: Cold Spring Harbor Laboratory Press.

Sans N, Petralia RS, Wang YX, Blahos J, 2nd, Hell JW, Wenthold RJ (2000) A developmental change in NMDA receptor-associated proteins at hippocampal synapses. J Neurosci 20:1260-1271.

Sanz-Clemente A, Nicoll RA, Roche KW (2013) Diversity in NMDA receptor composition: many regulators, many consequences. Neuroscientist 19:62-75.

Sawallisch C, Berhorster K, Disanza A, Mantoani S, Kintscher M, Stoenica L, Dityatev A, Sieber S, Kindler S, Morellini F, Schweizer M, Boeckers TM, Korte M, Scita G, Kreienkamp HJ (2009) The insulin receptor substrate of 53 kDa (IRSp53) limits hippocampal synaptic plasticity. J Biol Chem 284:9225-9236.

Scannevin RH, Huganir RL (2000) Postsynaptic organization and regulation of excitatory synapses. Nat Rev Neurosci 1:133-141.

Schaaf CP, Zoghbi HY (2011) Solving the autism puzzle a few pieces at a time. Neuron 70:806-808.

Schmeisser MJ, Ey E, Wegener S, Bockmann J, Stempel AV, Kuebler A, Janssen AL, Udvardi PT, Shiban E, Spilker C, Balschun D, Skryabin BV, Dieck S, Smalla KH, Montag D, Leblond CS, Faure P, Torquet N, Le Sourd AM, Toro R, Grabrucker AM, Shoichet SA, Schmitz D, Kreutz MR, Bourgeron T, Gundelfinger ED, Boeckers TM (2012) Autistic-like behaviours and hyperactivity in mice lacking ProSAP1/Shank2. Nature 486:256-260.

Scita G, Confalonieri S, Lappalainen P, Suetsugu S (2008) IRSp53: crossing the road of membrane and actin dynamics in the formation of membrane protrusions. Trends Cell Biol 18:52-60.

Segal M, Murphy DD (1998) CREB activation mediates plasticity in cultured hippocampal neurons. Neural Plast 6:1-7.

Sekerkova G, Loomis PA, Changyaleket B, Zheng L, Eytan R, Chen B, Mugnaini E, Bartles JR (2003) Novel espin actin-bundling proteins are localized to Purkinje cell dendritic spines and bind the Src homology 3 adapter protein insulin receptor substrate p53. J Neurosci 23:1310-1319.

Sindreu CB, Scheiner ZS, Storm DR (2007) Ca2+ -stimulated adenylyl cyclases regulate ERK-dependent activation of MSK1 during fear conditioning. Neuron 53:79-89.

Soltau M, Berhorster K, Kindler S, Buck F, Richter D, Kreienkamp HJ (2004) Insulin receptor substrate of 53 kDa links postsynaptic shank to PSD-95. J Neurochem 90:659-665.

Soltau M, Richter D, Kreienkamp HJ (2002) The insulin receptor substrate IRSp53 links postsynaptic shank1 to the small G-protein cdc42. Mol Cell Neurosci 21:575-583.

Squire LR (2009) The legacy of patient H.M. for neuroscience. Neuron 61:6-9.

Steward O, Worley PF (2001) A cellular mechanism for targeting newly synthesized mRNAs to synaptic sites on dendrites. Proc Natl Acad Sci U S A 98:7062-7068.

Stocca G, Vicini S (1998) Increased contribution of NR2A subunit to synaptic NMDA receptors in developing rat cortical neurons. J Physiol 507 ( Pt 1):13-24.

Suetsugu S, Kurisu S, Oikawa T, Yamazaki D, Oda A, Takenawa T (2006) Optimization of WAVE2 complex-induced actin polymerization by membrane-bound IRSp53, PIP(3), and Rac. J Cell Biol 173:571-585.

Suetsugu S, Toyooka K, Senju Y (2010) Subcellular membrane curvature mediated by the BAR domain superfamily proteins. Semin Cell Dev Biol 21:340-349.

Sweatt JD (1999) Toward a molecular explanation for long-term potentiation. Learn Mem 6:399-416.

Takahashi K, Suzuki K (2010) WAVE2 targeting to phosphatidylinositol 3,4,5-triphosphate mediated by insulin receptor substrate p53 through a complex with WAVE2. Cell Signal 22:1708-1716.

Tang W, Ehrlich I, Wolff SB, Michalski AM, Wolfl S, Hasan MT, Luthi A, Sprengel R (2009) Faithful expression of multiple proteins via 2A-peptide self-processing: a versatile and reliable method for manipulating brain circuits. J Neurosci 29:8621-8629.

Tang YP, Shimizu E, Dube GR, Rampon C, Kerchner GA, Zhuo M, Liu G, Tsien JZ (1999) Genetic enhancement of learning and memory in mice. Nature 401:63-69.

Tang YP, Wang H, Feng R, Kyin M, Tsien JZ (2001) Differential effects of enrichment on learning and memory function in NR2B transgenic mice. Neuropharmacology 41:779-790.

Teodorof C, Bae JI, Kim SM, Oh HJ, Kang YS, Choi J, Chun JS, Song WK (2009) SPIN90-IRSp53 complex participates in Rac-induced membrane ruffling. Exp Cell Res 315:2410-2419.

Thomas EA, Foye PE, Alvarez CE, Usui H, Sutcliffe JG (2001) Insulin receptor substrate protein p53 localization in rats suggests mechanism for specific polyglutamine neurodegeneration. Neurosci Lett 309:145-148.

Toma C, Hervas A, Balmana N, Vilella E, Aguilera F, Cusco I, del Campo M, Caballero R, De Diego-Otero Y, Ribases M, Cormand B, Bayes M (2011) Association study of six candidate genes asymmetrically expressed in the two cerebral hemispheres suggests the involvement of BAIAP2 in autism. J Psychiatr Res 45:280-282.

Tovar KR, Westbrook GL (1999) The incorporation of NMDA receptors with a distinct subunit composition at nascent hippocampal synapses in vitro. J Neurosci 19:4180-4188.

Towbin H, Staehelin T, Gordon J (1979) Electrophoretic transfer of proteins from polyacrylamide gels to nitrocellulose sheets: procedure and some applications. Proc Natl Acad Sci U S A 76:4350-4354.

Trifilieff P, Herry C, Vanhoutte P, Caboche J, Desmedt A, Riedel G, Mons N, Micheau J (2006) Foreground contextual fear memory consolidation requires two independent phases of hippocampal ERK/CREB activation. Learn Mem 13:349-358.

Vaggi F, Disanza A, Milanesi F, Di Fiore PP, Menna E, Matteoli M, Gov NS, Scita G, Ciliberto A (2011) The Eps8/IRSp53/VASP network differentially controls actin capping and bundling in filopodia formation. PLoS Comput Biol 7:e1002088.

van Gaalen MM, Steckler T (2000) Behavioural analysis of four mouse strains in an anxiety test battery. Behav Brain Res 115:95-106.

Veltman DM, Auciello G, Spence HJ, Machesky LM, Rappoport JZ, Insall RH (2011) Functional analysis of Dictyostelium IBARa reveals a conserved role of the I-BAR domain in endocytosis. Biochem J 436:45-52.

Viosca J, Malleret G, Bourtchouladze R, Benito E, Vronskava S, Kandel ER, Barco A (2009) Chronic enhancement of CREB activity in the hippocampus interferes with the retrieval of spatial information. Learn Mem 16:198-209.

Walf AA, Frye CA (2007) The use of the elevated plus maze as an assay of anxiety-related behavior in rodents. Nat Protoc 2:322-328.

Walsh CA, Morrow EM, Rubenstein JL (2008) Autism and brain development. Cell 135:396-400.

Wang Q, Liu L, Pei L, Ju W, Ahmadian G, Lu J, Wang Y, Liu F, Wang YT (2003) Control of synaptic strength, a novel function of Akt. Neuron 38:915-928.

Wang X, McCoy PA, Rodriguiz RM, Pan Y, Je HS, Roberts AC, Kim CJ, Berrios J, Colvin JS, Bousquet-Moore D, Lorenzo I, Wu G, Weinberg RJ, Ehlers MD, Philpot BD, Beaudet AL, Wetsel WC, Jiang YH (2011) Synaptic dysfunction and abnormal behaviors in mice lacking major isoforms of Shank3. Hum Mol Genet 20:3093-3108.

Won H, Lee HR, Gee HY, Mah W, Kim JI, Lee J, Ha S, Chung C, Jung ES, Cho YS, Park SG, Lee JS, Lee K, Kim D, Bae YC, Kaang BK, Lee MG, Kim E (2012) Autistic-like social behaviour in Shank2-mutant mice improved by restoring NMDA receptor function. Nature 486:261-265.

Yanagida-Asanuma E, Asanuma K, Kim K, Donnelly M, Young Choi H, Hyung Chang J, Suetsugu S, Tomino Y, Takenawa T, Faul C, Mundel P (2007) Synaptopodin protects against proteinuria by disrupting Cdc42:IRSp53:Mena signaling complexes in kidney podocytes. Am J Pathol 171:415-427.

Yang SN, Tang YG, Zucker RS (1999) Selective induction of LTP and LTD by postsynaptic [Ca2+]i elevation. J Neurophysiol 81:781-787.

Yeh TC, Ogawa W, Danielsen AG, Roth RA (1996) Characterization and cloning of a 58/53-kDa substrate of the insulin receptor tyrosine kinase. J Biol Chem 271:2921-2928.

Zhao H, Pykalainen A, Lappalainen P (2011) I-BAR domain proteins: linking actin and plasma membrane dynamics. Curr Opin Cell Biol 23:14-21.

Zhao WQ, Alkon DL (2001) Role of insulin and insulin receptor in learning and memory. Mol Cell Endocrinol 177:125-134.

Zheng CY, Seabold GK, Horak M, Petralia RS (2011) MAGUKs, synaptic development, and synaptic plasticity. Neuroscientist 17:493-512.

Zhou J, Jones DR, Duong DM, Levey AI, Lah JJ, Peng J (2013) Proteomic analysis of postsynaptic density in Alzheimer's disease. Clin Chim Acta 420:62-68.

Zolotukhin S, Byrne BJ, Mason E, Zolotukhin I, Potter M, Chesnut K, Summerford C, Samulski RJ, Muzyczka N (1999) Recombinant adeno-associated virus purification using novel methods improves infectious titer and yield. Gene Ther 6:973-985.

# Appendix

***Chemicals***

| Name | Source |
|---|---|
| 2-Propanol | Merck, Darmstadt, Germany |
| 30% Acrylamide/ Bis | BioRad, München, Germany |
| 5-Brom-4-chlor-3-indoxyl-β-D-galactopyranosid (X-Gal) | Thermo Scientific, Bonn, Germany |
| Acetic Acid | Merck, Darmstadt, Germany |
| Agar (Select) | Invitrogen, Kahrlsruhe, Germany |
| Agarose | Invitrogen, Kahrlsruhe, Germany |
| Albumin bovine serum (BSA) | Sigma-Aldrich, Steinheim, Germany |
| Ammonium persulfate (APS) | Sigma-Aldrich, Steinheim, Germany |
| Ampicillin | Sigma-Aldrich, Steinheim, Germany |
| Aqua PolyMount | Poly-Science, Eppelheim, Germany |
| Bacto tryton | AppliChem, Darmstadt, Germany |
| BBS | Sigma-Aldrich, Steinheim, Germany |
| Bicinchonic acid | Sigma-Aldrich, Steinheim, Germany |
| Bicinchoninic acid solution | Sigma-Aldrich, Steinheim, Germany |
| Bromphenol blue | Merck, Darmstadt, Germany |
| Calcium chloride | Sigma-Aldrich, Steinheim, Germany |
| Calcium chloride dehydrate | Merck, Darmstadt, Germany |
| Complete Mini, EDTA free | Roche Applied Science, Penzberg, Germany |
| Copper(II)sulfate solution | Sigma-Aldrich, Steinheim, Germany |
| D-glucose | Sigma-Aldrich, Steinheim, Germany |
| Dimethyl Sulfoxide | Sigma-Aldrich, Steinheim, Germany |
| Ethanol | Fluka, Taufkirchen, Germany |
| Ethidium bromide | Merck, Darmstadt, Germany |
| Ethylene glycol tetraacetic acid (EGTA) | Merck, Darmstadt, Germany |
| Ethylenediaminetetraacetic acid (EDTA) | Sigma-Aldrich, Steinheim, Germany |

| | |
|---|---|
| EZ-Link Sulfo-NHS-SS-Biotin | Thermo Scientific, Bonn, Germany |
| Glycerin | Carl Roth, Karlsruhe, Germany |
| Glycerol | Fluka, Taufkirchen, Germany |
| Glycin | Carl Roth, Karlsruhe, Germany |
| HEPES | Merck, Darmstadt, Germany |
| Hydrochloride acid | Merck, Darmstadt, Germany |
| Iodixanol (Optiprep) | Nycomed, Konstanz, Germany |
| Kanamycin | Sigma-Aldrich, Steinheim, Germany |
| Magnesium sulfate heptahydrate | Merck, Darmstadt, Germany |
| Methanol | Merck, Darmstadt, Germany |
| Methyleblue | Sigma-Aldrich, Steinheim, Germany |
| Nonindet P40 (NP-40) | Roche Applied Science, Penzberg, Germany |
| Normal goat serum (NGS) | Sigma-Aldrich, Steinheim, Germany |
| Paraform aldehyde (PFA) | Sigma-Aldrich, Steinheim, Germany |
| PhosStop | Roche Applied Science, Penzberg, Germany |
| Potassium chloride | Merck, Darmstadt, Germany |
| Potassium hexacyanoferrate(II) | Sigma-Aldrich, Steinheim, Germany |
| Potassium hexacyanoferrate(III) | Sigma-Aldrich, Steinheim, Germany |
| Potassium phosphate monobasic | Sigma-Aldrich, Steinheim, Germany |
| Sodium acide | Merck, Darmstadt, Germany |
| Sodium chloride | Sigma-Aldrich, Steinheim, Germany |
| Sodium dodecyl sulfate (SDS) | Sigma-Aldrich, Steinheim, Germany |
| Sodium doxycholat | Sigma-Aldrich, Steinheim, Germany |
| Sodium floride | Sigma-Aldrich, Steinheim, Germany |
| Sodium hydroxide solution | Merck, Darmstadt, Germany |
| Sodium orthovanandate | Merck, Darmstadt, Germany |
| Sodium tetraborate hydrate | Merck, Darmstadt, Germany |
| Tetramethylethylenediamine (TEMED) | BioRad, München Darmstadt |
| Triton-X-100 | Carl Roth, Karlsruhe, Germany |
| Trizma base | Sigma-Aldrich, Steinheim, Germany |
| Tween 20 | Sigma-Aldrich, Steinheim, Germany |
| Xylene | Merck, Darmstadt, Germany |
| β-glycerol phosphate | Merck, Darmstadt, Germany |
| β-Mercaptoethanol | Merck, Darmstadt, Germany |

***Consumable equipment***

| Name | Source |
|---|---|
| Agar plates | Greiner, Essen, Germany |
| AmiconUltra Concentrator, 100K | Merk Millipore, Darmstadt, Germany |
| BD Microlance | BD Bioscience, Heidelberg, Germany |
| BD Plastipak (50 ml) | BD Bioscience, Heidelberg, Germany |
| Cell scraper (28 cm) | Greiner Bio-One, Frickenhausen, Germany |
| Centrifuge tubes (250 ml) | Beckman, Palo Alto (CA), USA |
| Cover slides | Assistent, Sondheim, Germany |
| Cover slips (13 mm) | Assistent, Sondheim, Germany |
| Cronex5 X-ray fils | AGFA, Berlin, Germany |
| Cuvettes (10 x 4 x 45 mm) | Sarstedt, Nümbrecht, Germany |
| Gloves (rotiprotect-Latex) | Carl Roth, Karlsruhe, Germany |
| Heparin columns (1 ml) | GE Healthcare, Freiburg, Germany |
| Kimwipes | Kimberly-Clark, Kings Hill, UK |
| Microscope slides | Menzel Gläser, Braunschweig, Germany |
| Nitrocellulose transfer membrane (Protran) | Whatman, Dassel, Germany |
| Nunc Multiwell plates | Sigma Aldrich, Taugkirchen, Germany |
| Parafilm | Pechiney Plastic Packaging, Chicago, USA |
| Pasteur capillary pipettes (150 mm) | Carl Roth, Karlsruhe, Germany |
| PCR tubes | Sarstedt, Nümbrecht, Germany |
| Razor blades Personna | American Safety Razor blade Company, Verona (VA), USA |
| Reaction tube (15 ml; 50 ml) | Sarstedt, Nümbrecht, Germany |
| Reaction tubes (1.5 ml) | Sarstedt, Nümbrecht, Germany |
| Reaction tubes (2 ml) | Eppendorf, Hamburg, Germany |
| Rotilabs Syringe filter (0.40 µm) | Carl Roth, Karlsruhe, Germany |
| Serological pipetts (5 ml; 10 ml; 25 ml) | Sarstedt, Nümbrecht, Germany |
| Serological syringe (1 ml, 2 ml, 5 ml) | Henke Sass Wolf, Tuttlingen, Germany |
| Sterile filtre 0.20 µm | Sarstedt, Nümbrecht, Germany |
| Tips (10 µl; 20 µl; 200 µl; 1000 µl) | Sarstedt, Nümbrecht, Germany |
| Tissue culture dishes (10 cm) | Sarstedt, Nümbrecht, Germany |
| Whatman filter paper | Whatman, Dassel, Germany |

***Technical device***

| Device | Application | Source |
|---|---|---|
| ABI PRISM 3500 Genetic analyzer | Sequencing | ABI Applied Biosystems, Dresden, Germany |
| Assistent wather bath | Water bath | Assistent, Sondheim, Germany |
| Axiovert 40 CFL | Microscopy | Zeiss, Jena, Germany |
| BD FACS CantoII | FACS | BD Bioscience, Heidelberg, Germany |
| BertholdTech TriStar 1.04 | Protein concen-tration | Berthold Technologies, Bad Wildbad, Germany |
| Biometra T Gradient Thermo-cycler | PCR | Biometra GmbH, Göttingen, Germany |
| Biophotometer | various | Eppendorf, Hamburg, Germany |
| BioRad PowerPac 300 | Power Supply | BioRad, Munich, Germany |
| Centrifuge 5417R | Centrifuge | Eppendorf, Hamburg, Germany |
| ChemiDOC XRS | Detection | BioRad, Munich, Germany |
| Consort E833 | Power Supply | Amersham Bioscience, Freiburg, Germany |
| Graseby 3400 | Perfusion pump | Smith Medical, Grasbrunn, Germany |
| HERA safe Typ 12/2, 1995 | Hood | Heraeus, Hanau, Germany |
| Heraeus B5060 E | Incubator | Heraeus, Hanau, Germany |
| Hettich Mikro 20 | Centrifuge | Hettich, Tuttlingen, Germany |
| IKA-Combimag RCT | Magnetic stirrer | IKA, Staufen; Germany |
| Improvision LiveCell Spinning Disk | Microscopy | PerkinElmer, Rodgau, Germany |
| JLA 16.250 | Rotor | Beckman, Palo Alto (CA), USA |
| Lab scale PE 3600 | Calibrated scale | MWG, Ebersberg, Germany |
| Lamin Air Intruments | Hood | Heraeus, Hanau, Germany |
| Leica TCS SP5 | Microscopy | Leica, Wetzlar, Germany |
| Leica WILDM3Z | Bino | Leica, Wetzlar, Germany |
| LeicaVT1000S | Vibratom | Leica, Wetzlar, Germany |
| Microprocessor pH/ION meter pMX3000 | pH indicator | WTW , Weilheim, Germany |
| Milli-Q water purification sys-tem | various | Millipore , Schwalbach, Germany |
| Mini Trans-Blot cell | Western blot | BioRad, Munich, Germany |

| | | |
|---|---|---|
| Mini-PROTEAN 3 cell | SDS-Page | BioRad, Munich, Germany |
| MOUSE-E-MOTION | Activity monitoring system | INFRA-E-Motion, Hamburg, Germany |
| Nuova stirrer | various | Neolab, Heidelberg, Germany |
| OPTIMAX X-Ray Film Processor | Fluorescence microscopy | Protec, Oberstenfeld-Gronau, Germany |
| Orbital shaker | various | Infors, Bottmingen, CH |
| Pipetman | various | Gilson, Limburg-Offheim, Germany |
| Sartorius Scale | Calibrated scale | Sartorius AG, Göttingen, Germany |
| Serological Pipette | various | Thermo Scientific, Karlsruhe, Germany |
| Sorvall Superspeed RC2-B | Centrifuge | Thermo Scientific, Karlsruhe, Germany |
| Stoelting Tissue Slicer, Vernier Micrometer | Tissue slicer | Stoelting Co., Illinois, UK |
| Sub-Cell GT | Detection | BioRad, Munich, Germany |
| Thermomixer compact | various | Eppendorf, Hamburg, Germany |
| Transilluminator | Gel photo | Bachofer, Reutlingen, Germany |
| Vortex | various | Heidolph, Schwabach, Germany |
| Wather bath 1083 | Water bath | GFL, Burgwedel, Germany |

***Software***

| Software | Version | Source |
|---|---|---|
| 4D TBase | v12.5 | 4D, Echingen, Germany |
| Adobe Photoshop | CS4 | Adobe systems, San Jose (CA), USA |
| BD FACSDiva | 7.0 | BD Bioscience, Heidelberg, Germany |
| EditSeq | 8.0 | DNASTAR Lasergene, GATC, Konstanz, Germany |
| EnzymeX | 1.1 | http://mekentosj.com/enzymex7 |
| Gene Construction Kit | 2.5.10 | Textco Bio Software Inc., West Lebanon (NH), USA |
| GraphPad Prism | 6 | GraphPad Software, La Jolla (CA), USA |
| Image Lab | 2.0.1 | BioRad, Munich, Germany |
| ImageJ | 1.40 | NIH, Bethesda (MD), USA |
| JabRef | 2.7.2 | http://jabref.sourceforge.net |

| | | |
|---|---|---|
| LeicaLAS | 4.1 | Leica Microsystems, Wetzlar, Germany |
| Microsoft Excel | 2011 | Microsoft, Redmond (WA), USA |
| Microsoft Word | 2011 | Microsoft, Redmond (WA), USA |
| MircroWin2000 | 4.41 | Berthold Technologies, Bad Wildbad, Germany |
| SeqMan | 8.0 | DNASTAR Lasergene, GATC, Konstanz, Germany |
| Velocity | 6.1.0 | PerkinElmer, Rodgau, Germany |

# Acknowledgments

Initially, I would like to thank all, who contributed to this Dissertation by professional advice and moral support.

First, I thank PD Dr. Hans-Jürgen Kreienkamp for offering me the opportunity to work on this interesting topic and for providing great and patient supervision as well as frequent, helpful discussions during my whole project. Furthermore, I thank my appraiser Prof. Matthias Kneussel for kindly reviewing this manuscript.

Moreover, I would like to thank the AG Kreienkamp and the AG Kindler for professional advice throughout my research work and for critical discussions on my research project. In particular I would like to thank Julia Höft for her reliable and fatiguing help in the lab. Also, I thank Hans-Hinnrich Hönck, PhD Fabio Morellini, PhD Michaela Schweizer, Bernd Zobiak of the UKE Microscopic Imaging facility and the members of the FACS Sorting core unit of the UKE for providing professional instructions and assistance to essential techniques used in this manuscript. Furthermore, I thank Prof. Rolf Sprengel from the MPI for medical Research in Heidelberg providing me the Puzzle box as well as Prof. Seth Grant and PhD Marcelo Coba supplying me PSD fractionations from PSD95 deficient mice. I also thank Katrin Lehmann and Dr. Marc Willaredt for proofreading this manuscript.

Particularly, I would like to thank the whole Institute of Human Genetics for the friendly admission into their team, for their advice, help and the kind atmosphere throughout my research work.

Finally, my gratitude goes to my husband Markus and my family for always supporting me, offering valuable and professional advice and for assisting me by word and deed.